ABSTRACT

FRICK, KONOR L. Modeling and Design of a Sensible Heat Thermal Energy Storage System for Small Modular Reactors. (Under the direction of Dr. J. Michael Doster.)

The contribution of intermittent (renewable) energy sources such as wind and solar continues to increase as renewables improve in efficiency and price-point. However, since renewables have grid priority the variability of renewables generates additional challenges for the electric grid in the form of rapidly varying net electric loads.

Proposed options for accommodating this net load have included operating nuclear reactors in a load follow mode, or operating the reactor at or near steady state and bypassing steam directly to the condenser. Both strategies result in lost energy potential. In addition to lost energy potential, load follow operation results in increased stress on the fuel and other mechanical components. A more attractive approach is to operate the reactor at or near steady state and bypass excess steam to a thermal energy storage system. The thermal energy can then be recovered later, either for electric generation during periods of peak electric demand, or for use in ancillary applications such as desalination and chilled water production. Such systems are known as nuclear hybrid energy systems (NHES). Various methods of Thermal Energy Storage (TES) can be coupled to nuclear (or renewable) power sources to help absorb grid instabilities caused by daily electric demand changes and renewable intermittency.

Sensible Heat Thermal Energy Storage is a mature technology currently used in solar energy systems. This research focuses on the design and coupling of such a system to Small Modular Reactors (SMRs), typical of Integral Pressurized Water Reactor (IPWR) designs currently under development.

The goal of the coupled system is to match turbine output with demand, bypass steam to the TES system for storage, and maintain reactor power at approximately 100%. Simulations of the NHES dynamics are run in a high-fidelity FORTRAN model developed at NCSU. Results reveal a sensible heat storage system is capable of meeting turbine demand and maintaining reactor power constant, while providing enough thermal energy to operate the TES system as an electric or steam peaking unit.

Modeling and Design of a Sensible Heat Thermal Energy Storage System for Small Modular Reactors

by
Konor L Frick

A dissertation submitted to the Graduate Faculty of
North Carolina State University
in partial fulfillment of the
requirements for the Degree of
Doctor of Philosophy

Nuclear Engineering

Raleigh, North Carolina

2018

APPROVED BY:

_____	_____
Dr. J. Michael Doster Committee Chair	Dr. Stephen D. Terry
_____	_____
Dr. Shannon Bragg-Sitton	Dr. Mohamed A. Bourham

BIOGRAPHY

Konor Frick, an avid sports fan, was born 17 March 1993. He grew up across the eastern seaboard, having started school in North Carolina and ultimately graduating Shenendehowa High School in Upstate New York.

He earned his undergraduate degree at North Carolina State University (NCSU) in Nuclear Engineering during the spring of 2014. The following fall he began his graduate studies at NCSU under the direction of Dr. J. M. Doster in the hybrid energy field. In December 2016 he earned his Masters of Science in Nuclear Engineering. Konor's research interests lie in the efficient storage and usage of thermal energy from nuclear reactors.

Among his more redeeming qualities is his infatuation with haunted attractions. While in high school he became acquainted with the haunted attraction industry by assisting with the design of haunted attractions at major theme parks and hours of hands-on experience, honing the craft. Konor often remarks when asked about his haunted house experience, "There is no better job in world. I am paid to scare people; only downhill from here."

ACKNOWLEDGMENTS

I would first like to thank my thesis advisor Dr. J. Michael Doster of the Nuclear Engineering Department at North Carolina State University. The door to Dr. Doster's office was always open whenever I ran into technical difficulties. He always provided useful comments, remarks, and engagement throughout my dissertation tenure.

I would also like to acknowledge Dr. Mohamed Bourham, Dr. Stephen Terry, and Dr. Shannon Bragg-Sitton as committee members. I am gratefully indebted to them for their valuable comments on this thesis.

I would like to acknowledge funding support from the DOE-NE IUP Fellowship program through the NEUP office.

TABLE OF CONTENTS

LIST OF TABLES

LIST OF FIGURES

NOMENCLATURE

α	void fraction
A	area
ACV	auxiliary control valve
Aux	auxiliary
BOP	balance of plant
c_p	specific heat
FBV	feed bypass valve
FDCV	feed control valve
FCV	flow control valve
FV	flash vessel
GHG	greenhouse gas
h	enthalpy
H	height
HPT	high pressure turbine
HTSE	high temperature steam electrolysis
HVAC	heating ventilation and air conditioning
IHX	intermediate heat exchanger
IPWR	integral pressurized water reactor
K	loss coefficient
LCV	level control valve
$\dot{m}$	mass flow rate
M	mass
MGD	million gallons per day
MSF	multistage flash desalination
MWe	megawatts electric
MWt	megawatts thermal
NHES	nuclear hybrid energy system
Nu	nusselt number
OTSG	once through steam generator
P	pressure
ρ	density
ρu	energy per unit volume
PCV	pressure control valve
PRV	pressure relief valve
Pr	prandtl number
PV	photovoltaic
ΔP	pressure drop
$\dot{Q}$	heat transfer rate
R	universal gas constant
Re	reynolds number
RO	reverse osmosis
SMR	small modular reactor
Δt	change in time
t	time
T	temperature
$T_{IHXexit}$	temperature at exit of IHX (tube side)
TBV	turbine bypass valve

TES	thermal energy storage
u	internal energy
UA	overall heat transfer coefficient
v	velocity
ν	specific volume
V	volume
$\dot{W}$	work

Subscripts

Amb	ambient
Cond	condenser
CT	cold tank
f	saturated liquid
fg	range between saturated liquid and vapor
feed	feed flow
g	saturated vapor
HDR	header
HT	hot tank
IHX	intermediate heat exchanger
j	node “j”
l	liquid phase
Line	losses in lines
pump	pump
r	relative
ref	reference
sat	saturation value
SD	steam dome
SG	steam generator
TES	thermal energy storage
x	cross sectional area

Chapter 1 Introduction

1.1 Current State of Grid/Hybrid Energy Field

Renewable energy technologies continue to become more attractive with improvements in efficiency and price-point. However, the variability of renewables creates additional challenges for the electric grid. The most common forms of installed renewable energy are wind and solar. Wind and solar energy, while zero carbon footprint energy sources, have energy outputs which cannot be directly controlled and instead are subject to the variability found in nature. This implies the energy production side of the equation is no longer 100% dispatchable and, depending on the amount of solar and wind installed on the grid, could mean large, uncontrolled variations in energy production. This can lead to mismatches between energy demand and energy production and ultimately system instabilities and blackouts. Furthermore, the integration of renewable energy can lead to over-generation potential as shown in Figure 1.1. This over-generation potential can lead to negative electric prices where the utility is forced to pay customers who are willing to take the power produced. Negative prices occur when large amounts of inflexible power generation occur simultaneously with low demand [1]. This phenomenon occurs more frequently when a large amount of intermittent renewable energy is introduced to the grid.

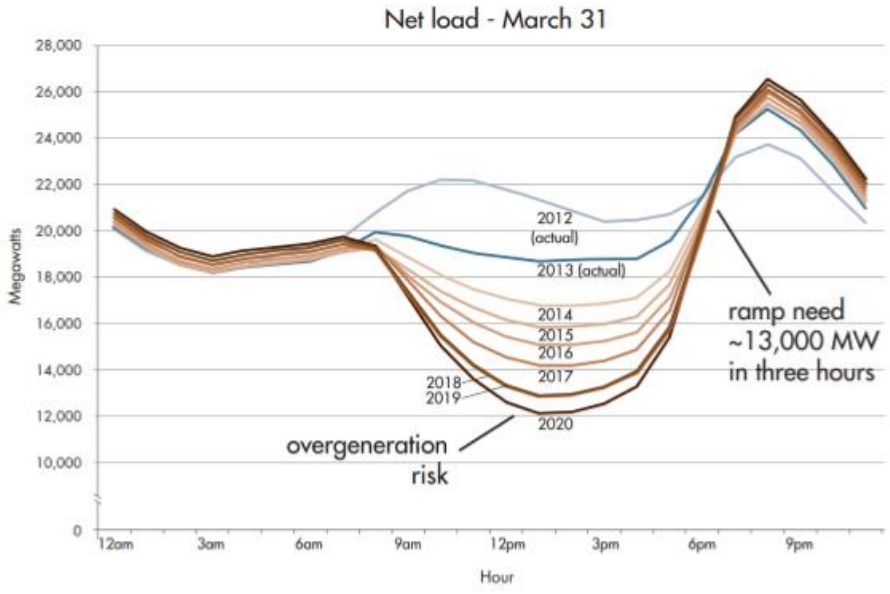

Figure 1.1: "Duck Curve" from substantial renewable energy (solar PV) integration in California [2]

It is likely that base load plants will still be required to maintain our current lifestyle. However, as the penetration of renewables increases, base load plants need to be more flexible in their operation as

illustrated in Figure 1.2 and Figure 1.3. Figure 1.2 gives a representative load profile for a hot summer day in an area with mixed commercial and residential characteristics [3]. Figure 1.3 shows representative energy profiles for wind and solar [4] and the energy output required of a plant operating in load follow mode if 65% of the peak energy demand can be provided by standard base load units. Without a plant designed to mitigate the load variability, the base load plants would need the ability to quickly increase and decrease power. An example of the relative load profile that might be experienced by the base load plants with 35% renewable penetration is illustrated in Figure 1.4.

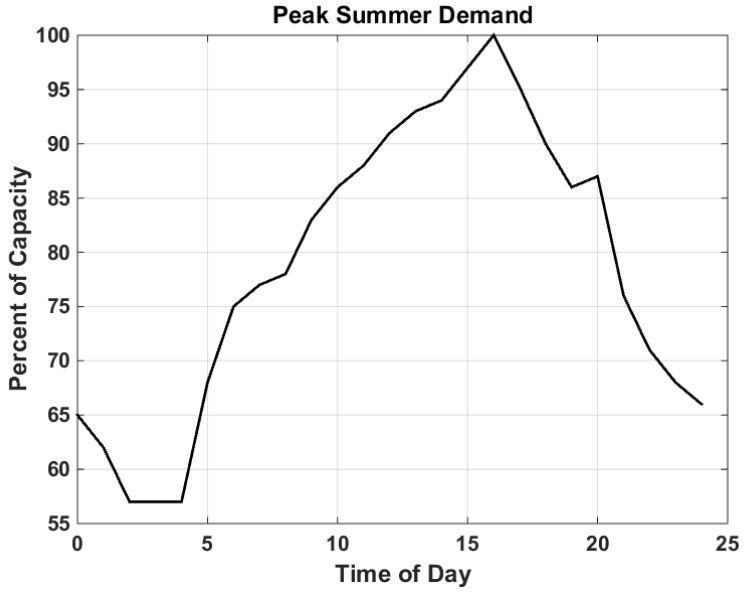

Figure 1.2: Representative Peak Summer Day Load Profile [2]

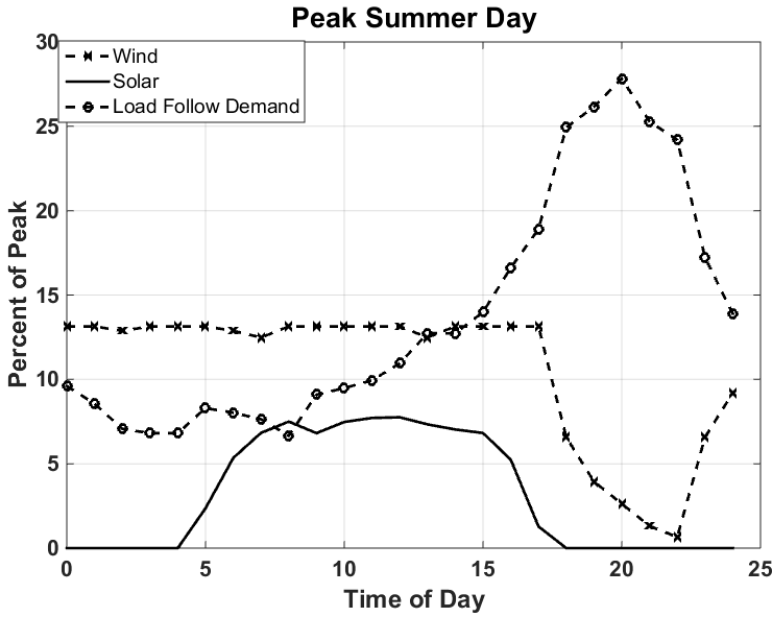

Figure 1.3: Peak Summer Day hourly demand with 65% power from base load units and 35% power from intermittent and load follow capacity [4].

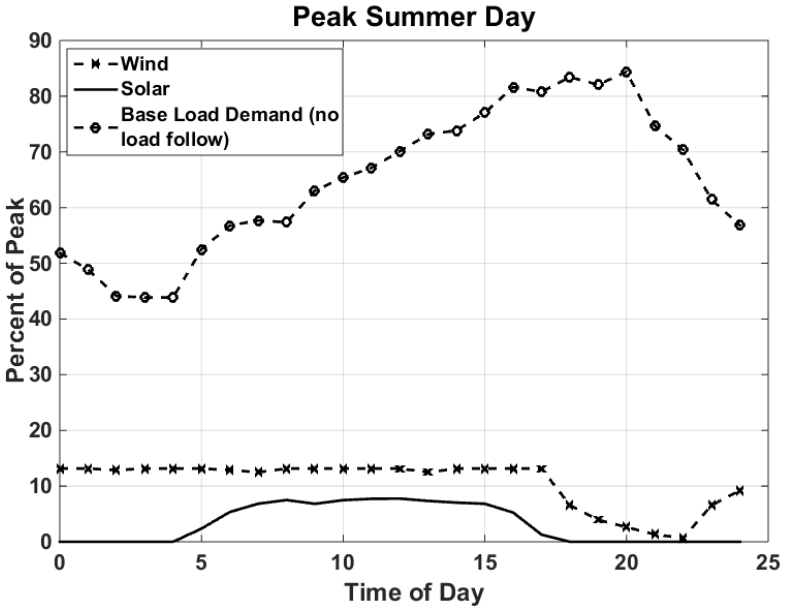

Figure 1.4: Peak summer day including intermittent generation of up to 35% penetration.

Under these conditions, the reactor can be subjected to significant time varying electric loads. Options for accommodating this load have included operating nuclear reactors in a load follow mode, or operating the reactor at or near steady state and bypassing steam directly to the condenser [5]. Both

strategies result in lost energy potential. Load follow operation can also result in additional stresses on the fuel and other mechanical components. A more attractive approach is to operate the reactor at or near steady state and store/use the excess energy in either a thermal energy storage unit (TES) or alternative applications. Such systems are known as nuclear hybrid energy systems (NHES). Integrated nuclear hybrid energy systems involve the design, integration and coordinated operation of several complex, standalone systems. The control algorithms involved are unique to each application and the particular design of the components. NHES architecture can include process steam applications, thermal energy storage, and the presence of intermittent energy sources such as wind and solar. An example NHES is shown in Figure 1.5. Potential alternative energy applications for excess power are considered below.

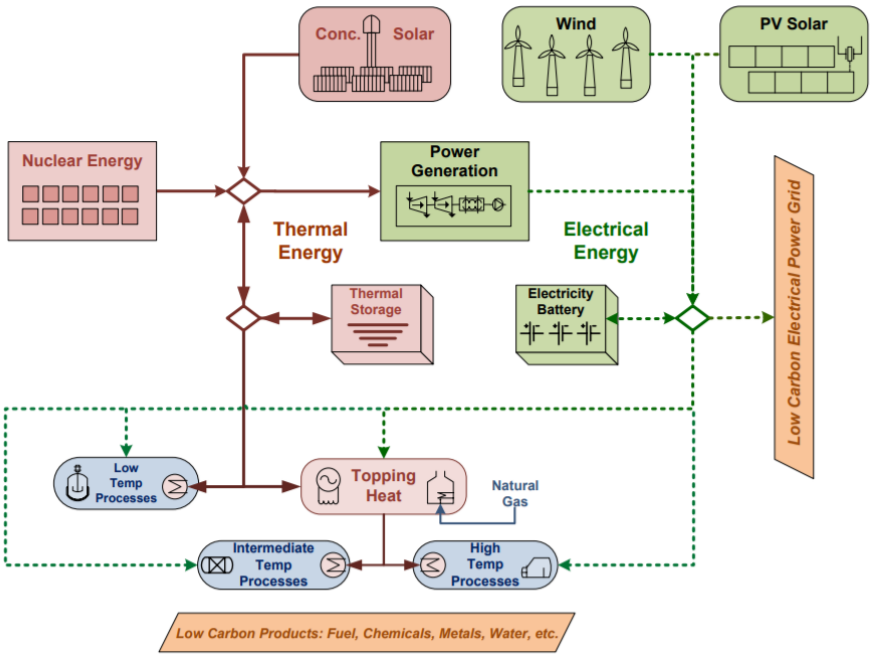

Figure 1.5: Example architecture for a tightly coupled NHES, as proposed by Idaho National Laboratory [6]

1.2 Candidate Ancillary Energy Applications

A benefit of NHES systems is the ability to store and use excess energy from the reactor for ancillary applications. However, not all ancillary applications are created equally. Some require process steam at high pressure and temperature, others require process steam at low pressure, and some only require electricity. This makes the selection of ancillary applications both region and NHES power source specific. Applications considered for use in this study include desalination of brackish water/ seawater, hydrogen production, and chilled water production using absorption chillers.

1.2.1. Desalination of Brackish/Sea Water

A promising alternative energy application is the desalination of sea water. This would be a particularly useful application in areas such as Southern California or the Southwestern United States where availability of potable drinking water is an increasing concern. To ensure adequate water supplies, desalination plants are being brought online yearly in Southern California, with the most recent in Carlsbad near San Diego in December 2015 [7], [8].

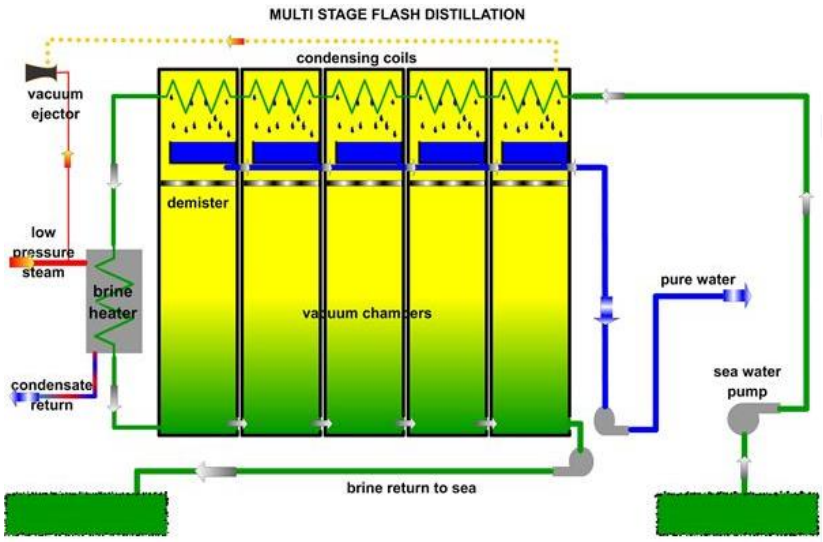

Figure 1.6: Example of a multistage flash desalination plant [9]

For desalination plants with a capacity of 4000 m^3/d and above the two main desalination technologies are multistage flash desalination (MSF) (69%) and reverse osmosis (RO) (23%) [10]. The process mechanics and energy requirements of the two are vastly different. Multistage flash desalination is based on heating seawater in a brine heater to around 90-110 degrees Celsius. The hot brine then enters a flash chamber which is held at vacuum. Since the water entering the chamber is above the boiling

temperature at vacuum, part of the water flashes to steam. This steam rises to condensing coils where it condenses into fresh water. A diagram of this process is shown in Figure 1.6.

Reverse Osmosis is the main competitor to multistage flash desalination. The RO process works by passing water at high pressures through fine membranes that only allow water molecules to pass. A typical RO plant works in two stages, the first being a pretreatment stage where chlorine and other chemical additives are used to remove biological organisms and control both the pH and hardness of the water. The water is then sent to the membrane filtration system where high pressure forces the water molecules through the membranes into an inner collection tube [11]. A representative diagram of an RO system is shown in Figure 1.7.

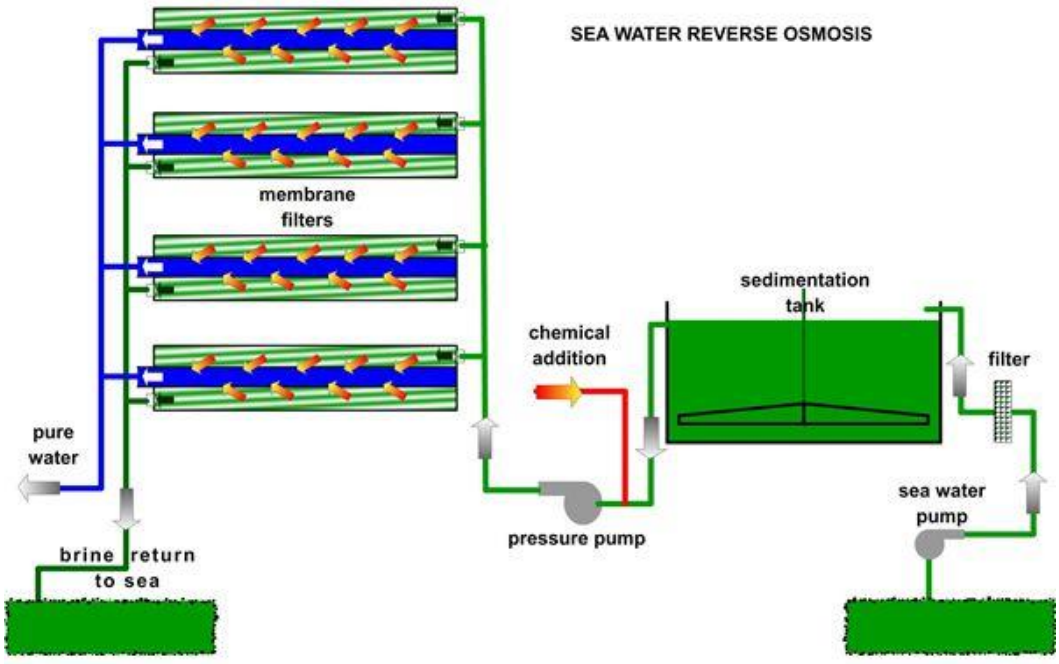

Figure 1.7: Example of a Reverse Osmosis (RO) plant [11].

MSF is a proven technology for water desalination. It is a simple and extremely reliable process that requires no moving parts other than pumps. Unfortunately, MSF is more energy intensive than current RO plants, requires a direct steam connection to the power plant, and typically runs at full capacity to limit potential system instabilities [12]. These challenges limit MSF applications when steam shedding is being used as a load leveling strategy.

Reverse Osmosis has the benefit of consuming less energy than MSF. RO also does not need a direct steam connection to the power plant as it only requires electric energy to run pumps and has simple start/stop operating capability [12]. Since RO is operated in modules, operation can be staged to take advantage of available excess energy instead of the all or nothing operation of MSF. These properties make RO a highly attractive secondary energy application for hybrid energy technologies.

1.2.2. Hydrogen Production

Excess thermal and electrical energy can be used for a wide range of alternative applications. One of the most intriguing currently is hydrogen production. The anticipated development and deployment of fuel cell technology and infrastructure into the transportation sector will create substantial additional demand for hydrogen. One of the motivations to switch to a hydrogen based infrastructure is to reduce greenhouse gas (GHG) emissions. However, significant GHG reduction will only occur if the hydrogen is produced from carbon-free sources.

Current large-scale hydrogen production is accomplished by stripping hydrocarbon fuel via steam-methane reforming [13]. In steam-methane reforming, methane reacts with steam in the presence of a catalyst to produce hydrogen and carbon monoxide. In a subsequent "water-gas shift reaction" the carbon monoxide and steam are reacted using a catalyst to produce carbon dioxide and hydrogen.

Steam methane reforming reaction:

$$CH_4 + H_2O + (\text{heat}) \rightarrow CO + 3H_2$$

Water-gas shift reaction:

$$CO + H_2O \rightarrow CO_2 + H_2 \ (+ \text{small amount of heat})$$

A byproduct of this reaction is CO_2, which does not meet the GHG reduction standards established in the Paris agreement [14], [15]. Fortunately, an alternative clean source of hydrogen, meaning zero CO_2 emissions, comes from the disassociation of water into hydrogen and oxygen via electrolysis. Currently, there are two ways of disassociating water via electrolysis: conventional (low temperature) electrolysis and High Temperature Steam Electrolysis (HTSE) [16]. HTSE is ~40% more efficient than conventional electrolysis but requires temperatures of $\sim 800^{o}C$ [16], [17]. HTSE uses approximately 79% electrical energy and 21% thermal energy [18].

A case study recently completed by NuScale [16] to establish a baseline cost for producing hydrogen via the HTSE process [16] showed that one 160MWth NuScale module could optimally produce 1,310

lb/hr of hydrogen using one matched HTSE module. The hydrogen would be 99% pure with no greenhouse gas emissions. The results of their economic analysis showed natural gas reforming to be more economical due to natural gas costs and the overall maturity of reforming technology. However, it also stated that a coupled hybrid technology plant for hydrogen production could become competitive as a result of different economic factors including increased natural gas prices, carbon emission penalties, and optimization of the HTSE process.

1.2.3. Chilled Water Production

Chilled water is used in large manufacturing facilities, college campuses, and district heating and cooling systems to satisfy cooling demands. During warmer months of the year, a large portion of a facility's electricity demand is generated from heating ventilation and air-conditioning (HVAC) equipment. Because building cooling loads regularly peak during the early to late afternoon hours, the HVAC equipment is sized to accommodate these peak loads. At night or during early morning hours when cooling loads are low, excess chiller capacity exists. Moreover, these facility cooling loads often coincide with peak electricity demands, thereby putting further strain on utilities. TES, in the form of chilled-water storage, is a way to combat peak cooling loads by shifting them from on-peak to off-peak hours [19].

Stratified chilled-water storage tanks have emerged as an effective option for storing chilled water [20]. In a stratified chilled-water storage tank, warm and cold water are stored in the same vessel with no structural interface. Instead, differences in density between cold and warm water cause a thin thermocline, or sharp temperature gradient, to form. Excess chilled water, produced when facility cooling demands are low, is deposited in the bottom of the tank via diffusers. Because the tank is a constant volume device, charging the tank with cold water means simultaneously removing warm water from the top of the tank to be sent to the chillers. Conversely, discharging the cold water to be used during times of peak facility cooling loads results in warm water being deposited in the top of the tank. Therefore, a fully charged tank implies the tank is full of chilled water, while a fully discharged tank implies the tank is full of warm water.

A previous case study examined using stratified chilled-water storage in conjunction with centrifugal electric chillers to offset cooling loads synonymous with a large office space or college campus in a NHES [21]. Results demonstrated that chilled-water storage can shift cooling loads to off-peak hours and help promote more steady-state reactor operation [21]. Another option for cooling water involves the use of single effect, lithium bromide absorption chillers, which use steam less than 205 kPa (15 psig) or hot water and the affinity between an absorbent and a refrigerant to create a chilling effect.

Absorption chillers become particularly attractive when a source of waste heat that would normally be rejected to the environment or some other low temperature sink is available. In a NHES, low-pressure steam can be diverted from waste heat reservoirs or low pressure sections of the energy conversion cycle to absorption chillers to make chilled water for facility cooling.

1.3 Region Selection

Since renewable energy tends to be highly region specific, it is important to determine the most economically feasible region in which to build a nuclear hybrid energy system. Three promising regions for deploying a nuclear hybrid energy system are presented below.

1.3.1 Southern California

The implementation of a nuclear hybrid energy system relies on three things: 1) sufficient renewable resources (wind, solar, etc.), 2) a use for the excess energy, and 3) availability of energy transmission lines to supply customers. The California Renewable Portfolio Standard set a goal of 33% of electricity generation to come from eligible renewable resources by 2020 [22]. Currently, California leads the nation in energy production from solar and biomass. As further evidence of their commitment to renewables, California recently completed construction of the world's largest solar thermal plant. The Ivanpah Solar Power Facility, located in San Bernardino County became operational on February 13, 2014 and is capable of producing upwards of 392MWe [23]. Excess energy generated during times of non-peak demand or times of high renewable output could be put to use by desalination plants or for hydrogen production.

As of February 2014, there were 17 proposed desalination plants in Southern California alone [24]. With the population density and recent extreme drought experienced in this area, the need for potable water is undeniable. Unfortunately, desalination of ocean water is an extremely energy intensive process that uses on average 15,000 kW-hr of power per million gallons of fresh water produced. This is compared to an estimated 3,300-8,300 kW-hr for potable water production by wastewater treatment [25]. The energy intensiveness of desalination creates opportunities for hybrid energy plants not only from an efficiency standpoint, but also from the environmental standpoint of little to no added carbon emissions.

By 2020 automakers expect to have thousands of hydrogen fuel cell based vehicles in California [26]. This transition to a hydrogen fuel cell based infrastructure will require hydrogen production facilities. The ability to produce hydrogen during times of low electric demand would add value to the facility.

Finally, Southern California is upgrading their grid transmission system. The recent installation of an extra 800 MW of transmission lines across southern California connecting renewable resources in southeast California to San Diego is a major step [27].

1.3.2 Southwest

Renewable energy resources in the southwest include wind, geothermal and solar photovoltaics. Arizona currently has the one of the world's largest solar photovoltaic facilities located in Yuma County, AZ completed in 2014 [28]. With further addition of photovoltaic facilities a stronger case can be made for an integrated nuclear-renewable system as the demand for grid flexibility increases.

As in Southern California, drought conditions in the southwest illustrate the need for additional sources of potable water. While current resources from the upper Colorado River Basin are sufficient, recent studies have shown this water supply to be dwindling [29]. With increasing population density and drought levels not seen in 1,250 years [29], the need for potable water is real.

The availability of transmission lines is another advantage the southwest has over other regions. Due to the possible closure of existing coal plants, the availability of existing grid infrastructure and the need for replacement generation would be conducive to installing an integrated nuclear-renewable system.

1.3.3 Agricultural Midwest

The Agricultural Midwest is considered to be the best opportunity for integrated nuclear-renewable systems at present [30]. The region has abundant wind energy supplies throughout the Great Plains. Second to Texas, Iowa is the leading producer of wind energy in the nation [31]. This, combined with the recent closures of coal fired power plants in the Midwest [32], could lead to a higher demand for renewable energy, making integrated nuclear-renewable systems more attractive.

Renewable energy technologies combined with industrial processes such as ammonia/fertilizer production lends additional benefit to these systems. During times of peak wind output or low electric demand, excess capacity could be diverted to ammonia production. An existing transmission infrastructure left over from coal plant closures also makes the Agricultural Midwest an extremely attractive option for these integrated nuclear-renewable systems.

1.4 TES System Configuration

Thermal Energy Storage (TES) systems have been proposed to store energy during periods of excess capacity and have already been employed in concentrated solar plants in the southwestern U.S. [33]. Thermal energy storage can be classified into three main types; sensible heat storage, thermochemical storage, and latent heat storage. Sensible heat storage (SHS) systems work by raising the temperature of a storage medium, usually a solid or a liquid. The storage materials undergo no change in phase over the temperature range of the storage process. A good SHS material has high heat capacity, relative molecular stability and durability over the temperature range of interest. Latent heat storage is an approximately isothermal process which takes advantage of the heat of fusion of the storage material as it changes phase. Thermochemical storage is a newer technology that relies on heat to drive reversible chemical reactions [34].

For the application proposed here, a sensible heat system was chosen. This allows for the simple bypass of steam to an intermediate heat exchanger, which transfers thermal energy to a thermal energy storage fluid. A two-tank direct system was chosen for this work. The two-tank system can accommodate molten salts or synthetic oils that are highly stable over the expected operating range of the system. Currently, the two-tank storage system is the most commercially mature technology [34].

Chapter 2 Reactor Simulator

2.1 Simulator Design

The target SMR in this work is an Integral Pressurized Water Reactor (IPWR) with operating parameters similar to those of the mPower reactor proposed by B&W [35]. Operating parameters are given in Table 2.1. IPWRs are characterized by having all major primary system components (core, steam generators, pressurizer, etc.) contained within the reactor vessel. A diagram of a typical IPWR is given in Figure 2.1.

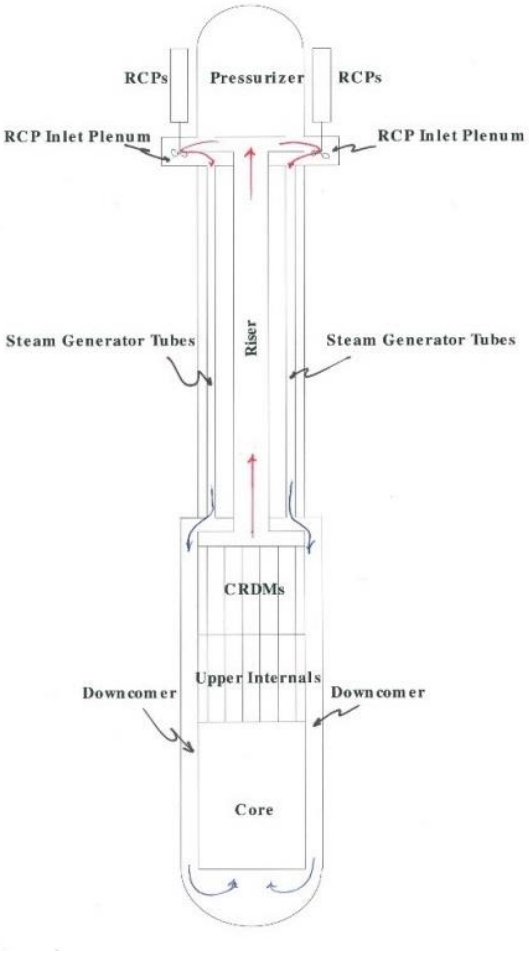

Figure 2.1: Representative Integral Pressurized Water Reactor

For the IPWR considered in this work the steam generators are a typical once through design, with steam generator pressure control via the turbine control valves (TCVs) located between the pressure equalization header and the high pressure turbine. Feed control valves modulate such that feed flow rate matches a feed demand signal that is proportional to the turbine load plus a shim that ensures

turbine output matches load. Steam generator level (boiling length) is allowed to float. In order to simulate the dynamics of an IPWR system, NCSU has developed high fidelity simulation tools for predicting the dynamic response of IPWR systems under normal and off-normal conditions [36] [37] [38] [39]. The reactor simulator is capable of simulating IPWRs operating under forced and natural circulation conditions. Additional features include: a) reactor kinetics with overlapping control rod banks, Xenon, fuel and moderator temperature feedback, b) decay heat, c) hot channel models including Critical Heat Flux and peak fuel centerline temperatures, d) pressurizer with heaters and sprays, e) conventional and helical coil Once Through Steam Generators, f) Balance of Plant and g) associated control functions. Models exist for IPWR concepts spanning a range of thermal outputs, including designs similar to the Westinghouse IRIS, B&W, mPower, and NuScale reactor concepts [35]. Primary loop nodalization is illustrated in Figure 2.2.

Table 2.1: SMR Design Parameters

Parameter	Value
Reactor Thermal Output	530 MWt
Electric Output	180 MWe
Primary System Pressure	14.134 MPa (2050 psia)
Core Inlet Temperature	296.6 °C (566 °F)
Core Exit Temperature	321.6 °C (611 °F)
Core Flow Rate	1.361 Mkg/hr (30 Mlbm/hr)
Steam Pressure	5.7 MPa (825 psia)
Steam Temperature	299.4 °C (571 °F)
Feed Temperature	212.2 °C (414 °F)
Steam Flow Rate	0.953 Mkg/hr (2.1Mlbm/hr)
Number of Tubes	7048
Tube Material	Inconel-690
Tube Inner Diameter	1.328 cm (0.523 inches)
Tube Outer Diameter	1.745 cm (0.687 inches)
Pitch	2.093 cm (0.824 inches)

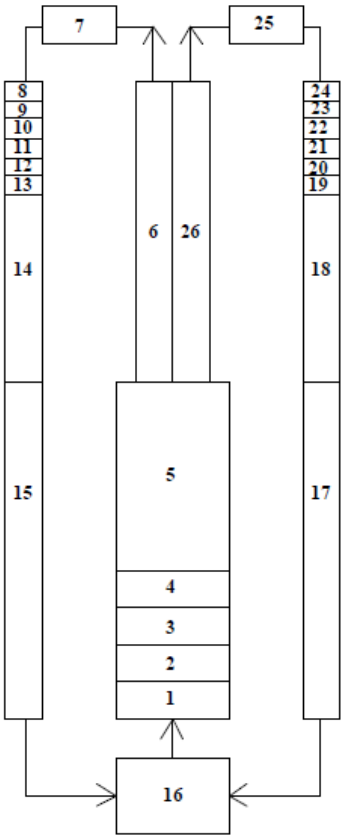

Nodes	Description
1 – 4	Reactor Core
5	Lower Riser
6, 26	Upper Riser
7, 25	RCP Inlet Plenum
8 – 13, 19 – 24	Steam Generator
14, 18	Upper Downcomer
15,17	Lower Downcomer
16	Lower Plenum

Figure 2.2: SMR Simulator Nodalization

Chapter 3 Thermal Energy Storage System

Sensible heat storage involves the heating of a solid or liquid without phase change and can be deconstructed into two operating modes: charging and discharging. A two-tank thermal energy storage system is a common configuration for liquid sensible heat systems. In the charging mode cold fluid is pumped from a cold tank through an Intermediate Heat Exchanger (IHX), heated, and stored in a hot tank while the opposite occurs in the discharge mode. Such systems have been successfully demonstrated in the solar energy field as a load management strategy [33].

3.1 Connection Point

The performance of a Thermal Energy Storage (TES) System is a strong function of the connection point to the secondary side of the IPWR. For plants incorporating Once Through Steam Generators (OTSG) the turbine control valves (TCVs) act as pressure control valves to maintain Steam Generator pressure at a given set point. Shown in Figure 3.1, Turbine Bypass Valves (TBVs) can be configured such that bypass steam can either be taken off the steam line at the pressure equalization header upstream of the turbine control valves (Aux 1), downstream of the turbine control valves prior to entering the high pressure turbine (Aux 2), or at some low pressure turbine tap (Aux 3). Steam off-take upstream of the TCVs provides approximately constant steam conditions but the system is only able to bypass ~50% nominal steam flow before losing pressure control. Should more steam flow be desired then placing the taps downstream of the TCVs is an option that has no steam flow limitation. However, steam conditions downstream of the TCVs are a strong function of the load profile. Taking bypass steam downstream of the turbine control valves can result in highly varying steam pressures and temperatures and unacceptably low IHX pressures. Further, if the TBVs are placed downstream of the TCVs then TBV operation must be uniform to maintain symmetric operation of the TCVs. For the sensible heat TES system assumed here, it is desirable to have roughly constant steam conditions since the shell side pressure in the Intermediate Heat Exchanger directly affects the TES fluid temperature leaving the IHX and ultimately stored in the hot tank. This makes taking bypass steam from the pressure equalization header upstream of the turbine control valves the preferred operating mode.

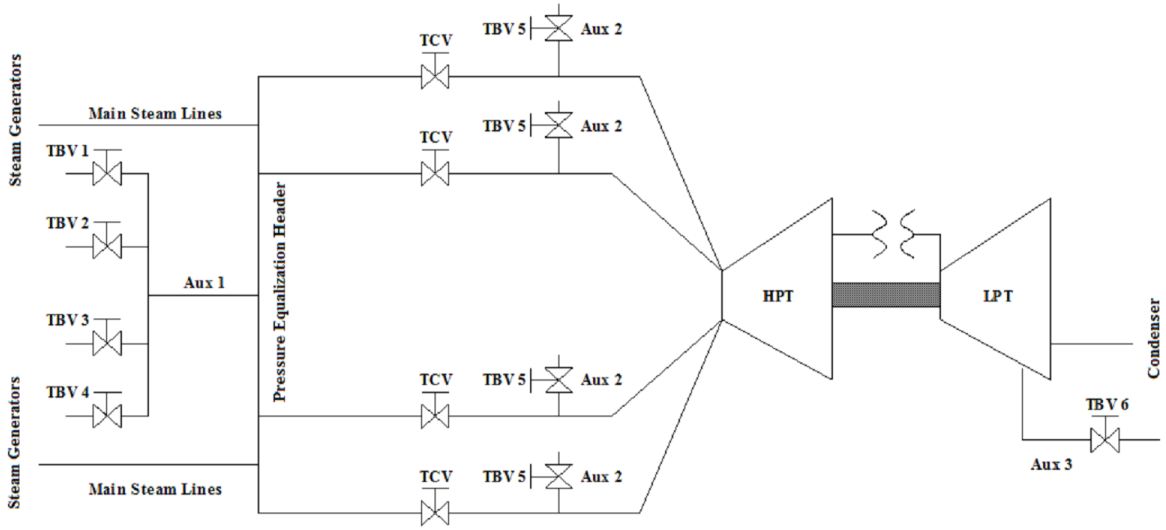

Figure 3.1: Bypass Steam Options

3.2 Charging System Design

The charging mode configuration of the proposed Thermal Energy Storage System is shown in the boxed region of Figure 3.2. An outer loop interfaces with the reactor's Balance of Plant (BOP) directly through four parallel auxiliary turbine bypass valves connected at the pressure equalization header, each staged to open at a certain percent of the maximum auxiliary flow demand. Bypass steam is directed through an intermediate heat exchanger and ultimately discharged to the main condenser. An inner loop containing a TES fluid consists of two large storage tanks along with several pumps to transport the TES fluid between the tanks, the IHX and a steam generator. Flow Bypass Valves are included in the discharge lines of both the Hot and Cold tanks to prevent deadheading the pumps when the Flow Control Valves are closed. Common TES fluid properties are given in Table 3.1. Therminol-66 is chosen as the TES fluid in this work as it is readily available, can be pumped at low temperatures, and offers thermal stability over the range (-3°C - 343°C) which covers the anticipated operating range of the TES system (203°C - 260°C). Molten salts (e.g. 48% NaNO3 – 52% KNO3) were not considered as the anticipated operating temperatures fall below their 222°C freezing temperature [40]. Other benefits of using Therminol-66 include its Material Safety Data Sheet (MSDS) classification as a nonhazardous material [41]. In addition, as hydrocarbons do not readily exchange hydrogen atoms with other materials [42], tritium migration would be mitigated in the rare event simultaneous leaks in

the steam generator and an IHX tube allowed activated primary water to mix with the TES fluid. In this event, the TES tanks would act as holding tanks for the activated water.

Table 3.1: Properties of Possible TES fluids at ~260 degrees Celsius (500 degrees Fahrenheit)

Heat Transfer Fluid	Boiling Point (°C)	Heat Storage (W*hr/m^{3}°C)	Operating Range (°C)
Therminol®-66 [43]	358 (678 °F)	1039 (576.95 W*hr/m^{3}°F)	-2.7 to 343.3 (27 °F to 650° F)
Therminol®-68 [44]	307 (586 °F)	1013 (563.03 W*hr/m^{3}°F)	-25.5 to 360 (-14 °F to 680 °F)
Therminol®-75 [45]	342 (649 °F)	992 (551.54 W*hr/m^{3}°F)	79.44 to 385 (175 °F to 725 °F)

The TES system is designed to allow the reactor to run continuously at ~100% power over a wide range of operating conditions. During periods of excess capacity, bypass steam is directed to the TES unit through the auxiliary bypass valves where it condenses on the shell side of the IHX. TES fluid is pumped from the Cold Tank to the Hot Tank through the tube side of the IHX at a rate sufficient to raise the temperature of the TES fluid to some set point. The TES fluid is then stored in the Hot Tank at constant temperature. Condensate is collected in a hot well below the IHX and drains back to the main condenser, or can be used for some other low pressure application such as chilled water production, desalination or feed-water heating. The system is discharged during periods of peak demand, or when process steam is desired, by pumping the TES fluid from the Hot Tank through a boiler (steam generator) to the Cold Tank. This process steam can then be reintroduced into the power conversion cycle for electricity production or directed to some other application through the Pressure Control Valve (PCV) at the exit of the steam dome. While the boiler in Figure 3.2 implies a Once Through Steam Generator (OTSG) design, a U-Tube design could just as easily be substituted. Pressure relief lines connect the shell side of the IHX with the condenser to prevent over pressurization of the heat exchanger during periods of low condensation rate. A nitrogen cover gas dictates the tank pressures during charging and discharging operation.

Note: Tank sizes are a direct function of the designed ΔT between the Hot Tank and Cold Tank. To achieve smaller tank sizes, increase the designed ΔT between the Cold Tank and Hot Tank.

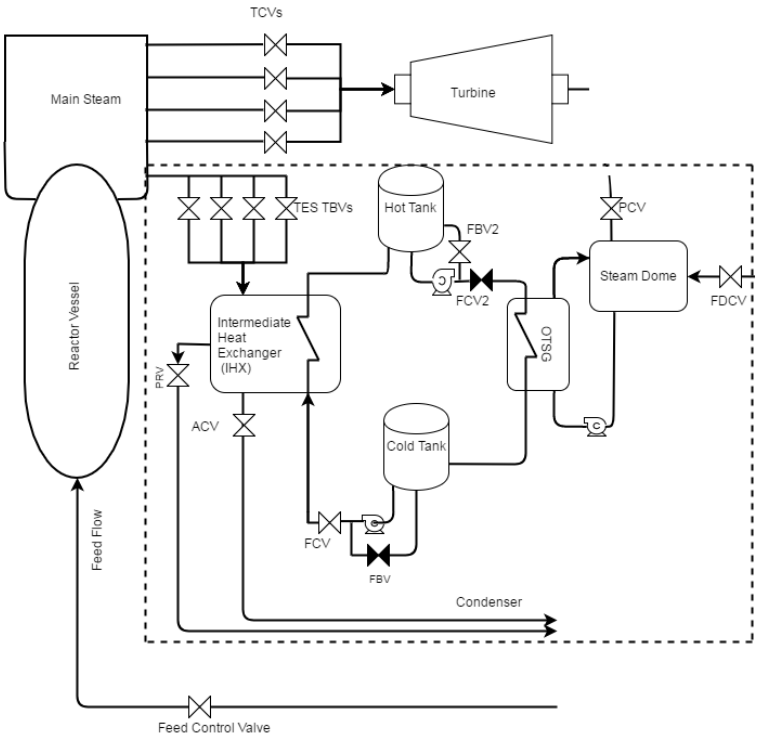

Figure 3.2: Schematic of an IPWR connected to a two-tank sensible heat thermal energy storage system, charging mode

3.2.1. Charging System Model

The time dependent behavior of the TES system is obtained by solving mass, energy and simple momentum balances on the Shell side of the IHX (Outer Loop), and the Tube side or Inner Loop.

System Equations for Shell Side (Outer Loop)

Energy Equation

$$V_{IHX}\frac{d(\rho u)}{dt}=\sum_{n}\dot{m}_{TBV_n}h_{SG}-\dot{m}_{IHX}h_f-\sum_{m}\dot{m}_{PRV_m}h_{IHX}-\dot{Q}_{IHX} \tag{3.1}$$

For n=1,2,…,n_{tbv} and m=1,2,…,$m_{prv.}$

Mass Equation

$$V_{IHX}\frac{d\rho}{dt}=\sum_{n}\dot{m}_{TBV_n}-\dot{m}_{IHX}-\sum_{m}\dot{m}_{PRV_m} \tag{3.2}$$

Momentum Equations

$$P_{HDR} = P_{IHX} + \frac{\left(K_{TBVline} + K_{TBV_n}\right)\dot{m}^2_{TBV_n}}{2A^2_{TBV_n}\rho_g} \tag{3.3}$$

$$P_{IHX} = P_{Cond} + \frac{\left(K_{ACVline} + K_{ACV}\right)\dot{m}^2_{IHX}}{2A^2_{ACV}\rho_f} \tag{3.4}$$

$$P_{IHX} = P_{Cond} + \frac{\left(K_{PRVline} + K_{PRV_m}\right)\dot{m}^2_{PRV_m}}{2A^2_{PRV_m}\rho_g} \tag{3.5}$$

State Equations

$$\rho = \alpha_l\rho_l + \alpha_g\rho_g \tag{3.6}$$

$$\rho u = \alpha_l\rho_l u_l + \alpha_g\rho_g u_g \tag{3.7}$$

Equations for tube side (Inner Loop) charging mode

Hot Tank Mass Balance

$$\frac{dM_{HT}}{dt} = \dot{m}_{TES} = \rho_{TES}A_{HT}\frac{dH_{HT}}{dt} \tag{3.8}$$

Cold Tank Mass Balance

$$\frac{dM_{CT}}{dt} = -\dot{m}_{TES} = \rho_{TES}A_{CT}\frac{dH_{CT}}{dt} \tag{3.9}$$

Momentum Equation

$$P_{CT} + \Delta P_{pump} = P_{HT} + \frac{\left(K_{FCV} + K_{FCVline}\right)\dot{m}^2_{TES}}{2A^2_{FCV}\rho_{TES}} \tag{3.10}$$

Hot tank energy balance

$$M_{HT}c_p\frac{dT_{HT}}{dt} = \dot{m}_{TES}c_pT_{IHX_{Exit}} - (UA)_{HT}\left(T_{HT} - T_{Amb}\right) \tag{3.11}$$

Hot Tank Pressure

$$P_{HT} = \rho_{HT}RT_{HT} \tag{3.12}$$

Cold Tank Pressure

$$P_{CT} = \rho_{CT} R T_{CT} \tag{3.13}$$

The heat transfer rate from equation (3.1) can be written as

$$\dot{Q}_{IHX} = (UA)_{IHX} \left(T_{sat} - \bar{T}_{TES} \right) \tag{3.14}$$

where $\bar{T}_{TES}$ is the average TES fluid temperature within the IHX. To obtain the average TES temperature we solve a simple energy balance on the fluid.

$$\dot{m}_{TES} c_p \frac{dT_{TES}}{dz} = (UP_w)_{IHX} \left(T_{sat} - T_{TES} \right)$$

$$\frac{dT_{TES}}{dz} = \frac{(UP_w)_{IHX}}{\dot{m}_{TES} c_p} \left(T_{sat} - T_{TES} \right) \Rightarrow \frac{dT_{TES}}{dz} = \frac{\beta}{L} \left(T_{sat} - T_{TES} \right)$$

where, $\beta = \dfrac{(UA)_{IHX}}{\dot{m}_{TES} c_p}$

$$\frac{dT_{TES}}{dz} + \frac{\beta}{L} T_{TES} = \frac{\beta}{L} T_{sat}$$

$$T_{TES}(\mathrm{z})\, \mathrm{e}^{\frac{\beta z}{L}} = T_{c_1} + \int_0^z \frac{\beta}{L} T_{sat} e^{\frac{\beta z'}{L}} dz' \Rightarrow T_{TES}(\mathrm{z})\, \mathrm{e}^{\frac{\beta z}{L}} = T_{c_1} + T_{sat} e^{\frac{\beta z'}{L}} \Big|_0^z$$

$$T_{TES}(\mathrm{z}) = T_{c_1}\, \mathrm{e}^{-\frac{\beta z}{L}} + T_{sat} \left\{ 1 - \mathrm{e}^{-\frac{\beta z}{L}} \right\} \tag{3.15}$$

Now defining $\bar{T}_{TES}$ as

$$\bar{T}_{TES} = \frac{1}{L} \int_0^L T_{TES}(\mathrm{z}) dz$$

where the TES fluid temperature is from equation (3.15)

$$\bar{T}_{TES} = \frac{1}{L} \int_0^L T_{c_1}\, \mathrm{e}^{-\frac{\beta z}{L}} dz + T_{sat} - \frac{T_{sat}}{L} \int_0^L \mathrm{e}^{-\frac{\beta z}{L}} dz$$

$$\bar{T}_{TES} = T_{sat} + \frac{\left(T_{sat} - T_{c_1}\right)}{L}\int_0^L \mathrm{e}^{-\frac{\beta z}{L}}\, dz$$

$$\bar{T}_{TES} = T_{sat} + \frac{\left(T_{sat} - T_{c_1}\right)}{L}\left(\frac{L}{\beta}\right)e^{-\frac{\beta z}{L}}\Bigg|_0^L$$

Rearranging gives the final equation.

$$\bar{T}_{TES} = T_{sat} - \frac{\left(T_{sat} - T_{c_1}\right)}{\beta}\left\{1 - e^{-\beta}\right\} \tag{3.16}$$

Further, the determination of Q_{IHX} requires the UA value

$$UA_{IHX} = \frac{2\pi nL}{\frac{1}{h_i r_i} + \frac{1}{k}\ln\left(\frac{r_o}{r_i}\right) + \frac{1}{h_o r_o}} \tag{3.17}$$

where an average condensation heat transfer coefficient is assumed for the shell side of the form,

$$h_o = h_{cond}\left(T_w\right) = 0.725\left[\frac{\rho_f\left(\rho_f - \rho_g\right)g h_{fg}^{'} k_f^3}{\mu_f d\left(T_{sat} - T_w\right)}\right]^{\frac{1}{4}} \tag{3.18}$$

$$h_{fg}^{'} = h_{fg}\left[1 + \frac{0.68 c_{p_f}\left(T_{sat} - T_w\right)}{h_{fg}}\right]$$

and T_w satisfies

$$h_{cond}\left(T_w\right) r_o\left(T_{sat} - T_w\right) = \left\{\frac{1}{k}\ln\left(\frac{r_o}{r_i}\right) + \frac{1}{h_i r_i}\right\}^{-1}\left(T_w - T_{c_{avg}}\right)$$

$$T_{c_{avg}} = \frac{T_{c_1} + T_{IHX_{exit}}}{2}$$

$$h_i = \frac{k_{TES} Nu_i}{De_{IHX}} \tag{3.19}$$

$$Nu_i = \max\left[0.023\,\mathrm{Re}^{0.8}\,\mathrm{Pr}^{0.4}, 4.66\right] \tag{3.20}$$

In the equations above, n = number of tubes, r_i = tube inner radius, r_o = tube outer radius, k = tube thermal conductivity, L= tube length, and d = tube outer diameter, and T_{C_1} = inlet temperature from cold tank. Equation (3.20) ensures non-zero heat transfer coefficients during periods of zero or very low TES flow rates.

3.2.2. Charging System Solution strategy

The TES system model requires solving a system of nonlinear equations. The solution method is outlined below.

Shell Side of IHX

A semi-implicit time discretization is chosen for the shell side equations of the form

Energy Equation

$$V_{IHX}\left\{\frac{\rho u^{t+\Delta t}-\rho u^{t}}{\Delta t}\right\}=\sum_{n}\dot{m}_{TBV_n}^{t+\Delta t}h_{SG}^{t}-\dot{m}_{IHX}^{t+\Delta t}h_{f}^{t}-\sum_{m}\dot{m}_{PRV_m}^{t+\Delta t}h_{IHX}^{t}-\dot{Q}_{IHX}^{t} \tag{3.21}$$

For n=1,2,…,n_{tbv} and m=1,2,…,$m_{prv.}$

Mass Equation

$$V_{IHX}\left\{\frac{\rho^{t+\Delta t}-\rho^{t}}{\Delta t}\right\}=\sum_{n}\dot{m}_{TBV_n}^{t+\Delta t}-\dot{m}_{IHX}^{t+\Delta t}-\sum_{m}\dot{m}_{PRV_m}^{t+\Delta t} \tag{3.22}$$

Momentum Equations

$$P_{HDR}^{t+\Delta t}=P_{IHX}^{t+\Delta t}+\frac{\left(K_{TBVline}+K_{TBV_n}\right)\left(\dot{m}_{TBV_n}^{2}\right)^{t+\Delta t}}{2A_{TBV_n}^{2}\rho_g} \tag{3.23}$$

$$P_{IHX}^{t+\Delta t}=P_{Cond}^{t+\Delta t}+\frac{\left(K_{ACVline}+K_{ACV}\right)\left(\dot{m}_{IHX}^{2}\right)^{t+\Delta t}}{2A_{ACV}^{2}\rho_f} \tag{3.24}$$

$$P_{IHX}^{t+\Delta t}=P_{Cond}^{t+\Delta t}+\frac{\left(K_{PRVline}+K_{PRV_m}\right)\left(\dot{m}_{PRV_m}^{2}\right)^{t+\Delta t}}{2A_{PRV_m}^{2}\rho_g} \tag{3.25}$$

State Equations

$$\rho^{t+\Delta t}=\alpha_l^{t+\Delta t}\rho_l^{t+\Delta t}+\alpha_g^{t+\Delta t}\rho_g^{t+\Delta t} \tag{3.26}$$

$$\rho u^{t+\Delta t} = \alpha_l^{t+\Delta t}\rho_l^{t+\Delta t}u_l^{t+\Delta t} + \alpha_g^{t+\Delta t}\rho_g^{t+\Delta t}u_g^{t+\Delta t} \tag{3.27}$$

These equations are nonlinear in the new time values. Applying a Newton-Iteration yields the following linear equations in the new iterate (k +1) values.

Energy Equation

$$V_{IHX}\left\{\frac{\rho u^{k+1} - \rho u^{t}}{\Delta t}\right\} = \sum_n \dot{m}_{TBV_n}^{k+1} h_{SG}^{t} - \dot{m}_{IHX}^{k+1} h_f^{t} - \sum_m \dot{m}_{PRV_m}^{k+1} h_{IHX}^{t} - \dot{Q}_{IHX}^{t} \tag{3.28}$$

For n=1,2,…,n_{tbv} and m=1,2,…,$m_{prv.}$

Mass Equation

$$V_{IHX}\left\{\frac{\rho^{k+1} - \rho^{t}}{\Delta t}\right\} = \sum_n \dot{m}_{TBV_n}^{k+1} - \dot{m}_{IHX}^{k+1} - \sum_m \dot{m}_{PRV_m}^{k+1} \tag{3.29}$$

Momentum Equations

$$P_{HDR}^{t+\Delta t} = P_{IHX}^{k+1} + \frac{\left(K_{TBVline} + K_{TBV_n}\right)}{2A_{TBV_n}^2\rho_g^{t}}\left(2\dot{m}_{TBVn}^{k+1} - \dot{m}_{TBn}^{k}\right)\dot{m}_{TBn}^{k} \tag{3.30}$$

$$P_{IHX}^{k+1} = P_{Cond}^{t+\Delta t} + \frac{\left(K_{ACVline} + K_{ACV}\right)}{2A_{ACV}^2\rho_f^{t}}\left(2\dot{m}_{IHX}^{k+1} - \dot{m}_{IHX}^{k}\right)\dot{m}_{IHX}^{k} \tag{3.31}$$

$$P_{IHX}^{k+1} = P_{Cond}^{t+\Delta t} + \frac{\left(K_{PRVline} + K_{PRV_m}\right)}{2A_{PRV_m}^2\rho_g^{t}}\left(2\dot{m}_{PRVm}^{k+1} - \dot{m}_{PRVm}^{k}\right)\dot{m}_{PRVm}^{k} \tag{3.32}$$

State Equations

$$\tilde{\rho}^{k} = \rho\left(\alpha_g^{k}, P_{IHX}^{k}\right) = \rho_f\left(P_{IHX}^{k}\right) + \alpha_g^{k}\left[\rho_g\left(P_{IHX}^{k}\right) - \rho_f\left(P_{IHX}^{k}\right)\right] \tag{3.33}$$

$$\rho u^{k} = \rho u\left(\alpha_g^{k}, P_{IHX}^{k}\right) = \rho_f\left(P_{IHX}^{k}\right)u_f\left(P_{IHX}^{k}\right) + \alpha_g^{k}\left[\rho_g\left(P_{IHX}^{k}\right)u_g\left(P_{IHX}^{k}\right) - \rho_f\left(P_{IHX}^{k}\right)u_f\left(P_{IHX}^{k}\right)\right] \tag{3.34}$$

$$\rho^{k+1} = \tilde{\rho}^{k} + \delta\alpha_g\left.\frac{\partial\rho}{\partial\alpha_g}\right|_k + \delta P_{IHX}\left.\frac{\partial\rho}{\partial P}\right|_k \tag{3.35}$$

$$\rho u^{k+1} = \rho u^{k} + \delta\alpha_g\left.\frac{\partial\rho u}{\partial\alpha_g}\right|_k + \delta P_{IHX}\left.\frac{\partial\rho u}{\partial P}\right|_k \tag{3.36}$$

Equations (3.28)-(3.36) can be reduced to a 4x4 matrix providing solutions for $\rho^{k+1}, \rho u^{k+1}, \delta\alpha_g, \mathrm{P}_{IHX}^{k+1}$. From these variables direct solves for the mass flows can be performed. The equations are iterated to

convergence based on the maximum relative difference for any single variable between iterations. The converged values become the solution for the new time values.

Tube Side Equations:

Tube side Energy Equation

$$V_{IHX}\rho_{TES}c_{p_{TES}}\left\{\frac{T_{IHX_{exit}}^{t+\Delta t}-T_{IHX_{exit}}^{t}}{\Delta t}\right\}+\dot{m}_{TES}^{t+\Delta t}c_{p_{TES}}\left\{T_{IHX_{exit}}^{t+\Delta t}-T_{C_1}\right\}=\dot{Q}_{IHX}^{t+\Delta t} \tag{3.37}$$

$$\dot{Q}_{IHX}^{t+\Delta t}=(UA)_{IHX}^{t}\left(T_{sat}-\bar{T}_{TES}^{t+\Delta t}\right) \tag{3.38}$$

$$\bar{T}_{TES}^{t+\Delta t}=T_{sat_{IHX}}-\frac{\left(T_{sat_{IHX}}-T_{c_1}\right)}{\beta}\left\{1-e^{-\beta}\right\},\quad \beta=\frac{(UA)_{IHX}^{t}}{\dot{m}_{TES}^{t+\Delta t}c_{p_{TES}}} \tag{3.39}$$

Hot Tank Mass Balance

$$\dot{m}_{TES}^{t+\Delta t}=\rho_{TES}A_{HT}\left\{\frac{H_{HT}^{t+\Delta t}-H_{HT}^{t}}{\Delta t}\right\} \tag{3.40}$$

Cold Tank Mass Balance

$$-\dot{m}_{TES}^{t+\Delta t}=\rho_{TES}A_{CT}\left\{\frac{H_{CT}^{t+\Delta t}-H_{CT}^{t}}{\Delta t}\right\} \tag{3.41}$$

Momentum Equation

$$P_{CT}^{t+\Delta t}+\Delta P_{pump}=P_{HT}^{t+\Delta t}+\frac{K_{FCV}^{t}\left(\dot{m}_{TES}^{t+\Delta t}\right)^2}{2A_{FCV}^{2}\rho_{TES}} \tag{3.42}$$

Hot tank energy balance

$$M_{HT}^{t}c_p\left\{\frac{T_{HT}^{t+\Delta t}-T_{HT}^{t}}{\Delta t}\right\}=\dot{m}_{TES}^{t+\Delta t}c_{p_{TES}}\left(T_{IHX_{Exit}}^{t+\Delta t}-T_{HT}^{t+\Delta t}\right)-(UA)_{HT}^{t}\left(T_{HT}^{t+\Delta t}-T_{Amb}\right) \tag{3.43}$$

Hot Tank Cover Gas

$$\rho_{HT}^{t+\Delta t}=\frac{M_{\text{Fillgas}_{\text{HT}}}^{o}}{A_{HT}\left(\text{Tank}_{\text{Height}}\text{-H}_{\text{HT}}^{\text{t+}\Delta\text{t}}\right)} \tag{3.44}$$

Cold Tank Cover Gas

$$\rho_{CT}^{t+\Delta t} = \frac{M^{o}_{\text{Fillgas}_{\text{CT}}}}{A_{CT}\left(\text{Tank}_{\text{Height}}\text{-H}_{\text{CT}}^{\text{t+}\Delta\text{t}}\right)} \tag{3.45}$$

Hot Tank Pressure (State Equation)

$$P_{HT}^{t+\Delta t} = \rho_{HT}^{t+\Delta t} R T_{HT}^{t+\Delta t} \tag{3.46}$$

Cold Tank Pressure (State Equation)

$$P_{CT}^{t+\Delta t} = \rho_{CT}^{t+\Delta t} R T_{CT}^{t} \tag{3.47}$$

Note: For the charging mode, cold tank temperature is assumed at past time. Conversely, in the discharge mode hot tank temperature is assumed at past time.

The tube side equations also form a non-linear system that must be solved iteratively. A general Newton-Raphson iteration for this system had poor convergence characteristics due to the stiffness of the system. As an alternate approach, the equations were cast as a single non-linear equation in the TES flow rate that could be solved iteratively by Brent's algorithm [46]. This provides for a much more robust search.

Tube side nonlinear search strategy:

For a given guess at the new iterate flow rate $\dot{m}_{TES}^{k+1}$, the tube side equations are solved in the following order:

Average TES fluid temperature

$$\bar{T}_{TES}^{k+1} = T_{sat_{IHX}} - \frac{\left(T_{sat_{IHX}} - T_{c_1}\right)}{\beta}\left\{1 - e^{-\beta}\right\}, \quad \beta = \frac{\left(UA\right)_{IHX}^{t}}{\dot{m}_{TES}^{k+1} c_{p_{TES}}} \tag{3.48}$$

Energy equation inside tubes

$$T_{IHX_{Exit}}^{k+1} = \frac{UA_{IHX}\left(T_{sat_{IHX}} - \bar{T}_{TES}^{k+1}\right) + \dot{m}_{TES}^{k+1} c_{p_{TES}} T_{CT} + \dfrac{V_{inner} c_{p_{TES}} \rho_{TES} T_{IHX_{Exit}}^{t}}{\Delta t}}{\dot{m}_{TES}^{k+1} c_{p_{TES}} + \dfrac{V_{inner} c_{p_{TES}} \rho_{TES}}{\Delta t}} \tag{3.49}$$

Hot tank energy equation

$$T_{HT}^{k+1} = \frac{\frac{M_{HT}^{t} c_{p_{TES}} T_{HT}^{t}}{\Delta t} + \dot{m}_{TES}^{k+1} c_{p_{TES}} T_{IHX_{Exit}}^{k+1} + UA_{HT}^{t} T_{Amb}}{\dot{m}_{TES}^{k+1} c_{p_{TES}} + (UA)_{HT}^{t} + \frac{M_{HT}^{t} c_{p_{TES}}}{\Delta t}} \tag{3.50}$$

Hot tank height

$$H_{HT}^{k+1} = \frac{\dot{m}_{TES}^{k+1} \Delta t}{\rho_{TES} A_{HT}} + H_{HT}^{t} \tag{3.51}$$

Cold tank height

$$H_{CT}^{k+1} = \frac{-\dot{m}_{TES}^{k+1} \Delta t}{\rho_{TES} A_{CT}} + H_{CT}^{t} \tag{3.52}$$

Hot tank density

$$\rho_{HT}^{k+1} = \frac{M_{\text{Fillgas}_{\text{HT}}}^{o}}{A_{HT}\left(\text{Tank}_{\text{Height}} - \text{H}_{\text{HT}}^{k+1}\right)} \tag{3.53}$$

Cold tank density

$$\rho_{CT}^{k+1} = \frac{M_{\text{Fillgas}_{\text{CT}}}^{o}}{A_{CT}\left(\text{Tank}_{\text{Height}} - \text{H}_{\text{CT}}^{k+1}\right)} \tag{3.54}$$

Hot tank pressure

$$P_{HT}^{k+1} = \rho_{HT}^{k+1} R T_{HT}^{k+1} \tag{3.55}$$

Cold tank pressure

$$P_{CT}^{k+1} = \rho_{CT}^{k+1} R T_{CT}^{t} \tag{3.56}$$

The momentum equation is used to determine how closely the equations are satisfied with the guess value of $\dot{m}_{TES}^{k+1}$

$$P_{CT}^{k+1} + \Delta P_{pump} - P_{HT}^{k+1} - \frac{K_{FCV}^{t}\left(\dot{m}_{TES}^{2}\right)^{k+1}}{2A_{FCV}^{2}\rho_{TES}} = error \tag{3.57}$$

When the error is within some specified tolerance the (k+1) iteration values become new time (t+Δt) values. Otherwise, a new guess value for $\dot{m}_{TES}^{k+1}$ is chosen according to Brent's algorithm.

For this algorithm it is necessary to bound the possible solution. To do this we consider the natural solution for the mass flow rate.

$$\dot{m}_{TES}^{t+\Delta t} = \sqrt{\frac{2\rho_{TES}\left(P_{CT}^{t+\Delta t} + \Delta P_{pump} - P_{HT}^{t+\Delta t}\right)}{K_{FCV} / A_{FCV}^2}} \tag{3.58}$$

The minimum flow possible is when the pressure of the cold tank is 0 psi. Likewise, the maximum possible flow is when pressure in the hot tank is 0 psi. Using the past time pressures as estimates of the new time values, gives an estimate of the bounds for the new time flow rate.

$$\dot{m}_{TES}^{t+\Delta t}\Big|_{\min} \approx \sqrt{\frac{2\rho_{TES}\left(\Delta P_{pump} - P_{HT}^{t}\right)}{K_{FCV} / A_{FCV}^2}} \tag{3.59}$$

$$\dot{m}_{TES}^{t+\Delta t}\Big|_{\max} \approx \sqrt{\frac{2\rho_{TES}\left(P_{CT}^{t} + \Delta P_{pump}\right)}{K_{FCV} / A_{FCV}^2}} \tag{3.60}$$

The nonlinear solver then does a number line search on a value of m_{TES}^{k+1} such that all of the equations associated with the tube side are satisfied. Once this value has been determined, m_{TES}^{k+1} is the solution for $m_{TES}^{t+\Delta t}$. This value is directly substituted into the tube side equations to determine $T_{IHX_{Exit}}^{t+\Delta t}, T_{HT}^{t+\Delta t}, H_{HT}^{t+\Delta t}, H_{CT}^{t+\Delta t}, \rho_{HT}^{t+\Delta t}, \rho_{CT}^{t+\Delta t}, \mathrm{P}_{HT}^{t+\Delta t}, \mathrm{P}_{CT}^{t+\Delta t}, Q_{IHX}^{t+\Delta t}, \overline{\mathrm{T}}_{TES}^{t+\Delta t}$.

A schematic of the Thermal Energy System solution strategy is illustrated in Figure 3.3.

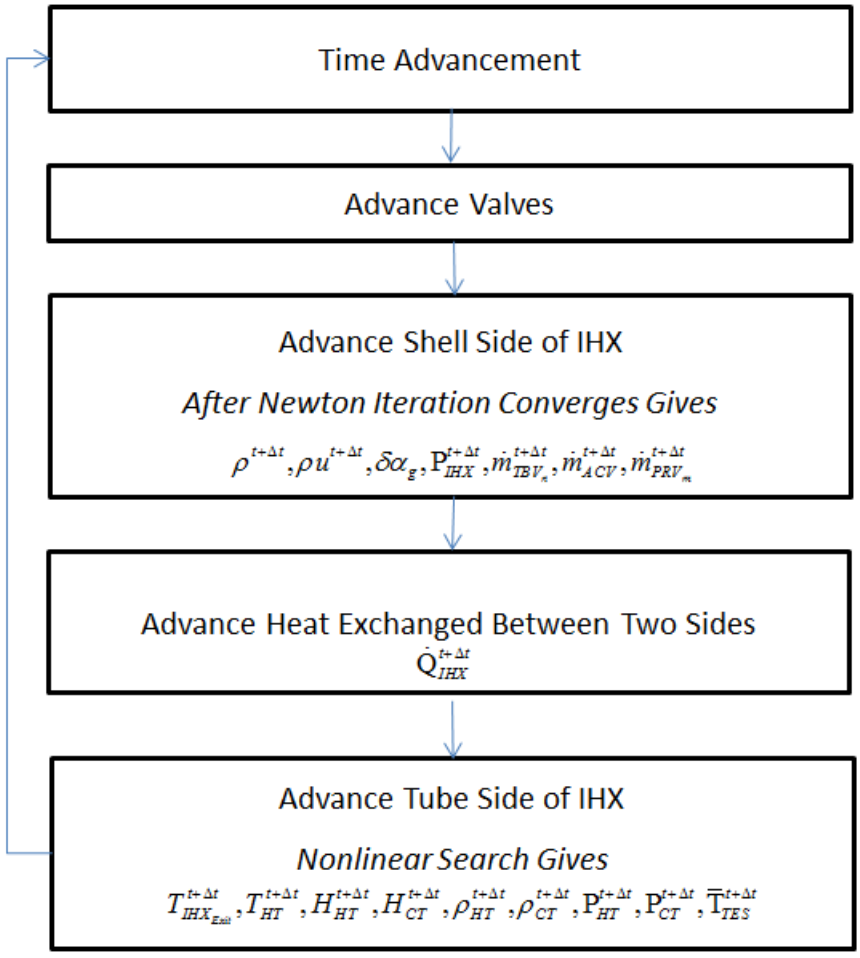

Figure 3.3: Thermal Energy Storage System Time Advancement Scheme (Charging Mode)

3.2.3. Charging System Control

The TES system has four sets of valves used to control system parameters: auxiliary bypass valves, the TES flow control valve, the auxiliary control valve, and pressure relief valves.

The goal of the bypass flow controller is to provide bypass steam to the TES system at a rate sufficient to maintain the reactor at or near its nominal steady state value. The bypass valve controller generates an error signal based on the difference between measured bypass flow and a bypass flow demand signal. The bypass demand signal assumes the required bypass flow is proportional to the relative difference between the nominal full power turbine output and the instantaneous electric load plus a correction term (shim). The shim term modifies the demand signal such that reactor power is kept approximately constant.

$$Signal_{TBV} = \frac{\dot{m}_{Bypass_{Demand}}}{\dot{m}_{Bypass_{\mathrm{Ref}}}} - \frac{\dot{m}_{Bypass}}{\dot{m}_{Bypass_{\mathrm{Ref}}}} \tag{3.61}$$

$$\dot{m}_{Bypass_{Demand}} = \dot{m}_{\mathrm{nominal}} \frac{W_{Fullpower} - W_{load}}{W_{load}} + Shim_{TES} \tag{3.62}$$

$$Shim_{TES}^{t+\Delta t} = Shim_{TES}^{t} + \frac{K_{Shim}\dot{m}_{\mathrm{nominal}}\left(Q_{Rx_{ref}} - Q_{Rx}\right)\Delta t}{Q_{Rx_{ref}}} \tag{3.63}$$

Flow from the cold tank to the hot tank is via a TES flow control valve. The TES flow control valve operates off a three element controller where the first error signal is designed to maintain the TES fluid temperature leaving the Intermediate Heat Exchanger at some reference value. The second error signal is designed to roughly match the heat input into the TES fluid with the heat bypassed to the IHX

$$Signal_{FCV} = G_1 Error_1 + G_2 Error_2 \tag{3.64}$$

$$Error_1 = \frac{T_{IHX_{Exit}} - T_{IHX_{Exitref}}}{T_{IHX_{Exitref}}} \tag{3.65}$$

$$\begin{aligned} Error_2 &= \frac{\dot{m}_{Bypass}}{\dot{m}_{Bypass_{\mathrm{Ref}}}} - \frac{\dot{m}_{TES}}{\dot{m}_{TES_{\mathrm{Ref}}}} \\ \dot{m}_{TES_{\mathrm{Ref}}} &= \frac{\dot{m}_{Bypass_{\mathrm{Ref}}}\left(h_{Steam} - h_f(\mathrm{P}_{IHX})\right)}{c_{p_{TES}}\left(T_{IHX_{\mathrm{Ref}}} - T_{CT}\right)} \end{aligned} \tag{3.66}$$

where $\dot{m}_{Bypass_{\mathrm{Ref}}}$ is the reference design bypass flow rate for the IHX.

The auxiliary control valve (ACV) maintains IHX hot well level. This valve operates on a three element controller based on the level of the IHX and the difference in mass flows into and out of the IHX as shown in equations (3.67)-(3.69) where G_1 and G_2 are error weighting gains. Gains were selected to allow for smooth operation of the ACV over foreseeable operating bands.

$$\mathrm{Signal}_{\mathrm{ACV}} = G_1 E_1 + G_2 E_2 \tag{3.67}$$

$$E_1 = \mathrm{Level\text{-}Level}_{\mathrm{Ref}} \tag{3.68}$$

$$E_2 = \dot{m}_{\mathrm{bypass}} - \dot{m}_{\mathrm{ACV}} \tag{3.69}$$

Pressure relief valves (PRV's) have been installed in the IHX to mitigate pressure increases. Should pressure reach an upper set point the valves will open and will not close until the pressure falls below a lower set point.

$$Signal_{PRV} = \frac{P_{IHX} - P_{IHX_{\text{Setpoint}}}}{P_{IHX_{\text{Setpoint}}}} \tag{3.70}$$

The only parameters directly controlled during charging mode operation of the TES system are the IHX exit temperature on the inner loop and the level in the IHX. All other variables including IHX pressure, tank levels, inner loop mass flow rate, and heat transfer across the IHX are determined from the mass, energy and momentum balances on the system.

A stop valve (not shown) is placed in the flow line between the cold tank and hot tank to ensure tank pressure and level stay below designated set points. Should either the pressure or level set points be exceeded the stop valve will close and TES fluid flow between the tanks will cease. A redundant control on level is that the volume of TES fluid in the system is less than the total volume of either tank.

3.3 Discharge System Design

Additional models are required to simulate discharge mode operation where energy is recovered by flowing the TES fluid from the hot tank, through a boiler, and back to the cold tank. For the configuration assumed here, the TES fluid flows through the tube side of a Once Through Steam Generator (OTSG) producing a saturated liquid-vapor mixture. This two-phase mixture flows to a steam dome where the steam dome will separate the gas and liquid phases and reintroduce the saturated steam into either the energy conversion cycle for electrical peaking or some industrial steam process. For electrical peaking, steam will be reintroduced prior to the moisture separator before entering the low pressure turbine. This allows the streams from the steam dome and high pressure turbine to combine and eliminate any moisture that may be present prior entering the low pressure turbine.

A schematic of the proposed discharge mode operation can be seen in Figure 3.4.

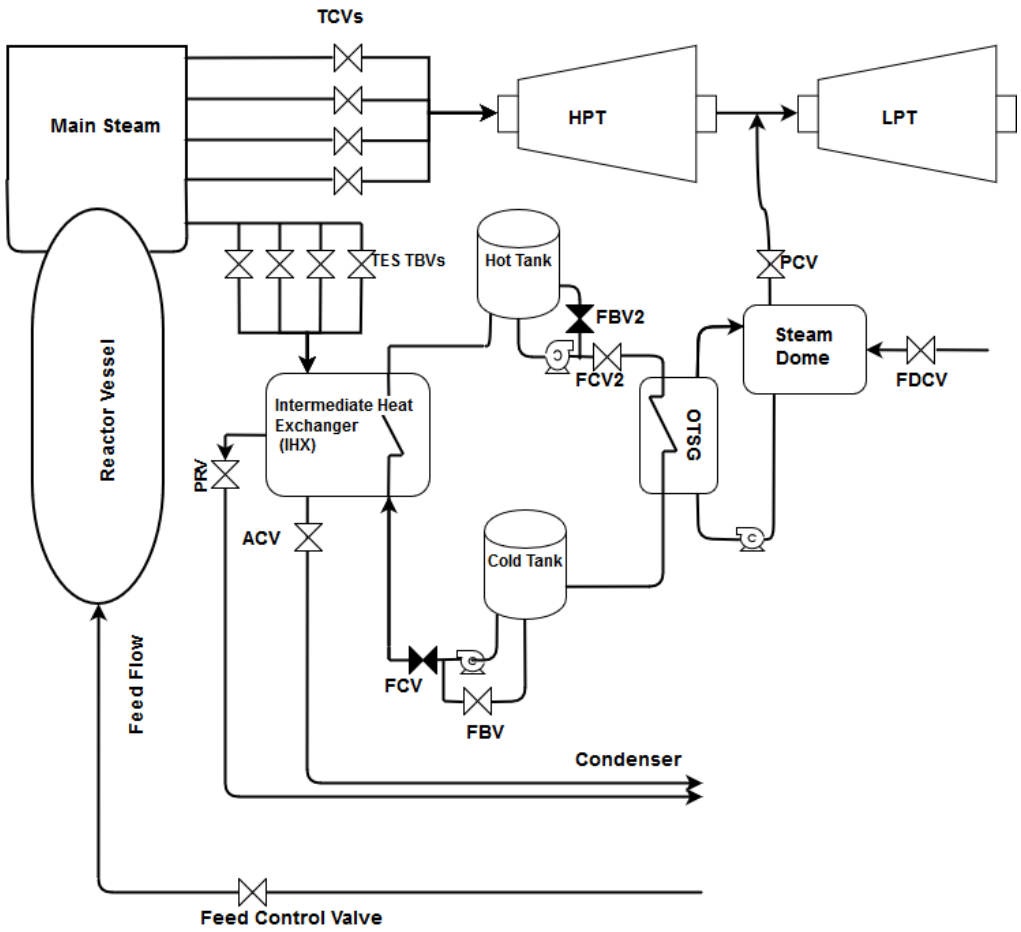

Figure 3.4: TES Discharge Mode Configuration

3.3.1. Discharge System Model

A three equation Global Compressibility Model is assumed for the shell side of the steam generator, where thermodynamic equilibrium is assumed between the phases. The steam dome model assumes the vapor region is saturated and the liquid region is subcooled. A pump is used to provide approximately constant flow between the steam dome and steam generator.

<u>OTSG (Shell Side) Equation Set</u>

Mass

$$V_{SG}\left\{\frac{d\rho}{dt}\right\}+\rho_{exit}v_{exit}A_{SG_{Exit}}-\rho_{inlet}v_{inlet}A_{SG_{inlet}}=0 \qquad (3.71)$$

Energy

$$V_{SG}\left\{\frac{d(\rho u)}{dt}\right\}+\left(\rho u\right)_{Exit} v_{exit}A_{SG_{Exit}}-\left(\rho u\right)_{inlet} v_{inlet}A_{SG_{inlet}}=$$
$$-P_{SG}\left\{v_{Exit}A_{SG_{Exit}}-v_{inlet}A_{SG_{Inlet}}\right\}+q_{SG}-\left\{\frac{\alpha_l\alpha_g\rho_f\rho_g}{\rho}\left(u_{fg}+P_{SG}v_{fg}\right)v_rA_{xSG}\right\}_{inlet}^{exit} \quad (3.72)$$

State Equations

$$\rho=\rho_l(u_l,P) \text{ or } \rho=\alpha_l\rho_l+\alpha_g\rho_g \quad (3.73)$$

$$\rho u=\rho(u_l,P)u_l \text{ or } \rho u=\alpha_l\rho_lu_l+\alpha_g\rho_gu_g \quad (3.74)$$

Steam Dome Equation Set

Liquid Mass

$$V_{SD}\left\{\frac{d\left(\alpha_l\rho_l\right)}{dt}\right\}=\rho_{FD}v_{FD}A_{FD}+\alpha_{lSG}\rho_fv_{SG}A_{xSG}$$
$$-\rho_{lSD}v_{FCV}A_{FCV}-\left.\frac{\alpha_l\alpha_g\rho_f\rho_gv_r}{\rho}\right|_{SG}A_{xSG} \quad (3.75)$$

Total Mass

$$V_{SD}\left\{\frac{d\rho_{SD}}{dt}\right\}=\rho_{FD}v_{FD}A_{FD}+\rho_{SG}v_{SG}A_{xSG}-\rho_{lSD}v_{FCV}A_{FCV}-\rho_gv_gA_{Steamline} \quad (3.76)$$

Total Energy

$$V_{SD}\left\{\frac{d\left(\rho u\right)_{SD}}{dt}\right\}=\left(\rho_{FD}u_{FD}+P_{SD}\right)\ v_{FD}A_{FD}+\left(\rho u_{SG}+P_{SD}\right)\ v_{SG}A_{xSG}$$
$$-\left(\rho_lu_{lSD}+P_{SD}\right)\ v_{FCV}A_{FCV}-\left(\rho_gu_g+P_{SD}\right)\ v_gA_{Steamline} \quad (3.77)$$
$$+\left\{\frac{\alpha_l\alpha_g\rho_f\rho_g}{\rho}\left(u_{fg}+P_{SD}v_{fg}\right)\ v_rA_{xSG}\right\}_{SG}$$

State Equations

$$\left(\alpha_l \rho_l\right)_{SD} = \alpha_{lSD} \rho_l(u_{lSD}, P_{SD}) \tag{3.78}$$

$$\rho_{SD} = \alpha_l \rho_l(u_{lSD}, P_{SD}) + \alpha_g \rho_g(P_{SD}) \tag{3.79}$$

$$\rho u_{SD} = \alpha_l \rho_l(u_{lSD}, P_{SD}) u_{lSD} + \alpha_g \rho_g(P_{SD}) u_g \tag{3.80}$$

Momentum Equations

$$P_{SD} + \Delta P_{pFCV} = P_{SG} + \rho_{lSD}\left(K_{FCVLine}\right)\frac{\left(v_{FCV}\right)^2}{2} \tag{3.81}$$

$$P_{SD} = P_{LPT} + \rho_{lSD}\left(K_{PCV} + K_{PCVLine}\right)\frac{\left(v_g\right)^2}{2} \tag{3.82}$$

$$P_{cond} + \Delta P_{pFD} = P_{SD} + \rho_{lcond}\left(K_{FDCV} + K_{FDCVLine}\right)\frac{\left(v_{FD}\right)^2}{2} \tag{3.83}$$

$$P_{SG} = P_{SD} + \rho_{SG}\left(K_{SG}\right)\frac{\left(v_{SG}\right)^2}{2} \tag{3.84}$$

Equations for tube side (Inner Loop) discharge mode

Hot Tank Mass Balance

$$\frac{dM_{HT}}{dt} = -\dot{m}_{TES} = \rho_{TES} A_{HT} \frac{dH_{HT}}{dt} \tag{3.85}$$

Cold Tank Mass Balance

$$\frac{dM_{CT}}{dt} = \dot{m}_{TES} = \rho_{TES} A_{CT} \frac{dH_{CT}}{dt} \tag{3.86}$$

Momentum Equation

$$P_{HT} + \Delta P_{pump2} = P_{CT} + \frac{\left(K_{FCV2} + K_{FCV2line}\right)\dot{m}_{TES}^2}{2A_{FCV2}^2 \rho_{TES}} \tag{3.87}$$

Cold tank energy balance

$$M_{CT} c_p \frac{dT_{CT}}{dt} = \dot{m}_{TES} c_p T_{OTSG_{Exit}} - (UA)_{CT} \left(T_{CT} - T_{Amb} \right) \tag{3.88}$$

Hot Tank Pressure

$$P_{HT} = \rho_{HT} R T_{HT} \tag{3.89}$$

Cold Tank Pressure

$$P_{CT} = \rho_{CT} R T_{CT} \tag{3.90}$$

3.3.2. Solution strategy

The TES discharge system model requires solving a system of nonlinear equations. The solution method is outlined below.

Shell Side of discharge model

A semi-implicit time discretization is chosen for the shell side equations of the form shown below with "n" nodes.

OTSG (Shell Side) Equation Set

Mass

$$V_j \left\{ \frac{\rho_j^{t+\Delta t} - \rho_j^t}{\Delta t} \right\} + \rho_{j+1/2}^t v_{j+1/2}^{t+\Delta t} A_{j+1/2} - \rho_{j-1/2}^t v_{j-1/2}^{t+\Delta t} A_{j-1/2} = 0 \tag{3.91}$$

Energy

$$\begin{aligned} &V_j \left\{ \frac{\rho u_j^{t+\Delta t} - \rho u_j^t}{\Delta t} \right\} + \rho u_{j+1/2}^t v_{j+1/2}^{t+\Delta t} A_{j+1/2} - \rho u_{j-1/2}^t v_{j-1/2}^{t+\Delta t} A_{j-1/2} = \\ &-P^t \left\{ v_{j+1/2}^{t+\Delta t} A_{j+1/2} - v_{j-1/2}^{t+\Delta t} A_{j-1/2} \right\} + q_j^t - \left\{ \frac{\alpha_l \alpha_g \rho_f \rho_g}{\rho} \left(u_{fg} + P_{SG} \nu_{fg} \right) v_r A_{xSG} \right\}_{j-1/2}^{j+1/2,t} \end{aligned} \tag{3.92}$$

State Equations

$$\rho^{t+\Delta t} = \rho(u_l^{t+\Delta t}, P^{t+\Delta t}) \quad \text{or} \quad \rho^{t+\Delta t} = \alpha_l^{t+\Delta t} \rho_l^{t+\Delta t} + \alpha_g^{t+\Delta t} \rho_g^{t+\Delta t} \tag{3.93}$$

$$\rho u^{t+\Delta t} = \rho(u_l^{t+\Delta t}, P^{t+\Delta t}) u_l^{t+\Delta t} \quad \text{or} \quad \rho u^{t+\Delta t} = \alpha_l^{t+\Delta t} \rho_l^{t+\Delta t} u_l^{t+\Delta t} + \alpha_g^{t+\Delta t} \rho_g^{t+\Delta t} u_g^{t+\Delta t} \tag{3.94}$$

Steam Dome Equation Set

Liquid Mass

$$V_{SD}\left\{\frac{\left(\alpha_l\rho_l\right)^{t+\Delta t}-\left(\alpha_l\rho_l\right)^{t}}{\Delta t}\right\}=\rho_{FD}^{t}v_{FD}^{t+\Delta t}A_{FD}+\alpha_{lSG}^{t}\rho_f^{t}v_{SG}^{t+\Delta t}A_{xSG}$$
$$-\rho_{lSD}^{t}v_{FCV}^{t+\Delta t}A_{FCV}-\frac{\alpha_l\alpha_g\rho_f\rho_g v_r}{\rho}\Bigg|_{SG}^{t}A_{xSG} \tag{3.95}$$

Total Mass

$$V_{SD}\left\{\frac{\rho_{SD}^{t+\Delta t}-\rho_{SD}^{t}}{\Delta t}\right\}=\rho_{FD}^{t}v_{FD}^{t+\Delta t}A_{FD}+\rho_{SG}^{t}v_{SG}^{t+\Delta t}A_{xSG}-\rho_{lSD}^{t}v_{FCV}^{t+\Delta t}A_{FCV}-\rho_g^{t}v_g^{t+\Delta t}A_{Steamline} \tag{3.96}$$

Total Energy

$$V_{SD}\left\{\frac{\rho u_{SD}^{t+\Delta t}-\rho u_{SD}^{t}}{\Delta t}\right\}=\left(\rho_{FD}u_{FD}+P_{SD}\right)^{t}v_{FD}^{t+\Delta t}A_{FD}+\left(\rho u_{SG}+P_{SD}\right)^{t}v_{SG}^{t+\Delta t}A_{xSG}$$
$$-\left(\rho_l u_{lSD}+P_{SD}\right)^{t}v_{FCV}^{t+\Delta t}A_{FCV}-\left(\rho_g u_g+P_{SD}\right)^{t}v_g^{t+\Delta t}A_{Steamline} \tag{3.97}$$
$$+\left\{\frac{\alpha_l\alpha_g\rho_f\rho_g}{\rho}\left(u_{fg}+P_{SD}v_{fg}\right)^{t}v_r A_{xSG}\right\}_{SG}^{t}$$

State Equations

$$\left(\alpha_l\rho_l\right)_{SD}^{t+\Delta t}=\alpha_{lSD}^{t+\Delta t}\rho_l(u_{lSD}^{t+\Delta t},P_{SD}^{t+\Delta t}) \tag{3.98}$$

$$\rho_{SD}^{t+\Delta t}=\alpha_{lSD}^{t+\Delta t}\rho_l(u_{lSD}^{t+\Delta t},P_{SD}^{t+\Delta t})+\alpha_g^{t+\Delta t}\rho_g(P_{SD}^{t+\Delta t}) \tag{3.99}$$

$$\left(\rho u_{SD}\right)^{t+\Delta t}=\alpha_{lSD}^{t+\Delta t}\rho_l(u_{lSD}^{t+\Delta t},P_{SD}^{t+\Delta t})u_{lSD}^{t+\Delta t}+\alpha_g^{t+\Delta t}\rho_g(P_{SD}^{t+\Delta t})u_g^{t+\Delta t} \tag{3.100}$$

Momentum Equations

$$P_{SD}^{k+1}+\Delta P_{pFCV}=P_{SG}^{k+1}+\frac{\rho_{lSD}^{t}\left(K_{FCVLine}\right)\left(v_{FCV}^{t+\Delta t}\right)^2}{2} \tag{3.101}$$

$$P_{SD}^{t+\Delta t}=P_{LPT}^{t+\Delta t}+\rho_{lSD}^{t}\left(K_{PCV}^{t}+K_{PCVLine}\right)\frac{\left(v_g^{t+\Delta t}\right)^2}{2} \tag{3.102}$$

$$P_{cond} + \Delta P_{pFD} = P_{SD}^{t+\Delta t} + \rho_{lcond}^{t}\left(K_{FDCV}^{t} + K_{FDCVLine}\right)\frac{\left(v_{FD}^{t+\Delta t}\right)^2}{2} \tag{3.103}$$

$$P_{SG}^{t+\Delta t} = P_{SD}^{t+\Delta t} + \rho_{SG}^{t}\left(K_{SG}\right)\frac{\left(v_{SG}^{t+\Delta t}\right)^2}{2} \tag{3.104}$$

These equations are nonlinear in the new time values. Applying a Newton-Iteration yields the following linear equations in the new iterate (k +1) values.

OTSG (Shell Side) Equation Set

Mass

$$V_j\left\{\frac{\rho_j^{k+1} - \rho_j^{t}}{\Delta t}\right\} + \rho_{j+1/2}^{t} v_{j+1/2}^{k+1} A_{j+1/2} - \rho_{j-1/2}^{t} v_{j-1/2}^{k+1} A_{j-1/2} = 0 \tag{3.105}$$

Energy

$$\begin{aligned} &V_j\left\{\frac{\rho u_j^{k+1} - \rho u_j^{t}}{\Delta t}\right\} + \rho u_{j+1/2}^{t} v_{j+1/2}^{k+1} A_{j+1/2} - \rho u_{j-1/2}^{t} v_{j-1/2}^{k+1} A_{j-1/2} = \\ &-P^{t}\left\{v_{j+1/2}^{k+1} A_{j+1/2} - v_{j-1/2}^{k+1} A_{j-1/2}\right\} + q_j^{t} - \left\{\frac{\alpha_l \alpha_g \rho_f \rho_g}{\rho}\left(u_{fg} + P_{SG} v_{fg}\right) v_r A_{xSG}\right\}_{j-1/2}^{j+1/2,t} \end{aligned} \tag{3.106}$$

State Equations

If the node is subcooled the state equations are

$$\rho^{k} = \rho_l(u_j^{k}, P_{SG}^{k}) \tag{3.107}$$

$$\rho u^{k} = \rho_l(u_j^{k}, P_{SG}^{k}) u_j^{k} \tag{3.108}$$

$$\rho^{k+1} = \tilde{\rho}^{k} + \delta u_j \left.\frac{\partial \rho}{\partial u_l}\right|_k + \delta P_{SG} \left.\frac{\partial \rho}{\partial P}\right|_k \tag{3.109}$$

$$\rho u^{k+1} = \rho u^{k} + \delta u_j \left.\frac{\partial (\rho u)}{\partial u_l}\right|_k + \delta P_{SG} \left.\frac{\partial (\rho u)}{\partial P}\right|_k \tag{3.110}$$

If the node is two phase the state equations become

$$\tilde{\rho}^{k} = \rho\left(\alpha_g^{k}, P_{SG}^{k}\right) = \rho_f\left(P_{SG}^{k}\right) + \alpha_g^{k}\left[\rho_g\left(P_{SG}^{k}\right) - \rho_f\left(P_{SG}^{k}\right)\right] \tag{3.111}$$

$$\rho u^{k} = \rho u\left(\alpha_g^{k}, P_{SG}^{k}\right) = \rho_f\left(P_{SG}^{k}\right) u_f\left(P_{SG}^{k}\right) + \alpha_g^{k}\left[\rho_g\left(P_{SG}^{k}\right) u_g\left(P_{SG}^{k}\right) - \rho_f\left(P_{SG}^{k}\right) u_f\left(P_{SG}^{k}\right)\right] \tag{3.112}$$

$$\rho^{k+1} = \tilde{\rho}^{k} + \delta\alpha_g \left.\frac{\partial\rho}{\partial\alpha_g}\right|_k + \delta P_{SG} \left.\frac{\partial\rho}{\partial P}\right|_k \tag{3.113}$$

$$\rho u^{k+1} = \rho u^{k} + \delta\alpha_g \left.\frac{\partial\rho u}{\partial\alpha_g}\right|_k + \delta P_{SG} \left.\frac{\partial\rho u}{\partial P}\right|_k \tag{3.114}$$

Steam Dome Equation Set

Liquid Mass

$$\begin{aligned} V_{SD}\left\{\frac{(\alpha_l\rho_l)^{k+1} - (\alpha_l\rho_l)^{t}}{\Delta t}\right\} &= \rho_{FD}^{t} v_{FD}^{k+1} A_{FD} + \alpha_{lSG}^{t}\rho_f^{t} v_{SG}^{k+1} A_{xSG} \\ -\rho_{lSD}^{t} v_{FCV}^{k+1} A_{FCV} &- \left.\frac{\alpha_l\alpha_g\rho_f\rho_g v_r}{\rho}\right|_{SG}^{t} A_{xSG} \end{aligned} \tag{3.115}$$

Total Mass

$$V_{SD}\left\{\frac{\rho_{SD}^{k+1} - \rho_{SD}^{t}}{\Delta t}\right\} = \rho_{FD}^{t} v_{FD}^{k+1} A_{FD} + \rho_{SG}^{t} v_{SG}^{k+1} A_{xSG} - \rho_{lSD}^{t} v_{FCV}^{k+1} A_{FCV} - \rho_g^{t} v_g^{k+1} A_{Steamline} \tag{3.116}$$

Total Energy

$$\begin{aligned} V_{SD}\left\{\frac{\rho u_{SD}^{k+1} - \rho u_{SD}^{t}}{\Delta t}\right\} &= \left(\rho_{FD}u_{FD} + P_{SD}\right)^{t} v_{FD}^{k+1} A_{FD} + \left(\rho u_{SG} + P_{SD}\right)^{t} v_{SG}^{k+1} A_{xSG} \\ -\left(\rho_l u_{lSD} + P_{SD}\right)^{t} v_{FCV}^{k+1} A_{FCV} &- \left(\rho_g u_g + P_{SD}\right)^{t} v_g^{k+1} A_{Steamline} \\ + \left\{\frac{\alpha_l\alpha_g\rho_f\rho_g}{\rho}\left(u_{fg} + P_{SD}\nu_{fg}\right)^{t} v_r A_{xSG}\right\}_{SG}^{t} & \end{aligned} \tag{3.117}$$

State Equations

$$\left(\alpha_l\rho_l\right)_{SD}^{k} = \alpha_l^{k}\rho_l(u_{lSD}^{k}, P_{SD}^{k}) \tag{3.118}$$

$$\left(\alpha_l\rho_l\right)_{SD}^{k+1} = \left(\alpha_l\rho_l\right)_{SD}^{k} + \delta\alpha_g \left.\frac{\partial\left(\alpha_l\rho_l\right)}{\partial\alpha_g}\right|_k + \delta P_{SD} \left.\frac{\partial\left(\alpha_l\rho_l\right)}{\partial P}\right|_k + \delta u_{lSD} \left.\frac{\partial\left(\alpha_l\rho_l\right)}{\partial u_l}\right|_k \tag{3.119}$$

$$\rho_{SD}^{k} = \alpha_{gSD}^{k}\rho_g\left(P_{SD}^{k}\right) + \alpha_{lSD}^{k}\rho_l(u_{lSD}^{k}, P_{SD}^{k}) \tag{3.120}$$

$$\rho_{SD}^{k+1} = \rho_{SD}^{k} + \delta\alpha_g \left.\frac{\partial\rho}{\partial\alpha_g}\right|_k + \delta P_{SD} \left.\frac{\partial\rho}{\partial P}\right|_k + \delta u_{lSD} \left.\frac{\partial\rho}{\partial u_l}\right|_k \tag{3.121}$$

$$\rho u_{SD}^{k} = \alpha_{gSD}^{k}\rho_g\left(P_{SD}^{k}\right)u_g\left(P_{SD}^{k}\right) + \alpha_{lSD}^{k}\rho_l(u_{lSD}^{k}, P_{SD}^{k})u_{lSD}^{k} \tag{3.122}$$

$$\rho u_{SD}^{k+1} = \rho u_{SD}^{k} + \delta\alpha_g \left.\frac{\partial(\rho u)}{\partial\alpha_g}\right|_k + \delta P_{SD} \left.\frac{\partial(\rho u)}{\partial P}\right|_k + \delta u_{lSD} \left.\frac{\partial(\rho u)}{\partial u_l}\right|_k \tag{3.123}$$

Momentum Equations

$$P_{SD}^{k+1} + \Delta P_{pFCV} = P_{SG}^{k+1} + \frac{\rho_{lSD}^{t}\left(K_{FCVLine}\right)\left(2v_{FCV}^{k+1} - v_{FCV}^{k}\right)\left|v_{FCV}^{k}\right|}{2} \tag{3.124}$$

$$P_{SD}^{k+1} = P_{LPT}^{t+\Delta t} + \rho_{lSD}^{t}\left(K_{PCV}^{t} + K_{PCVLine}\right)\frac{\left(2v_g^{k+1} - v_g^{k}\right)\left|v_g^{k}\right|}{2} \tag{3.125}$$

$$P_{cond}^{t+\Delta t} + \Delta P_{pFD} = P_{SD}^{k+1} + \rho_{lcond}^{t}\left(K_{FDCV}^{t} + K_{FDCVLine}\right)\frac{\left(2v_{FD}^{k+1} - v_{FD}^{k}\right)\left|v_{FD}^{k}\right|}{2} \tag{3.126}$$

$$P_{SG}^{k+1} = P_{SD}^{k+1} + \rho_{SG}^{t}\left(K_{SG}\right)\frac{\left(2v_{SG}^{k+1} - v_{SG}^{k}\right)\left|v_{SG}^{k}\right|}{2} \tag{3.127}$$

Using the Newton-Iteration scheme, equations (4.1)-(4.14) can be reduced to a (n+2) x (n+2) matrix providing solutions for the new iterate (k+1) values $v_{FCV}^{k+1}, v_{1+1/2,\ldots,}^{k+1} v_{j+1/2}^{k+1}, v_{SG}^{k+1}, P_{SG}^{k+1}, P_{SD}^{k+1}$, where n is the number of steam generator nodes. The remaining new iterate values can be obtained directly by back substitution. The equations are iterated to convergence based on the maximum relative difference for any single variable between iterations. The converged values become the solution for the new time values.

Tube Side Equations

Tube Side Energy Equation

$$V_j\rho_{TES}c_{pTES}\left\{\frac{T_j^{t+\Delta t} - T_j^{t}}{\Delta t}\right\} + \dot{m}_{TES}^{t+\Delta t}c_{pTES}\left(T_j^{t+\Delta t} - T_{j-1}^{t+\Delta t}\right) = -\dot{q}_j^{t+\Delta t} \tag{3.128}$$

$$\dot{q}_j^{t+\Delta t} = (UA)_j^t \left(T_j^{t+\Delta t} - T_{SGj}^t\right) \tag{3.129}$$

Rearranging

$$T_j^{t+\Delta t} = \frac{\frac{V_j \rho_{TES} c_{pTES}}{\Delta t} T_j^t + (UA)_j^t T_{SG_j}^t + \dot{m}_{TES}^{t+\Delta t} c_{pTES} T_{j-1}^{t+\Delta t}}{\frac{V_j \rho_{TES} c_{pTES}}{\Delta t} + (UA)_j^t + \dot{m}_{TES}^{t+\Delta t} c_{pTES}} \tag{3.130}$$

For node 1, $T_{j-1} = T_{HT}$

Hot Tank Mass Balance

$$-\dot{m}_{TES}^{t+\Delta t} = \rho_{TES} A_{HT} \left\{ \frac{H_{HT}^{t+\Delta t} - H_{HT}^t}{\Delta t} \right\} \tag{3.131}$$

Cold Tank Mass Balance

$$\dot{m}_{TES}^{t+\Delta t} = \rho_{TES} A_{CT} \left\{ \frac{H_{CT}^{t+\Delta t} - H_{CT}^t}{\Delta t} \right\} \tag{3.132}$$

Momentum Equation

$$P_{HT}^{t+\Delta t} + \Delta P_{pump2} = P_{CT}^{t+\Delta t} + \frac{K_{FCV2}^t \left(\dot{m}_{TES}^{t+\Delta t}\right)^2}{2 A_{FCV2}^2 \rho_{TES}} \tag{3.133}$$

Cold tank energy balance

$$M_{CT}^t c_p \left\{ \frac{T_{CT}^{t+\Delta t} - T_{CT}^t}{\Delta t} \right\} = \dot{m}_{TES}^{t+\Delta t} c_{p_{TES}} \left(T_{OTSG_{Exit}}^{t+\Delta t} - T_{CT}^{t+\Delta t}\right) - (UA)_{CT}^t \left(T_{CT}^{t+\Delta t} - T_{Amb}\right) \tag{3.134}$$

Hot Tank Cover Gas

$$\rho_{HT}^{t+\Delta t} = \frac{M_{\text{Fillgas}_{\text{HT}}}^o}{A_{HT} \left(\text{Tank}_{\text{Height}} - \text{H}_{\text{HT}}^{\text{t+\Delta t}}\right)} \tag{3.135}$$

Cold Tank Cover Gas

$$\rho_{CT}^{t+\Delta t} = \frac{M_{\text{Fillgas}_{\text{CT}}}^o}{A_{CT} \left(\text{Tank}_{\text{Height}} - \text{H}_{\text{CT}}^{\text{t+\Delta t}}\right)} \tag{3.136}$$

Hot Tank Pressure (State Equation)

$$P_{HT}^{t+\Delta t} = \rho_{HT}^{t+\Delta t} R T_{HT}^{t+\Delta t} \tag{3.137}$$

Cold Tank Pressure (State Equation)

$$P_{CT}^{t+\Delta t} = \rho_{CT}^{t+\Delta t} R T_{CT}^t \tag{3.138}$$

The tube side equations also form a non-linear system that must be solved iteratively. Similar to the solution strategy during charging mode operation, the equations were cast as a single non-linear equation in the TES flow rate that could be solved iteratively by Brent's algorithm [46]. This provides for a much more robust search.

Tube side nonlinear search strategy:

Guess $\dot{m}_{TES}^{k+1}$ and solve the tube side equations in the following order

$$T_j^{k+1} = \frac{\frac{V_j \rho_{TES} c_{pTES}}{\Delta t} T_j^t + (UA)_j^t T_{SG_j}^t + \dot{m}_{TES}^{k+1} c_{pTES} T_{j-1}^{k+1}}{\frac{V_j \rho_{TES} c_{pTES}}{\Delta t} + (UA)_j^t + \dot{m}_{TES}^{k+1} c_{pTES}} \tag{3.139}$$

For node 1, $T_{j-1} = T_{HT}$

Cold tank energy

$$T_{CT}^{k+1} = \frac{\frac{M_{CT}^t c_{p_{TES}} T_{CT}^t}{\Delta t} + \dot{m}_{TES}^{k+1} c_{p_{TES}} T_{OTSG_{Exit}}^{k+1} + UA_{CT}^t T_{Amb}}{\dot{m}_{TES}^{k+1} c_{p_{TES}} + (UA)_{CT}^t + \frac{M_{CT}^t c_{p_{TES}}}{\Delta t}} \tag{3.140}$$

Hot tank height

$$H_{HT}^{k+1} = \frac{-\dot{m}_{TES}^{k+1} \Delta t}{\rho_{TES} A_{HT}} + H_{HT}^t \tag{3.141}$$

Cold tank height

$$H_{CT}^{k+1} = \frac{\dot{m}_{TES}^{k+1} \Delta t}{\rho_{TES} A_{CT}} + H_{CT}^t \tag{3.142}$$

Hot tank density

$$\rho_{HT}^{k+1} = \frac{M_{\text{Fillgas}_{\text{HT}}}^o}{A_{HT}\left(\text{Tank}_{\text{Height}} - \text{H}_{\text{HT}}^{k+1}\right)} \tag{3.143}$$

Cold tank density

$$\rho_{CT}^{k+1} = \frac{M_{\text{Fillgas}_{\text{CT}}}^o}{A_{CT}\left(\text{Tank}_{\text{Height}} - \text{H}_{\text{CT}}^{k+1}\right)} \tag{3.144}$$

Hot tank pressure

$$P_{HT}^{k+1} = \rho_{HT}^{k+1} R T_{HT}^{k+1} \tag{3.145}$$

Cold tank pressure

$$P_{CT}^{k+1} = \rho_{CT}^{k+1} R T_{CT}^{t} \tag{3.146}$$

The momentum equation is used to determine how closely the equations are satisfied with the guess value of $\dot{m}_{TES}^{k+1}$

$$P_{HT}^{k+1} + \Delta P_{pump2} - P_{CT}^{k+1} - \frac{K_{FCV}^{t} \left(\dot{m}_{TES}^{2} \right)^{k+1}}{2 A_{FCV2}^{2} \rho_{TES}} = error \tag{3.147}$$

When the error is within some specified tolerance the (k+1) iteration values become new time (t+Δt) values. Otherwise, a new guess value for $\dot{m}_{TES}^{k+1}$ is chosen according to Brent's algorithm.

For this algorithm it is necessary to bound the possible solution. To do this we consider the natural solution for the mass flow rate.

$$\dot{m}_{TES}^{t+\Delta t} = \sqrt{\frac{2\rho_{TES} \left(P_{HT}^{t+\Delta t} + \Delta P_{pump2} - P_{CT}^{t+\Delta t} \right)}{K_{FCV} / A_{FCV2}^{2}}} \tag{3.148}$$

The minimum flow possible is when the pressure of the hot tank is 0 psi. Likewise, the maximum possible flow is when pressure in the cold tank is 0 psi. Using the past time pressures as estimates of the new time values, gives an estimate of the bounds for the new time flow rate.

$$\dot{m}_{TES}^{t+\Delta t}\Big|_{\min} \approx \sqrt{\frac{2\rho_{TES} \left(\Delta P_{pump2} - P_{CT}^{t} \right)}{K_{FCV} / A_{FCV2}^{2}}} \tag{3.149}$$

$$\dot{m}_{TES}^{t+\Delta t}\Big|_{\max} \approx \sqrt{\frac{2\rho_{TES} \left(P_{HT}^{t} + \Delta P_{pump2} \right)}{K_{FCV} / A_{FCV2}^{2}}} \tag{3.150}$$

The nonlinear solver then does a number line search on a value of m_{TES}^{k+1} such that all of the equations associated with the tube side are satisfied. Once this value has been determined, m_{TES}^{k+1} is the solution for $m_{TES}^{t+\Delta t}$. This value is directly substituted into the tube side equations to determine the values at new time.

3.3.3. Control

The discharge mode can be operated in two different modes. It can operate either as an electrical peaking unit to supplement the electric grid during times of high demand, or it can be used as a source of steam for ancillary industrial applications. Both modes are considered, each with its' own set of control algorithms.

3.3.3.1. Electrical Peaking Unit

The electrical peaking unit control strategy assumes three control valves. A Pressure Control Valve (PCV) on the steam dome to ensure constant pressure steam conditions in the steam generator, a Feed Control Valve to allow for level control within the steam dome and a Flow Control Valve on the tube side of the steam generator to regulate the amount of TES flow from the hot tank to the cold tank. Feed control is based on a standard three element controller where the error signals are level and steam flow/feed flow mismatch. The TES flow control assumes the TES flow required is proportional to relative demand of the maximum design TES flow plus a correction term (shim). The shim term modifies the demand signal such that the instantaneous electric load is met.

$$Signal_{FCV2} = \frac{\dot{m}_{TES2demand} - \dot{m}_{TES}}{m_{TES2ref}} \tag{3.151}$$

$$\dot{m}_{TES2demand} = \dot{m}_{TES2ref}\left(\frac{\dot{W}_{\text{target}}}{\dot{W}_{\text{Peaking}_{Max}}}\right) + \dot{m}_{TES_{shim}} \tag{3.152}$$

$$\dot{m}_{TES_{shim}}^{t+\Delta t} = \dot{m}_{TES_{shim}}^{t} + \frac{K_{TES_{Shim}}\dot{m}_{TES_{ref}}\left(\dot{W}_{\text{target}} - \dot{W}_{\text{discharge}}\right)\Delta t}{\dot{W}_{\text{Peaking}_{Max}}} \tag{3.153}$$

During times of discharge the reactor power is held constant by changing the feed demand on the main system feed control valve that modulates flow through the main steam generator.

$$Feed_{demand} = Flow_{SG_{\text{Nominal}}} + Feed_{Shim} \tag{3.154}$$

$$Feed_{Shim}^{t+\Delta t} = Feed_{Shim}^{t} + \frac{K_{Shim}Flow_{SG_{\text{Nominal}}}\left(Q_{\text{Ref}} - Q_{th}\right)\Delta t}{Q_{\text{Ref}}} \tag{3.155}$$

This modification allows the reactor to remain at approximately 100 percent power while the thermal energy storage system matches the demand of the turbine.

3.3.3.2. Industrial Steam Production

As when configured as an electrical peaking unit, the control strategy for industrial steam production also assumes three control valves. A Pressure Control Valve (PCV) on the steam dome ensures constant pressure steam conditions in the steam generator, a Feed Control Valve allows for level control within the steam dome and a Flow Control Valve on the tube side of the steam generator regulates the amount of TES flow from the hot tank to the cold tank. Feed control is based on a standard three element controller where the error signals are steam dome level and steam flow/feed flow mismatch. The TES flow control assumes the TES flow required is proportional to the maximum design TES flow plus a correction term (shim). The shim term modifies the demand signal such that the instantaneous steam demand is met.

$$Signal_{FCV2} = \frac{\dot{m}_{TES2demand} - \dot{m}_{TES}}{m_{TES2ref}} \tag{3.156}$$

$$\dot{m}_{TES2demand} = \dot{m}_{TES2ref}\left(\frac{\dot{m}_{\text{Steamtarget}}}{\dot{m}_{\text{Steampeakref}}}\right) + \dot{m}_{TES_{shim}} \tag{3.157}$$

$$\dot{m}_{TES_{shim}}^{t+\Delta t} = \dot{m}_{TES_{shim}}^{t} + \frac{K_{TES_{Shim}}\dot{m}_{TES_{ref}}\left(\dot{m}_{\text{Steamtarget}} - \dot{m}_{\text{Steam}}\right)\Delta t}{\dot{m}_{\text{Steampeakref}}} \tag{3.158}$$

3.4 Charging/Discharge Cycle Realignment

Over the course of time, whether it is days, weeks, or months, there will come a point where the discrepancy in time spent charging and discharging will cause one of the tanks to fill while leaving the other empty. When this occurs one of the two operating modes, charging or discharging, will need to be suspended until such a time that the tanks levels have realigned. Options to mitigate such scenarios are outlined below.

Scenario 1: Hot Tank is nearly full, and the system is charging

1. Decrease charging by decreasing the reactor power. This can be planned and does not require switching to full load follow operation.

2. Should the Hot Tank fill up the pressure relief valves in the IHX will open when the stop valve between the Cold Tank and Hot Tank closes, shutting off TES fluid flow. Thus, all the bypass

flow into the IHX will bypass through the pressure relief valves directly to the condenser, allowing the reactor to maintain operation at 100% power.

Scenario 2: Cold Tank is nearly full, and the system is discharging

1. Turn on additional peaking units. These can be smaller fossil fuel peaking units.

The mitigation of scenario 1 is easier in terms of infrastructure, especially if the system is deployed on a constrained grid. With this in mind, most of the systems presented will be designed such that more time is spent charging than discharging when subjected to typical electric demands (electric or steam).

Chapter 4 Condenser Model

4.1 Design

The presence of the TES system places additional demands on the condenser, and its time dependent behavior is necessary to predict overall system performance. The condenser model is sufficient to handle all foreseeable operating modes. Included in the Condenser model are flows from the turbine and the TES system's ACV and PRVs. The condenser model will provide the time varying condenser pressure and associated system dynamics. Condenser parameters for an mPower sized reactor/TES system are given in Table 4.1.

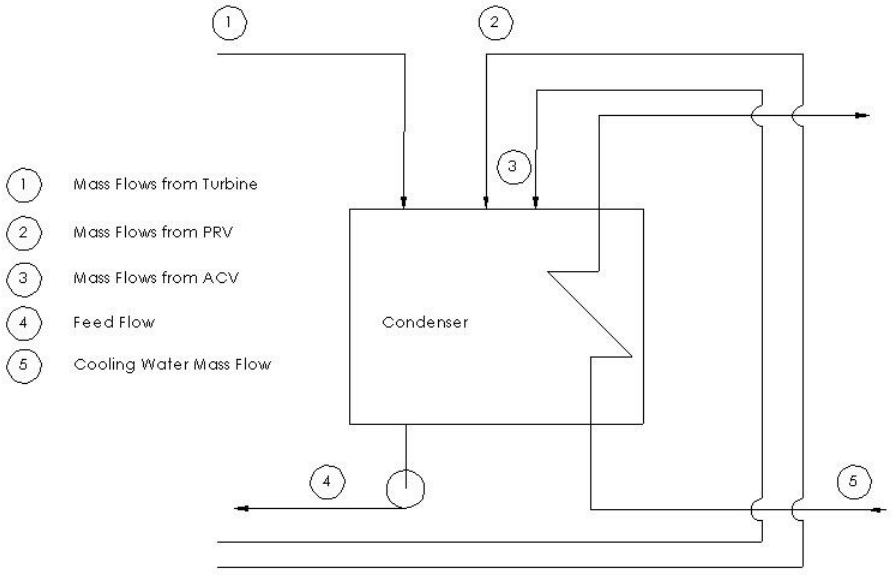

Figure 4.1: Condenser Configuration

4.2 Condenser equation set

To model the Condenser, an equation set similar to that for the Intermediate heat exchanger is used.

Energy Equation

$$V_{cond}\frac{d\rho u}{dt} = \sum_{n}\dot{m}_{IHX}h_{f_{@\,P_{IHX}}} + \sum_{m}\dot{m}_{PRV_{IHX}}h_{g_{@\,P_{IHX}}} + \sum_{l}\dot{m}_{turb_{exh}}h_{exh_l} - \dot{m}_{Feed}h_{f_{@\,P_{Cond}}} - \dot{Q}_{Cond} \quad (4.1)$$

Mass Equation

$$V_{cond}\frac{d\rho}{dt}=\sum_{n}\dot{m}_{IHX}+\sum_{m}\dot{m}_{PRV_{IHX}}+\sum_{l}\dot{m}_{turb_{exh}}-\dot{m}_{Feed} \tag{4.2}$$

State Equations

$$\rho = \alpha_l\rho_l+\alpha_g\rho_g \tag{4.3}$$

$$\rho u = \alpha_l\rho_l u_l+\alpha_g\rho_g u_g \tag{4.4}$$

Differencing in time gives

$$V_{cond}\left\{\frac{\rho u^{t+\Delta t}-\rho u^{t}}{\Delta t}\right\}=\sum_{n}\dot{m}_{IHX}^{t+\Delta t}h_{f_{@P_{IHX}}}^{t+\Delta t}+\sum_{m}\dot{m}_{PRV_{IHX}}^{t+\Delta t}h_{g_{@P_{IHX}}}^{t+\Delta t}+\sum_{l}\dot{m}_{turb_{exh}}^{t+\Delta t}h_{exh_l}^{t+\Delta t}-\dot{m}_{Feed}^{t+\Delta t}h_{f_{@P_{Cond}}}^{t+\Delta t}-\dot{Q}_{Cond}^{t} \tag{4.5}$$

$$V_{cond}\left\{\frac{\rho^{t+\Delta t}-\rho^{t}}{\Delta t}\right\}=\sum_{n}\dot{m}_{IHX}^{t+\Delta t}+\sum_{m}\dot{m}_{PRV_{IHX}}^{t+\Delta t}+\sum_{l}\dot{m}_{turb_{exh}}^{t+\Delta t}-\dot{m}_{Feed}^{t+\Delta t} \tag{4.6}$$

State Equations

$$\rho^{t+\Delta t}=\alpha_l^{t+\Delta t}\rho_l^{t+\Delta t}+\alpha_g^{t+\Delta t}\rho_g^{t+\Delta t} \tag{4.7}$$

$$\rho u^{t+\Delta t}=\alpha_l^{t+\Delta t}\rho_l^{t+\Delta t}u_l^{t+\Delta t}+\alpha_g^{t+\Delta t}\rho_g^{t+\Delta t}u_g^{t+\Delta t} \tag{4.8}$$

Assuming the inlet flows and enthalpies are known, casting the problem as a Newton Iteration gives for the new iterate values

$$V_{cond}\left\{\frac{\rho u^{k+1}-\rho u^{t}}{\Delta t}\right\}=\sum_{n}\dot{m}_{IHX}^{t+\Delta t}h_{f_{@P_{IHX}}}^{t+\Delta t}+\sum_{m}\dot{m}_{PRV_{IHX}}^{t+\Delta t}h_{g_{@P_{IHX}}}^{t+\Delta t}+\sum_{l}\dot{m}_{turb_{exh}}^{t+\Delta t}h_{exh_l}^{t+\Delta t}-\dot{m}_{Feed}^{t+\Delta t}h_{f_{@P_{Cond}}}^{t+\Delta t}-\dot{Q}_{Cond}^{t} \tag{4.9}$$

$$V_{cond}\left\{\frac{\rho^{k+1}-\rho^{t}}{\Delta t}\right\}=\sum_{n}\dot{m}_{IHX}^{t+\Delta t}+\sum_{m}\dot{m}_{PRV_{IHX}}^{t+\Delta t}+\sum_{l}\dot{m}_{turb_{exh}}^{t+\Delta t}-\dot{m}_{Feed}^{t+\Delta t} \tag{4.10}$$

$$\tilde{\rho}^{k}=\rho\left(\alpha_g^{k},P_{Cond}^{k}\right)=\rho_f\left(P_{Cond}^{k}\right)+\alpha_g^{k}\left[\rho_g\left(P_{Cond}^{k}\right)-\rho_f\left(P_{Cond}^{k}\right)\right] \tag{4.11}$$

$$\rho u^{k}=\rho u\left(\alpha_g^{k},P_{Cond}^{k}\right)=\rho_f\left(P_{Cond}^{k}\right)u_f\left(P_{Cond}^{k}\right)+\alpha_g^{k}\left[\rho_g\left(P_{Cond}^{k}\right)u_g\left(P_{Cond}^{k}\right)-\rho_f\left(P_{Cond}^{k}\right)u_f\left(P_{Cond}^{k}\right)\right] \tag{4.12}$$

$$\rho^{k+1}=\tilde{\rho}^{k}+\delta\alpha_g\left.\frac{\partial\rho}{\partial\alpha_g}\right|_k+\delta P_{Cond}\left.\frac{\partial\rho}{\partial P}\right|_k \tag{4.13}$$

$$\rho u^{k+1}=\rho u^{k}+\delta\alpha_g\left.\frac{\partial\rho u}{\partial\alpha_g}\right|_k+\delta P_{Cond}\left.\frac{\partial\rho u}{\partial P}\right|_k \tag{4.14}$$

The system of equations can be rewritten as a direct solve for $\rho u^{k+1}, \rho^{k+1}, \delta\alpha_g, \delta P_{Cond}$. Upon convergence, the heat transfer rate for the next time step ($\dot{Q}^t_{Cond}$) can be obtained from $\dot{Q}_{Cond} = UA_{cond}\Delta T_m$ where

$$\Delta T_m = \frac{\left(T_{sat} - T_{Cond_{exit}}\right) - \left(T_{sat} - T_{Cond_{inlet}}\right)}{\ln\left[\frac{T_{sat} - T_{Cond_{exit}}}{T_{sat} - T_{Cond_{inlet}}}\right]} \tag{4.15}$$

$$UA_{cond} = \frac{2\pi nL}{\frac{1}{h_i r_i} + \frac{1}{k}\ln\left(\frac{r_o}{r_i}\right) + \frac{1}{h_o r_o}} \tag{4.16}$$

The heat transfer coefficients h_i and h_o are obtained in the same manner as in the intermediate heat exchanger equations (3.18) and (3.19).

It will be assumed that the mass flow rate of the cooling water is constant and known along with the cooling water inlet temperature and pressure. This gives $T_{Cond_{inlet}}$. To calculate $T_{Cond_{exit}}$ an energy balance can be applied between the tube and shell side of the condenser.

$$V_{Cond}\rho_{flow}c_{p_{flow}}\left\{\frac{T^{t+\Delta t}_{Cond_{exit}} - T^{t}_{Cond_{exit}}}{\Delta t}\right\} + \dot{m}_{Cond}c_{p_{flow}}\left\{T^{t+\Delta t}_{Cond_{exit}} - T_{Cond_{inlet}}\right\} = \dot{Q}^t_{Cond} \tag{4.17}$$

Rearranging gives for $T^{t+\Delta t}_{Cond_{exit}}$

$$T^{t+\Delta t}_{Cond_{exit}} = \frac{\dot{Q}^t_{Cond}}{\zeta} + \frac{\dot{m}_{Cond}c_{p_{flow}}T_{Cond_{inlet}}}{\zeta} + \frac{T^t_{Cond_{exit}}\dfrac{V_{Cond}\rho_{flow}c_{p_{flow}}}{\Delta t}}{\zeta} \tag{4.18}$$

Where, $\zeta = \dfrac{V_{Cond}\rho_{flow}c_{p_{flow}}}{\Delta t} + \dot{m}_{Cond}c_{p_{flow}}$.

Table 4.1: Condenser Parameters for mPower sized Reactor/TES system.

Parameter	Value
Design Heat Transfer Rate	530 MWt
Temperature of Cooling Water	10 °C (50 °F)
Volume of Condenser	215.4 m^3 (7607 ft^3)
Number of Tubes in Condenser	76824
Length of Tubes	7.34 m (24.1 ft)
Mass Flow of Cooling Water	1.547×10^7 kg/hr (3.411×10^7 lbm/hr)
Condenser Tube Inner Diameter	0.013 m (0.044 ft)
Condenser Tube Outer Diameter	0.018 m (0.058 ft)

Chapter 5 Flash Vessel Model

Once the bypass steam has been condensed in the Intermediate Heat Exchanger it is no longer useful to the TES system, and would normally be directed to the condenser. However, for the system operating parameters assumed here, this condensate is sitting at a pressure of approximately 4.82MPa (700psia), making it high grade waste heat for other applications. To utilize this waste heat for low pressure applications such as chilled water production, the condensate from the IHX is dropped across a let down orifice to produce a low pressure steam/water mixture. This two phase mixture is sent to a flash vessel where the liquid and vapor phases are separated. The saturated steam is then sent to an ancillary application to utilize the high grade waste heat byproduct produced in the TES system. A potential configuration for chilled water production is illustrated in Figure 5.1, where the chilled water is assumed to be stored in a stratified storage tank [47]. Other potential applications include using the waste heat for desalination or in an additional feedwater heater placed at the end of the feed train to minimize feed temperature variations with turbine load.

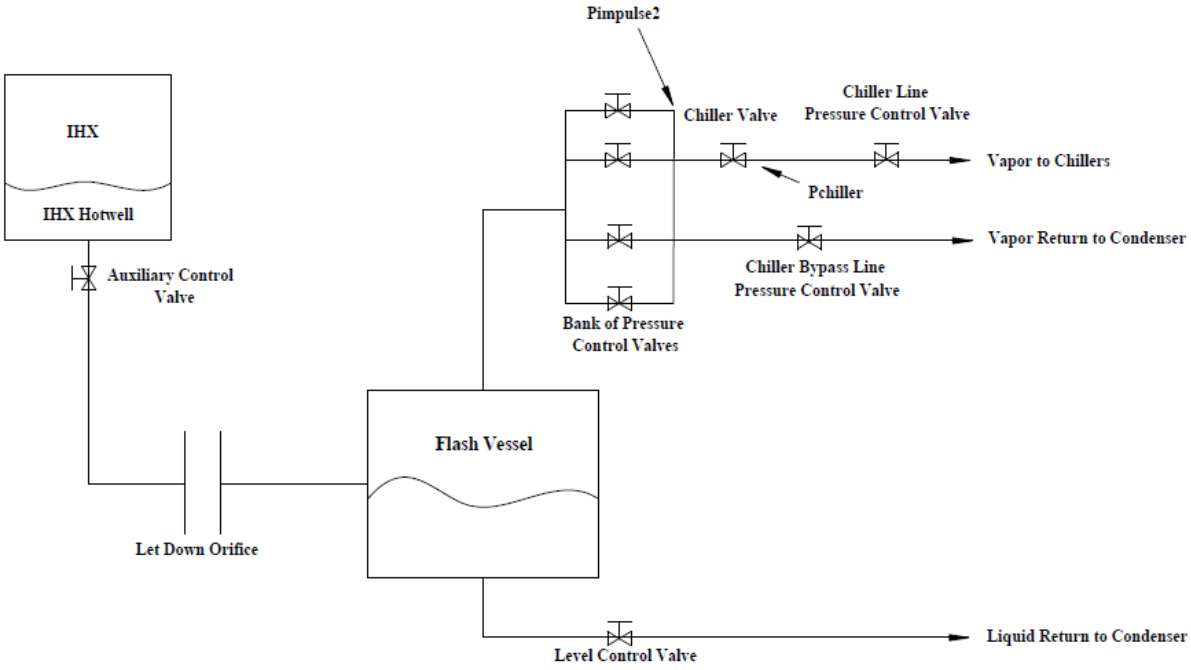

Figure 5.1: Flash Vessel Configuration

5.1 Flash Vessel Equation Set

The flash vessel is assumed to be ideal and works to separate the steam/water mixture into saturated liquid and vapor.

Mass Balance

$$V_{FV}\frac{d\rho_{FV}}{dt}=\dot{m}_{IHX}-\dot{m}_{PCV}-\dot{m}_{Cond_2} \tag{5.1}$$

Energy Balance

$$V_{FV}\frac{d\rho u_{FV}}{dt}=\dot{m}_{IHX}h_{f_{IHX}}-\dot{m}_{PCV}h_{g_{FV}}-\dot{m}_{Cond_2}h_{f_{FV}} \tag{5.2}$$

State Equations

$$\rho_{FV}=\rho_f\left(P_{FV}\right)-\alpha_{g_{FV}}\left(\rho_f\left(P_{FV}\right)-\rho_g\left(P_{FV}\right)\right) \tag{5.3}$$

$$\rho u_{FV}=\rho_f u_{f_{FV}}-\alpha_{g_{FV}}\left(\rho_f u_{f_{FV}}-\rho_g u_{g_{FV}}\right) \tag{5.4}$$

Momentum Equations

$$P_{IHX}=P_{FV}+\frac{\left(K_{ACV}+K_{Letdown}\right)\dot{m}_{IHX}^2}{2A_{ACV}^2\rho_{f_{IHX}}} \tag{5.5}$$

$$P_{FV}=P_{impulse2}+\frac{\left(K_{PCV_n}+K_{PCVline}\right)\dot{m}_{PCV_n}^2}{2A_{PCV_n}^2\rho_{g_{FV}}} \tag{5.6}$$

$$P_{FV}=P_{cond}+\frac{\left(K_{LCV}+K_{LCVline}\right)\dot{m}_{cond_2}^2}{2A_{LCV}^2\rho_{f_{FV}}} \tag{5.7}$$

$$P_{impulse2}=P_{cond}+\frac{\left(K_{Chiller}+K_{Chillerline}\right)\dot{m}_{chiller}^2}{2A_{Chiller}^2\rho_{g_{FV}}} \tag{5.8}$$

$$P_{impulse2}=P_{cond}+\frac{\left(K_{Bypass}+K_{Bypassline}\right)\dot{m}_{bypass}^2}{2A_{Bypass}^2\rho_{g_{FV}}} \tag{5.9}$$

5.2 Flash Vessel Control

The Flash Vessel has six sets of valves used to control system parameters: the auxiliary control valve, level control valve, three sets of pressure control valves, and a chiller valve.

The auxiliary control valve modulates to maintain level in the Intermediate Heat Exchanger. Thus during times of high bypass steam flow, there will be a corresponding high condensate flow exiting the IHX. The goal of the first bank of pressure control valves is to maintain the flash vessel at some user specified pressure. The second pressure control valve is located at the exit of the chiller line. This pressure control valve modulates to maintain a user specified pressure downstream of the chiller valve. The chiller valve operates on a binary signal such that if the thermocline level in the stratified storage

tank is below some lower set point the valve goes to its full open position. Conversely when the thermocline level hits some upper set point the valve shuts. The third pressure control valve located on the bypass line around the chiller modulates to maintain a user defined pressure downstream of the main pressure control valve bank, this point is called *Pimpulse2* in Figure 5.1.

$$Signal_{PCV_{bank}} = \frac{P_{FlashVessel} - P_{FlashVessel_{design}}}{P_{FlashVessel_{design}}} \tag{5.10}$$

$$Signal_{PCV_{Chiller}} = \frac{P_{Chiller} - P_{Chiller_{design}}}{P_{Chiller_{design}}} \tag{5.11}$$

$$Signal_{PCV_{bypass}} = \frac{P_{\mathrm{Impulse2}} - P_{\mathrm{Impulse2}_{design}}}{P_{\mathrm{Impulse2}_{design}}} \tag{5.12}$$

The level control valve, located at the bottom of the flash vessel maintains Flash Vessel level. This valve operates on a three element controller based on the level of the flash vessel and difference in mass flows into and out of the flash vessel.

$$\mathrm{Signal}_{LCV} = G_1 E_1 + G_2 E_2 \tag{5.13}$$

$$E_1 = \mathrm{Level\text{-}Level}_{\mathrm{Ref}} \tag{5.14}$$

$$E_2 = \dot{m}_{IHX} - \dot{m}_{PCV} - \dot{m}_{Cond_2} \tag{5.15}$$

Parameters directly controlled in the flash vessel model are the flash vessel level, flash vessel pressure, pressure downstream of the first pressure control bank, and pressure downstream of the chiller valve.

Chapter 6 NHES Dynamic Simulation Results

The goal of this work is to eliminate stressors on the reactor associated with load follow operation by storing thermal energy during periods of excess reactor capacity in a TES system to be recovered at a later time. To fully demonstrate such capabilities several sets of simulations were performed. The first set of simulations show the system's ability to move stressors away from the primary and secondary sides of the reactor system over to the TES system. The second set demonstrates the ability of TES systems to operate as electrical peaking units. The last set of simulations demonstrates the potential for ancillary applications ranging from chilled water production to desalination. For these simulations an mPower style reactor with the geometry and design parameters specified in Table 2.1 was utilized. TES design parameters and set point values are given in Table 6.1. For all simulations the term "electric demand" refers to the net demand required of the Reactor/TES system.

Table 6.1: TES Design Parameters for connection with an mPower size IPWR

Parameter	Value
TES Fluid	Therminol®-66
Hot Tank Volume	226,535 m^3
Cold Tank Volume	226,535 m^3
IHX Reference Exit Temperature	260 ˚C (500 ˚F)
Number of TBV's	4
TES Maximum Steam Accommodation	~45% nominal steam flow
Pressure Relief Valve Upper Setpoint	5.377 MPa (780 psia)
Pressure Relief Valve Lower Setpoint	5.240 MPa (760 psia)
Turbine Header Pressure	5.688 MPa (825 psia)
Shell Side (outer loop) IHX Volume	101.94 m^3 (3600 ft^3)
Number of Tubes	19140
Length of Tubes	11.25 m (36.9 ft)
Tube Inner Diameter	0.013 m (0.044 ft)
Tube Outer Diameter	0.018 m (0.058 ft)
Steam Dome Reference Pressure	1.379 MPa (200 psia)
Steam Dome Volume	509.7 m^3 (18000 ft^3)
LPT reentrance point	1.207 MPa (175 psia)
TES Steam Generator tube count	32761
TES Steam Generator volume	42.475 m^3 (1500 ft^3)
TES Steam Generator Height	9.144 m (30 ft)
TES Steam Generator Thermal Conductivity	10.3 Btu/hr-ft-˚F
TES Steam Generator pitch to diameter ratio	1.606

Components on the charging system were designed to accommodate 45% nominal steam flow from an mPower size IPWR while maintaining IHX pressure above 4.826MPa (700 psia). Discharge components were sized to accommodate approximately 45MWe of peaking capacity assuming a 33% balance of plant conversion rate.

6.1 Charging System Capability

The first set of simulations highlights the advantage of having a thermal storage system attached to the reactor as opposed to simply operating the reactor in load follow mode. These simulations focus only on the charging mode of the TES system. Operation of the TES system as a peaking unit will be discussed later. A 24-hour simulation was run with an electric load profile representative of a typical summer day in an area with mixed commercial and residential characteristics [3]. The load profile has been scaled such that the minimum load is approximately 60% of nominal full power. Time zero corresponds to midnight. A 24 hour cycle was chosen because it is the minimum amount of time required to show a full daily cycle for a region during a season. Week or month long runs will show the same general trends as the daily cycle with the only distinction being in tank level.

6.1.1. Load Follow Operation

As a basis for comparison, the SMR is operated in Load Follow mode, where the reactor power is modulated to match the electric demand. As shown in Figure 6.1 and Figure 6.2, the system is able to maneuver such that the turbine output is effectively identical to the electric demand, and the reactor power follows the load. For this simulation, a constant T_{ave} program was assumed with the corresponding control rod positions given in Figure 6.4. Four control banks are modeled. At the beginning of the maneuver, banks A-C are fully withdrawn, with D bank approximately 50% inserted. Over the course of the maneuver bank D moves to its full out position, and by the end of the transient has returned to its approximate starting point. The average primary coolant temperature varies by 4 degrees Celsius over the course of the run as illustrated in Figure 6.5. The changes in core coolant temperatures, along with changes in core power distribution and associated fuel temperatures add additional thermal stresses to the system, especially if repeated for multiple cycles. Figure 6.6 gives the variation in steam generator dryout location. Over the course of the simulation the dryout location varies by 15% of the tube length. The dryout location represents a sharp temperature gradient, and repeated cycling of this location can induce stresses that decrease the lifetime of the steam generator tubes. Of additional interest is the steam pressure downstream of the TCV (Turbine Impulse Pressure). As stated previously, steam conditions at this location are a strong function of the load profile and create

additional challenges if connections to the TES system are made downstream of this point. Variations in turbine impulse pressure directly impact the downstream pressures at all turbine taps and as a result impact feedwater temperature as illustrated in Figure 6.8. Cycling of feed temperature adds additional stresses to the steam generator tubes.

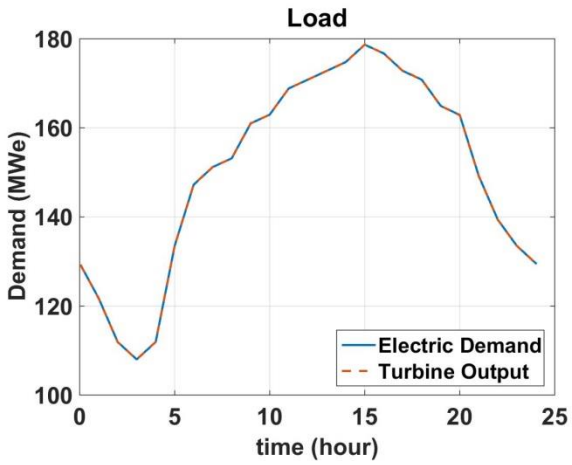

Figure 6.1: Turbine Output and Demand

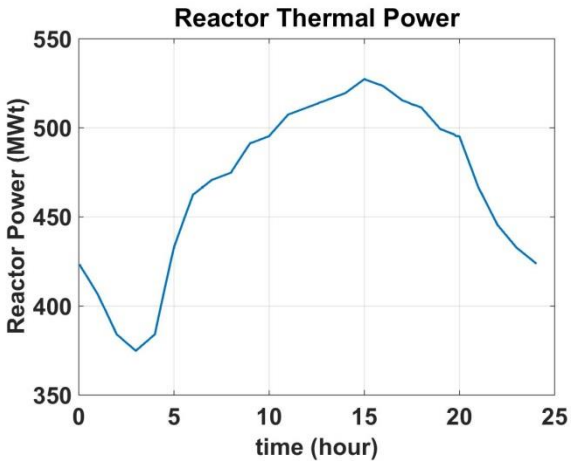

Figure 6.2: Reactor Power

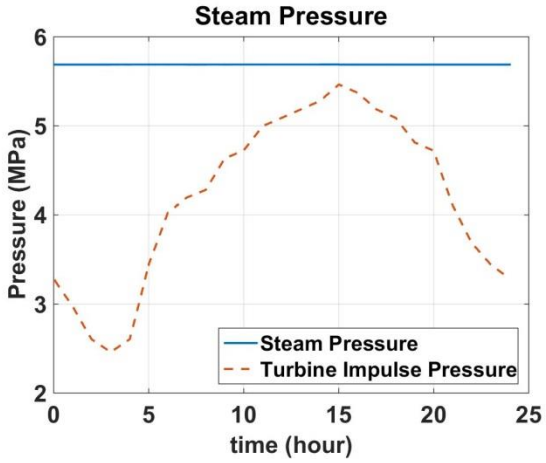

Figure 6.3: Steam Pressure

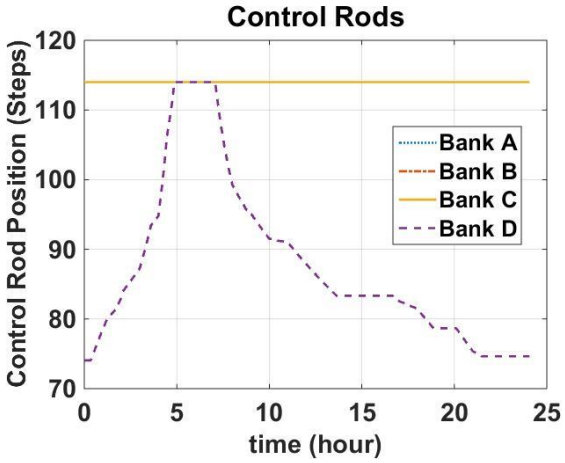

Figure 6.4: Control Rod Position

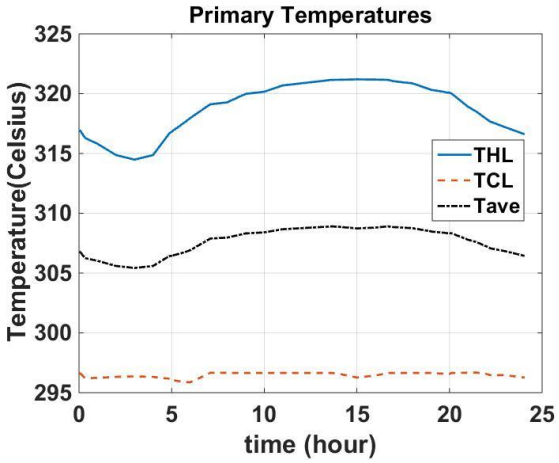

Figure 6.5: Primary Temperatures

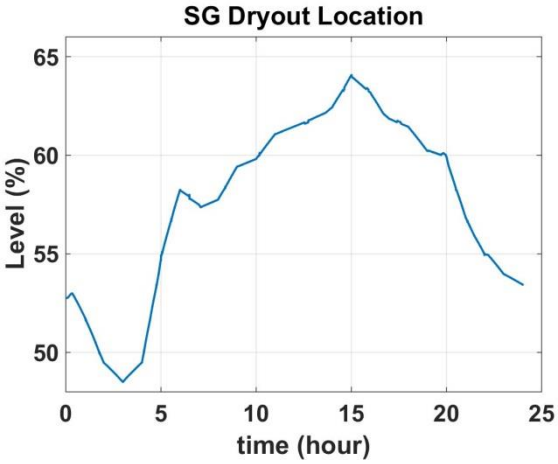

Figure 6.6: Steam Generator Dryout Location

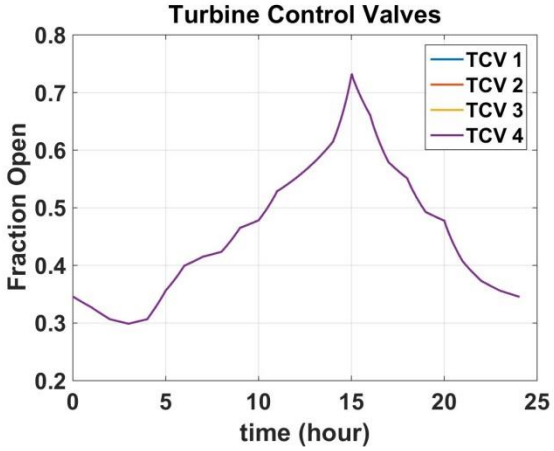

Figure 6.7: Turbine Control Valve Position (all TCVs move to same position)

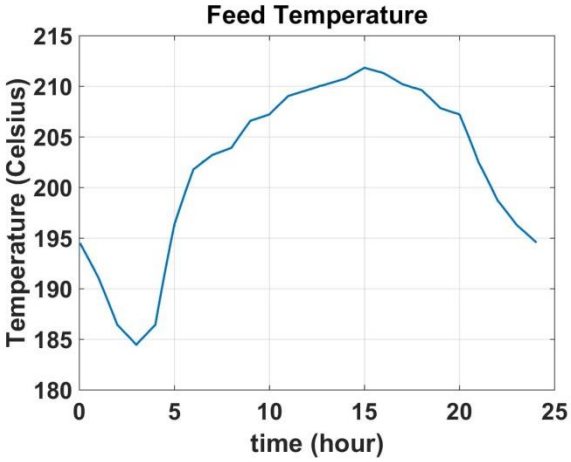

Figure 6.8: Temperature of feed water entering bottom of Steam Generator

6.1.2. Reactor Coupled with TES Storage System (Charging only Operation)

The same 24 hour run was simulated with the TES system active. As illustrated in Figure 6.9 and Figure 6.10, the plant is able to maneuver such that the electric demand is satisfied while keeping reactor power effectively constant. Since reactor power and reactor coolant temperatures were essentially constant, this maneuver could be executed without control rod movement and thermal stresses associated with changes in temperatures and power distributions. The corresponding bypass flow to the TES system is shown in Figure 6.13. As would be expected, the bypass flow rate is essentially the

inverse of the load profile. The steam generator dryout location varies by only 2% of the steam generator tube length for this simulation as compared with the 15% variation present during straight load follow. The TES fluid flow rate is shown in Figure 6.14 and closely follows the bypass flow rate. Steam generator and turbine impulse pressure are essentially unchanged from the Load Follow simulations.

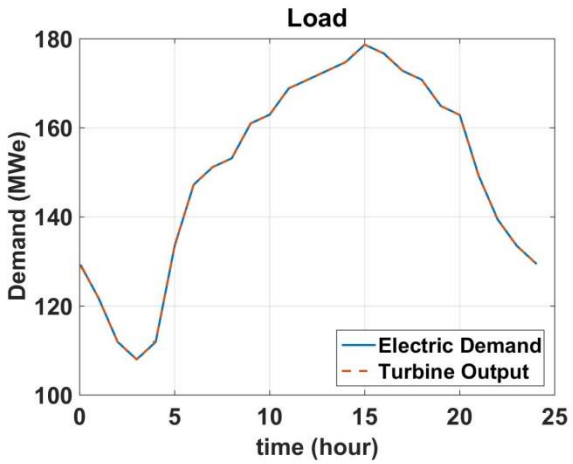

Figure 6.9: Turbine Output and Demand

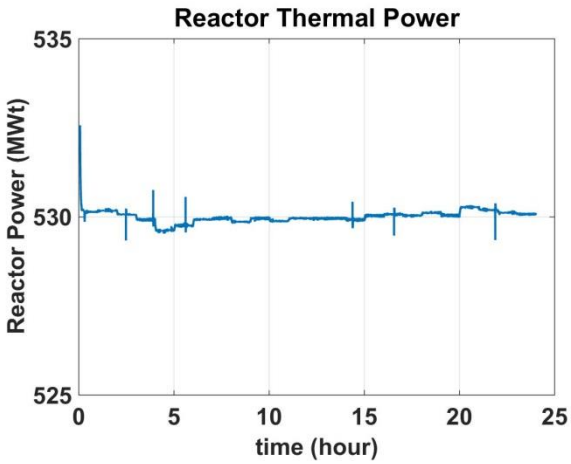

Figure 6.10: Reactor Power

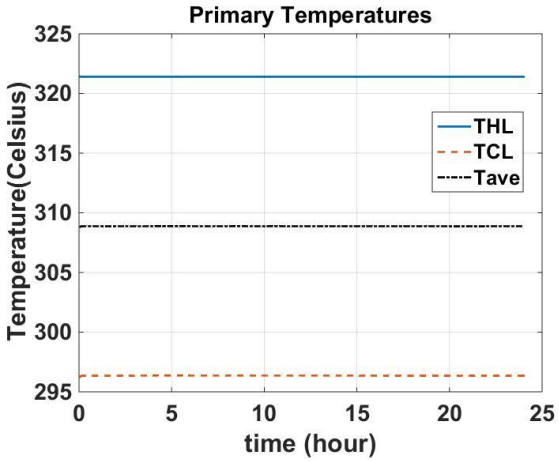

Figure 6.11: Primary Temperatures

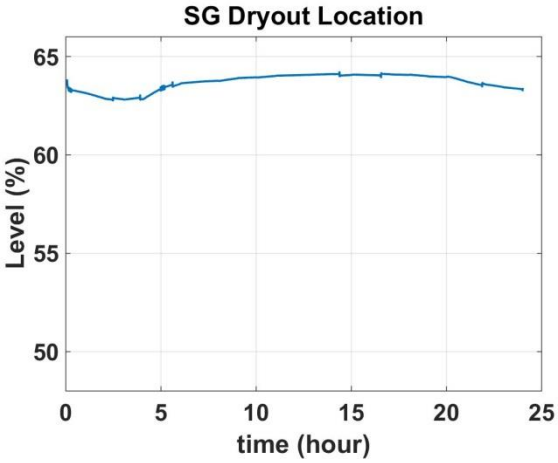

Figure 6.12: Steam Generator Dryout Location

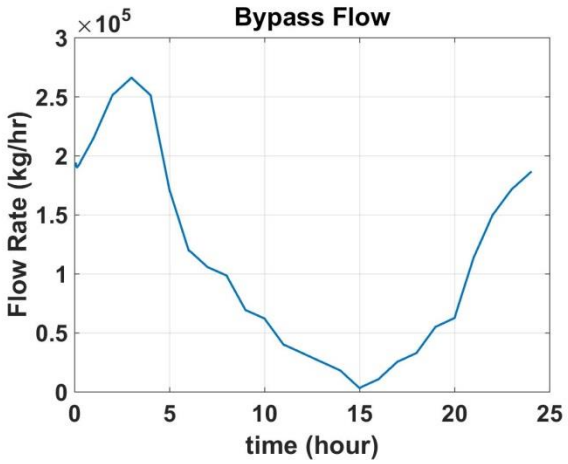

Figure 6.13: Bypass Flow into TES system

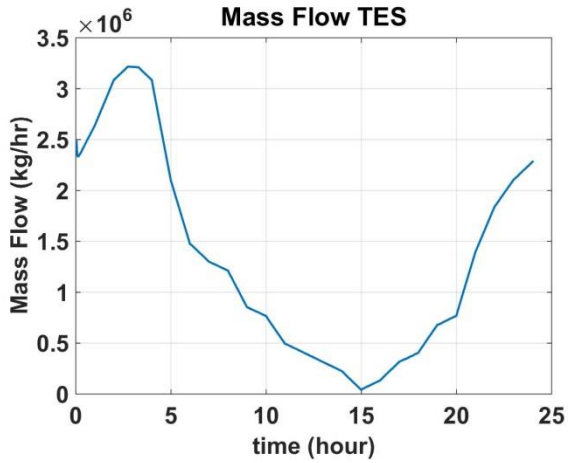

Figure 6.14: Flow of TES Fluid from Cold Tank to Hot Tank

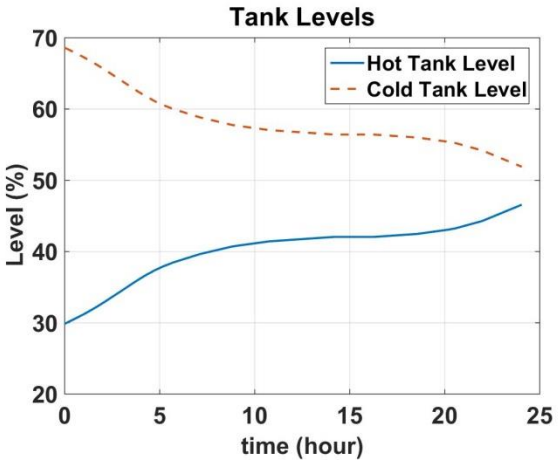

Figure 6.15: Hot and Cold Tank Levels

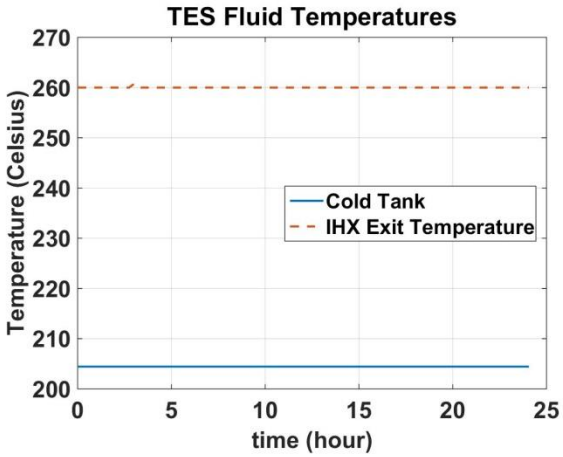

Figure 6.16: TES Temperatures

Figure 6.16 demonstrates that the flow controller for the TES flow control valve (FCV) is effective in keeping the IHX exit fluid temperature at its target value. The hot and cold storage tank levels are given in Figure 6.15. For the load profile considered here, the tanks have more than enough capacity to accommodate the excess thermal energy in the system.

6.1.3. Reactor Coupled with TES Storage System and intermittent renewables

An advantage of the TES system is the ability to accommodate the presence of intermittent energy sources on the grid, particularly solar energy generation that can vary depending on time of day or cloud cover. To illustrate these effects the load profile was modified to reflect upwards of 40MWe installed solar capacity as shown in Figure 6.17 and Figure 6.18. Over the course of the simulation, turbine load is met while thermal power stays approximately constant as illustrated in Figure 6.19 and Figure 6.20. The response of other system parameters is similar to that shown previously for the typical summer day. The TES system has the capacity to charge for the full 24 hour run as tank levels go from 30% to 57%, shown in Figure 6.22. Similar results have been obtained for a variety of load profiles with varying levels of renewable resources [48].

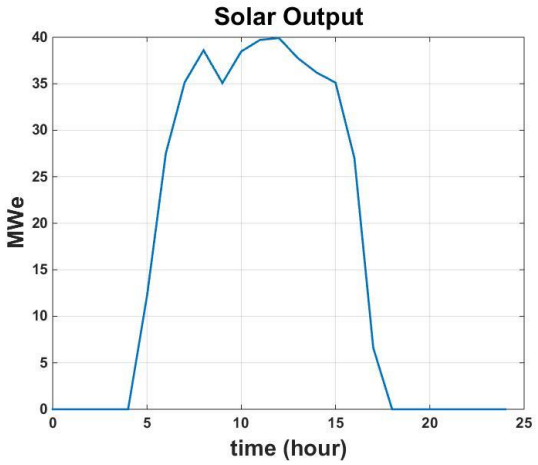

Figure 6.17: Typical Solar Output for a Summer Day

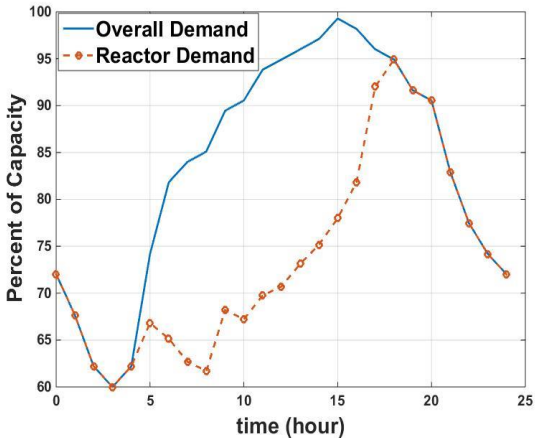

Figure 6.18: Demand profiles of a Typical Summer Day with and without Solar

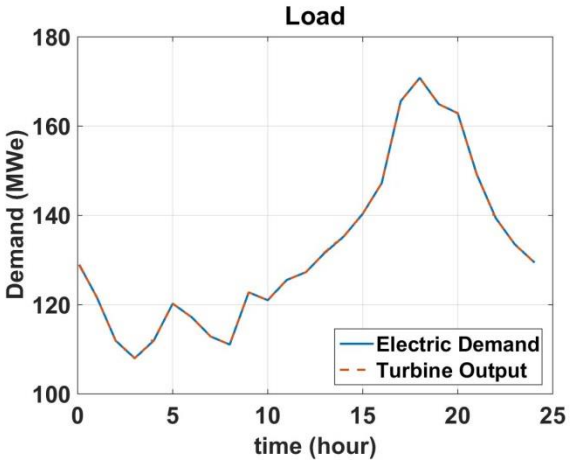

Figure 6.19: Turbine Load and Output

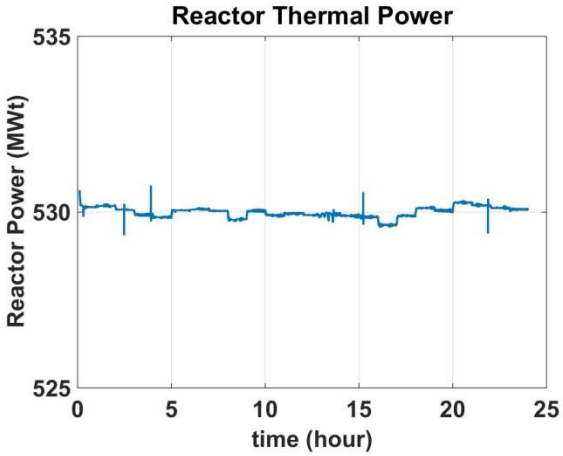

Figure 6.20: Reactor Power

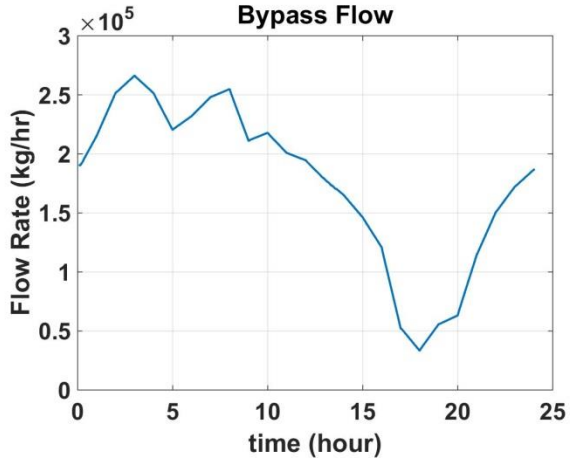

Figure 6.21: Auxiliary Bypass Flow

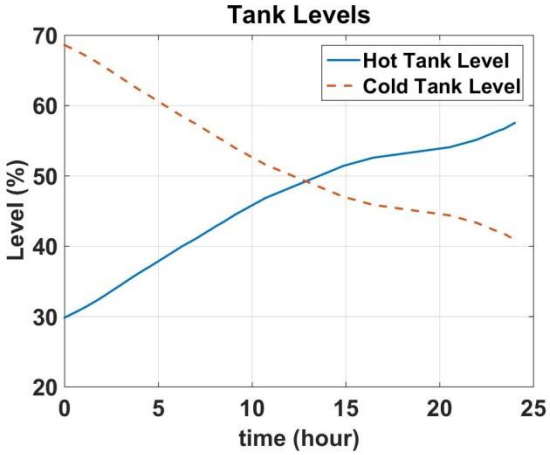

Figure 6.22: Hot and Cold Tank Levels

6.2 Electrical Peaking Unit

The "charging only" results show the advantages of having a TES system attached to the reactor as a means of heat storage and load variability control. This second set of simulations highlight the TES system's ability to operate as an electrical peaking unit. The electrical peaking unit is designed to accommodate ~35MWe peaking potential. To give a representative charge/discharge cycle the 24-hour electric load for a typical summer day was scaled so that for a typical summer day the integral amount of energy spent charging is 52.5% of the total energy spent charging and discharging as illustrated in Figure 6.23. The deployability of these systems necessitates that a single design be able to

accommodate a large range of load profiles. To test this capability, three scenarios were run: a typical summer day, a typical summer day with 15% (31.76Mwe) maximum solar penetration to the grid, and a typical winter day. For these runs the amount of therminol-66 in the tanks has been drastically reduced from the charging only model since the cost of this fluid is substantial [49]. Rather than having enough TES fluid to fill 226,500m^3 (height=18.28m) the volume has been reduced to 61,164m^3 (height=18.28m). It should be noted that a load profile could be chosen purely for economic reasons. A system with this storage capacity could operate to store heat during times of low electric prices and then discharge during times of high electric prices. Simulations run here assume the system is the main source of power as opposed to a piece in a larger network where such a dispatch strategy is feasible.

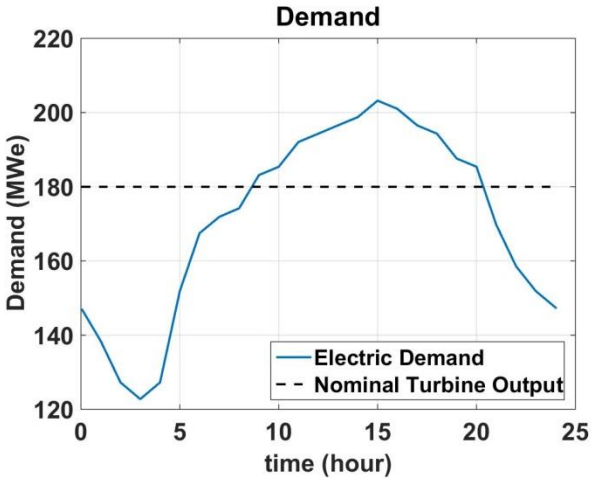

Figure 6.23: Electric Demand for a Typical Summer Day in a region scaled for charge/discharge operation with standard residential and commercial electrical needs.

6.2.1. Typical Summer Day

As illustrated in Figure 6.24 and Figure 6.25, the TES system is able to maneuver such that the electric demand is satisfied while keeping reactor power effectively constant. As the demand begins to exceed the maximum nominal turbine output of 180 MWe the peaking unit activates as shown in Figure 6.33. The primary and secondary loops of the reactor remain unchanged from when the system was operated in the charging only mode as seen in Figure 6.26 and Figure 6.27. Bypass flow into the charging system, illustrated in Figure 6.28, is approximately an x-axis reflection of the load profile up until the load reaches the nominal "rated" output of 180MWe. At this point the charging mode shuts off and the electrical peaking mode automatically activates. The mass flowing from the cold tank to the hot tank follows this same shape as seen in Figure 6.29. From about 8am to 9pm the system is operating as an

electrical peaking unit as illustrated in Figure 6.33. During this time the mass flow from the hot tank to the cold tank is modulated to ensure the electrical demand is being met as seen in Figure 6.32. Over the course of the day the tank levels oscillate about 25% of maximum, arriving back at approximately the same level as at the start of the day as illustrated in Figure 6.30. The TES fluid temperature entering the hot tank is maintained at the reference set point as seen in Figure 6.31.

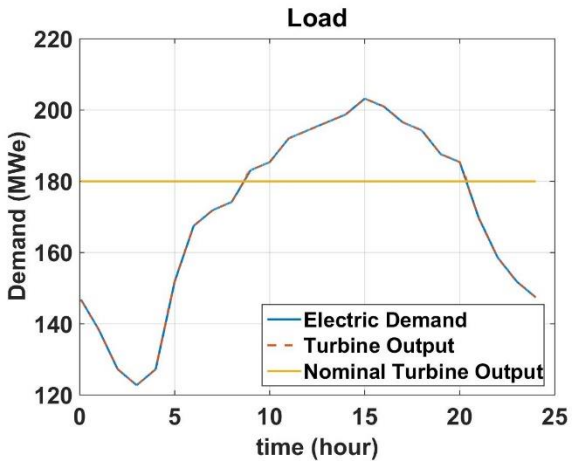

Figure 6.24: Turbine Load and Output

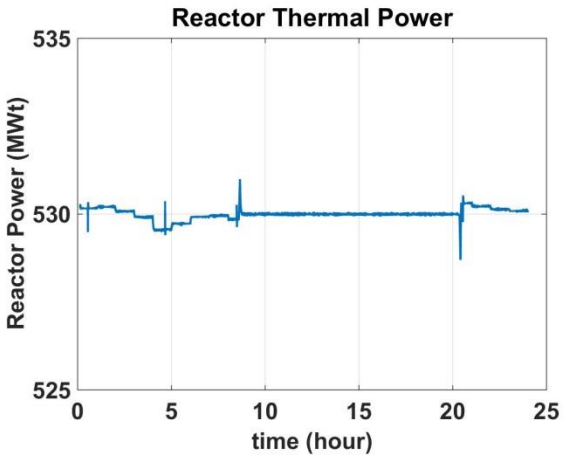

Figure 6.25: Reactor Power

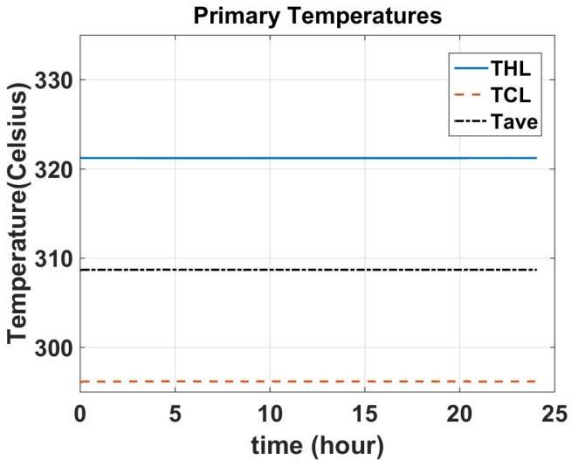

Figure 6.26: Primary Loop Temperatures

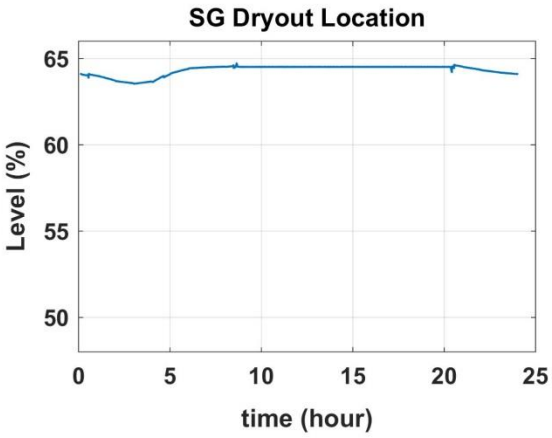

Figure 6.27: Steam Generator Dryout Location

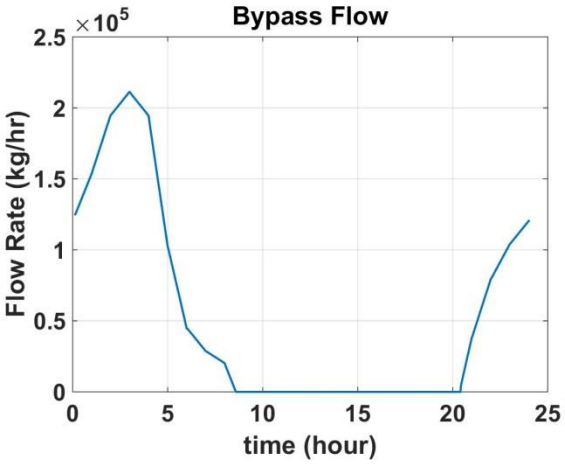

Figure 6.28: Auxiliary Bypass Flow

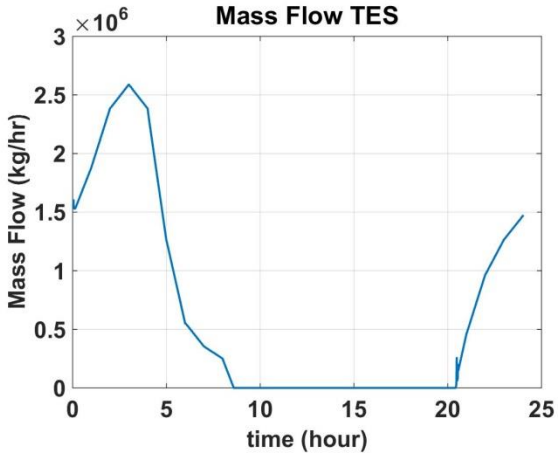

Figure 6.29: Flow of TES Fluid from Cold Tank to Hot Tank

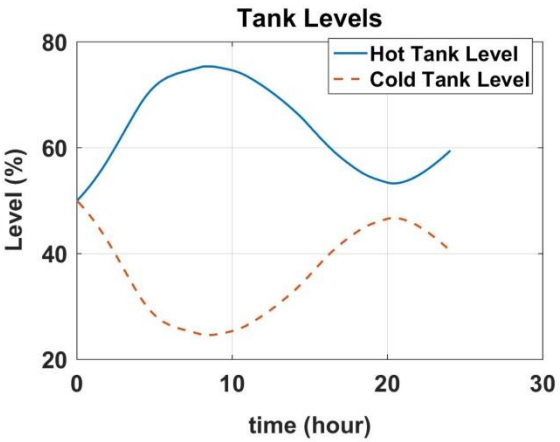

Figure 6.30: Hot Tank and Cold Tank Level

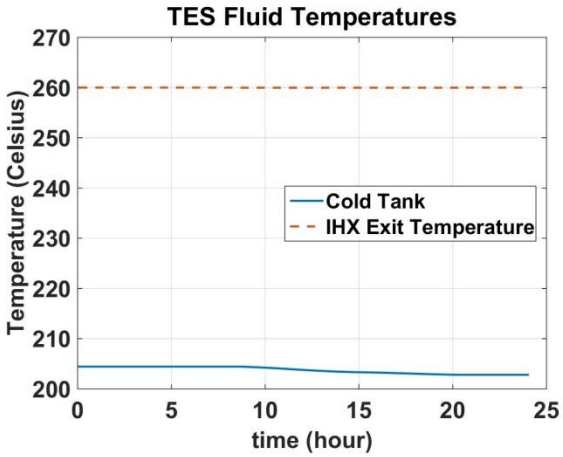

Figure 6.31: TES Fluid Temperature

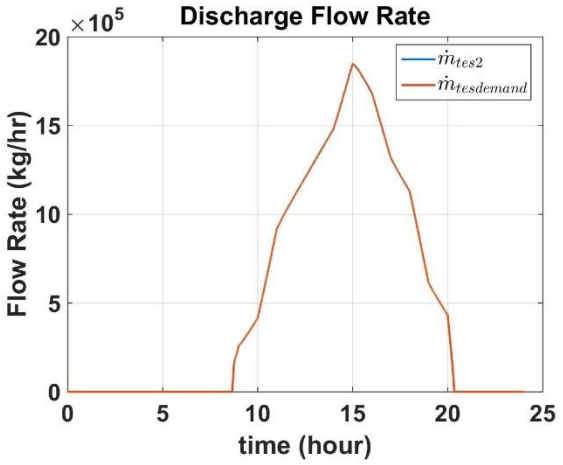

Figure 6.32: Flow of TES Fluid from Hot Tank to Cold Tank

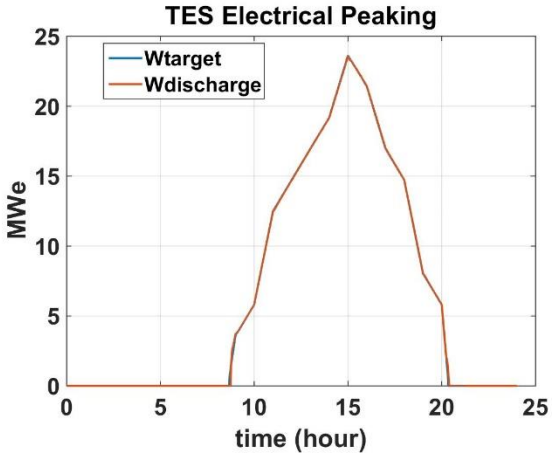

Figure 6.33: Electrical Peaking Output

6.2.2. Typical Summer Day with 15% Solar Penetration

For this simulation, 15% solar PV is assumed along with the reactor and TES system operating as an electric peaking unit. Figure 6.34 and Figure 6.35 show the TES system is able to maneuver such that the electric demand is satisfied while keeping reactor power effectively constant. The primary and secondary loops of the reactor remain unchanged. As before bypass flow into the charging system, illustrated in Figure 6.36, is approximately an x-axis reflection of the load profile up until the load reaches the nominal turbine "rated" output of 180MWe. At this point the charging mode automatically shuts off and the electrical peaking unit turns on. The mass flow from the cold tank to the hot tank follows this same shape as seen in Figure 6.37. The TES fluid temperature entering the hot tank is maintained at the reference set point as seen in Figure 6.39 throughout the course of the day. Once demand goes above 180MWe the system is operating as an electrical peaking unit. During this time the mass flow from the hot tank to the cold tank is modulated to ensure the electrical demand is being met as shown in Figure 6.40. Over the course of the day the tank levels oscillate about 50% of maximum arriving at a new point that is much higher than at the start of the day, as illustrated in Figure 6.38. This means that the system as sized would not be suitable as a long term solution with this amount of solar penetration. However, should this be the desired operating mode then the combined system would be designed such that the charging mode would operate less, either through grid design or through addition of ancillary applications.

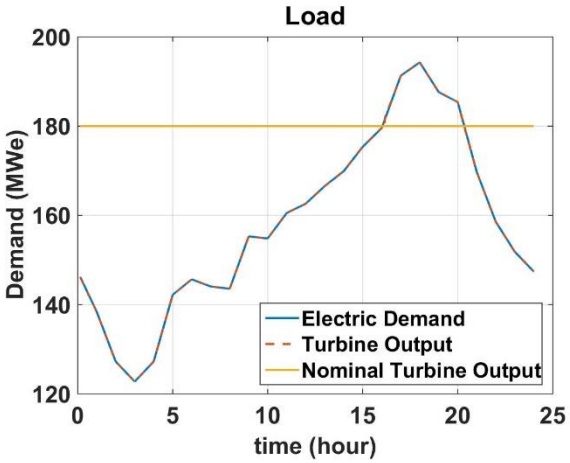

Figure 6.34: Turbine Output and Demand

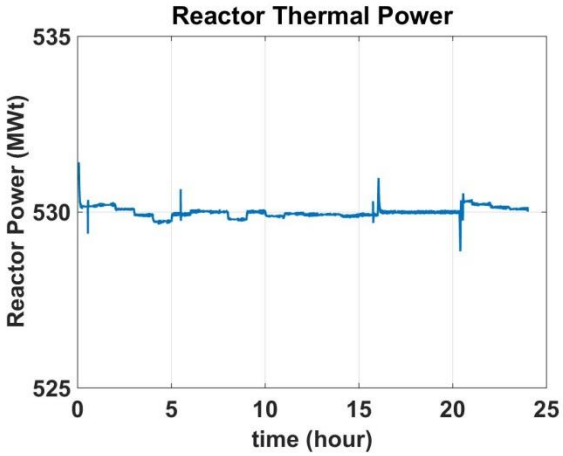

Figure 6.35: Reactor Power

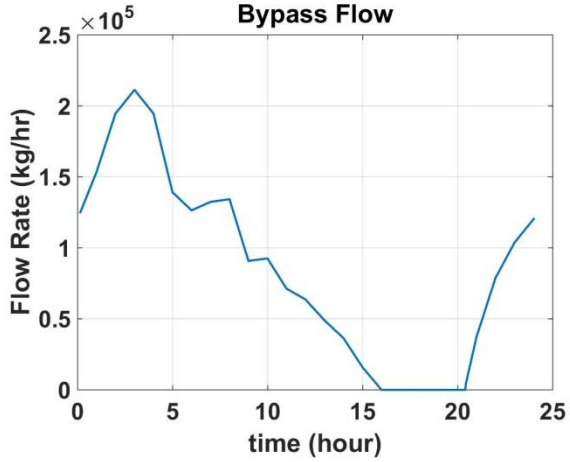

Figure 6.36: Auxiliary Bypass Flow

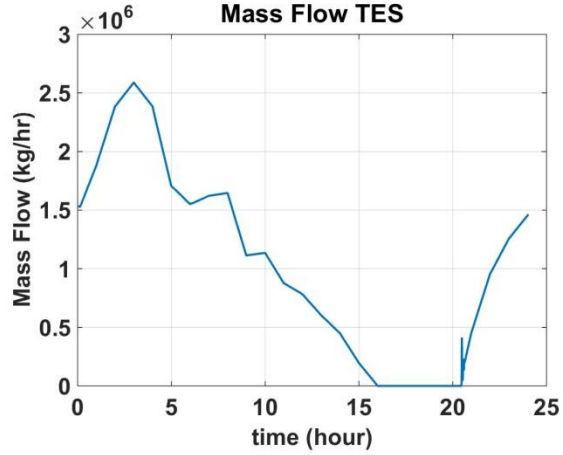

Figure 6.37: Flow of TES Fluid from Cold Tank to Hot Tank

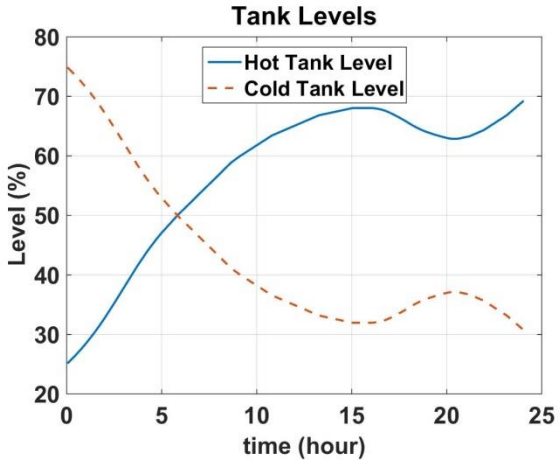

Figure 6.38: Hot Tank and Cold Tank Level

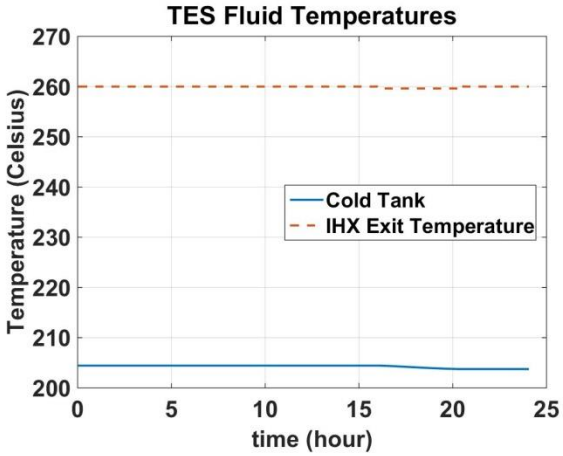

Figure 6.39: TES Fluid Temperature

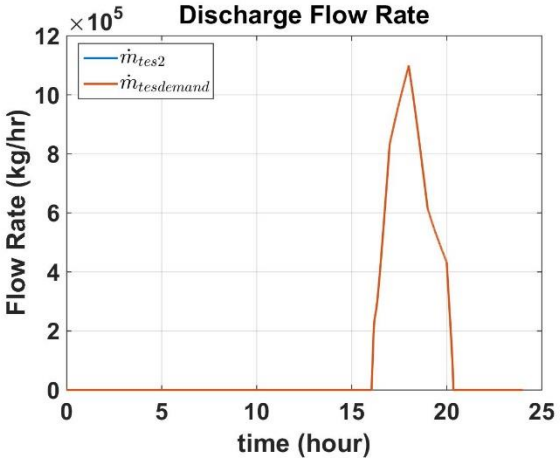

Figure 6.40: Flow of TES Fluid from Hot Tank to Cold Tank

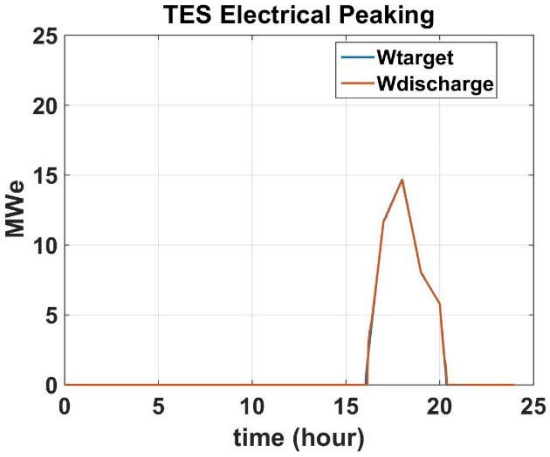

Figure 6.41: Electrical Peaking Output

6.2.3. Winter Day

Along with typical diurnal electric demand there is also seasonal demand. The 24-hour simulation below is that of a typical winter day in the southeast United States [50]. As illustrated in Figure 6.42 and Figure 6.43 the load is met throughout the entire day while maintaining reactor thermal power at the nominal level, just as in the summer day simulations. Primary and secondary loop dynamics remain unchanged from previous TES system runs. The bypass flow into the intermediate heat exchanger and the flow from the cold tank to the hot tank is approximately an x-axis reflection of the load up to the

180MWe line, as seen in Figure 6.44 and Figure 6.45. Over the course of the day the tank levels oscillate about 25% with the hot tank being about 12-13% fuller than at the start of the day. The temperature of the fluid leaving the top of the IHX going into the hot tank is held at the reference setpoint temperature of 260°C (500°F). Figure 6.48 and Figure 6.49 show that when demand increases above the 180MWe nominal reactor limit the electrical peaking unit turns on and fluid is released from the hot tank to heat fluid in the OTSG.

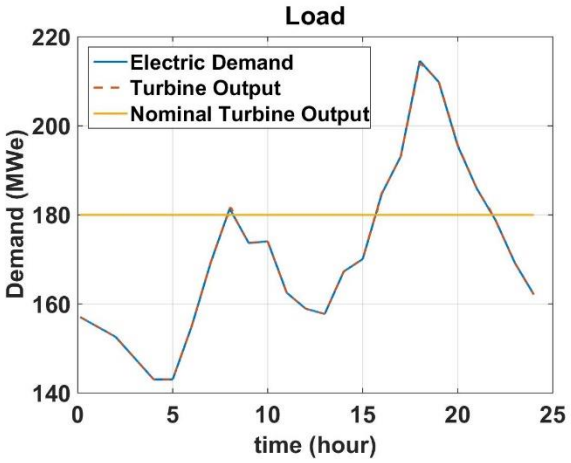

Figure 6.42: Turbine Output and Demand

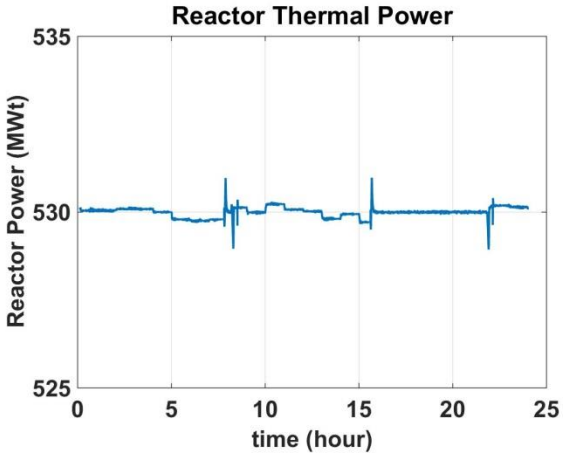

Figure 6.43: Reactor Power

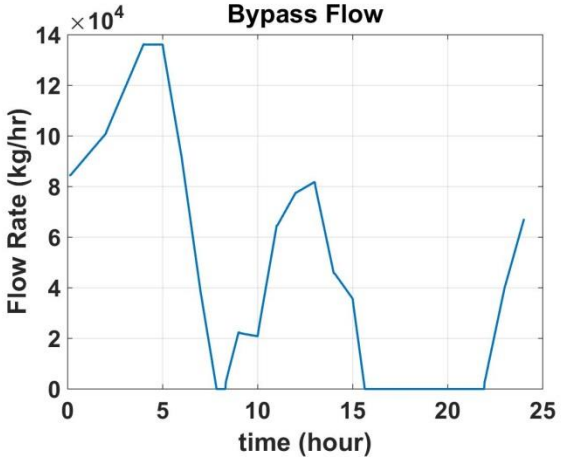

Figure 6.44: Auxiliary Bypass Flow

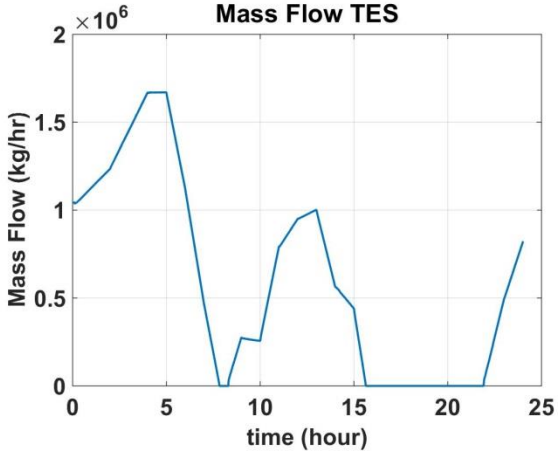

Figure 6.45: Flow of TES Fluid from Cold Tank to Hot Tank

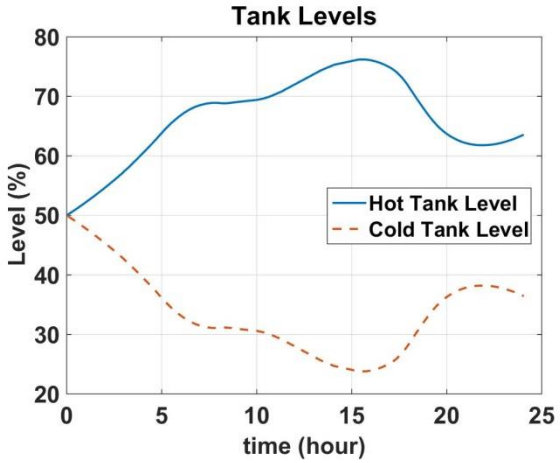

Figure 6.46: Hot Tank and Cold Tank Level

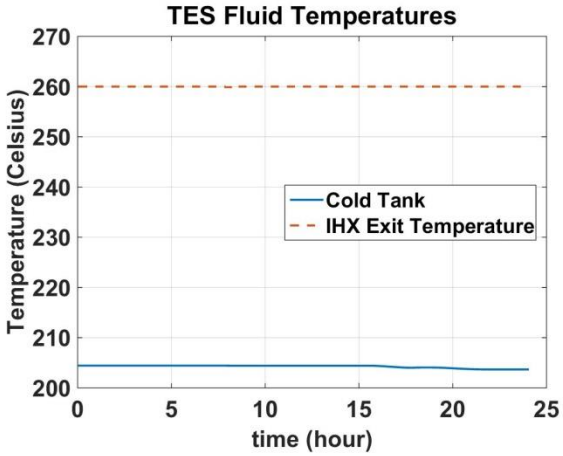

Figure 6.47: TES Fluid Temperature

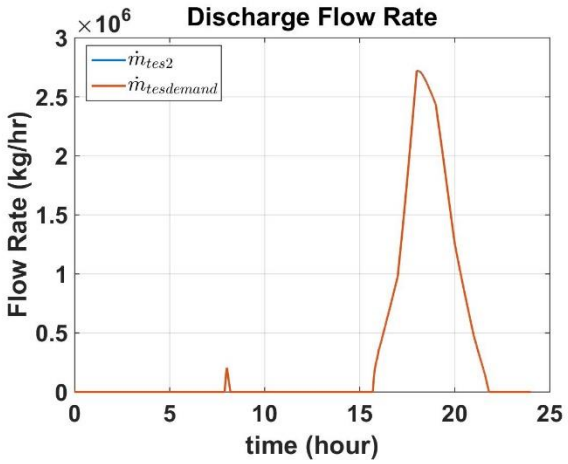

Figure 6.48: Flow of TES Fluid from Hot Tank to Cold Tank

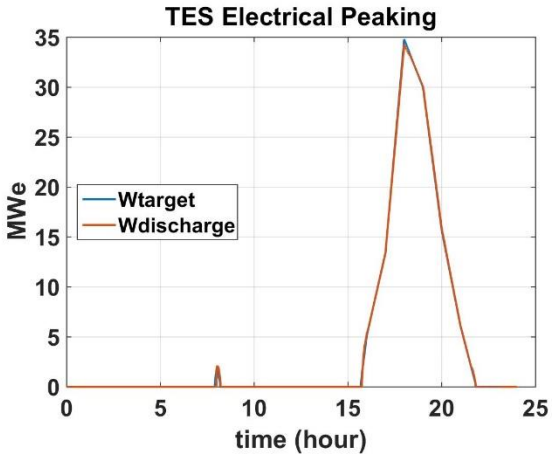

Figure 6.49: Electrical Peaking Output

6.3 Extended Runs

To further show the robustness of the system and the impact of tank sizing (61,164 m^3), the system was subjected to three different three day runs. The first run is three consecutive summer days with 15% solar PV, the second run is three typical summer days with 15% solar PV where the third day is cloudy, and the third run is three winter days with 15% solar PV where day two is cloudy. On cloudy or rainy days solar panels are assumed to run at only 10% capacity [51]. These runs highlight the versatility of the system over time and that the assumed tank sizing is appropriate to accommodate such loads. For

these runs the systems electric demand was shifted upward so that on a typical summer day with 15% solar penetration the hot tank fills more than the cold tank. This allows the system to be more adaptable to times of low solar output (e.g. rain or cloud cover).

6.3.1. Three Summers Days with 15% Solar Penetration

The first of the simulations is three consecutive sunny summer days with 15% solar penetration. Figure 6.50 and Figure 6.51 demonstrate that load is met throughout the entire 72 hour run while maintaining nominal reactor thermal power. Bypass flow into the TES system and TES fluid flow from the cold tank to the hot tank is roughly the inverse of the load as shown in Figure 6.52 and Figure 6.53. Figure 6.54 illustrates the oscillatory nature of the tank levels over the course of the three day run, with the hot tank ending up 30% fuller at the end of day three than at the start of day one. Cold tank temperature is not controlled and over the three day run the cold tank temperature fluctuates about five degrees Celsius. However, TES fluid temperature entering the hot tank is still maintained at the reference set point as seen in Figure 6.55.

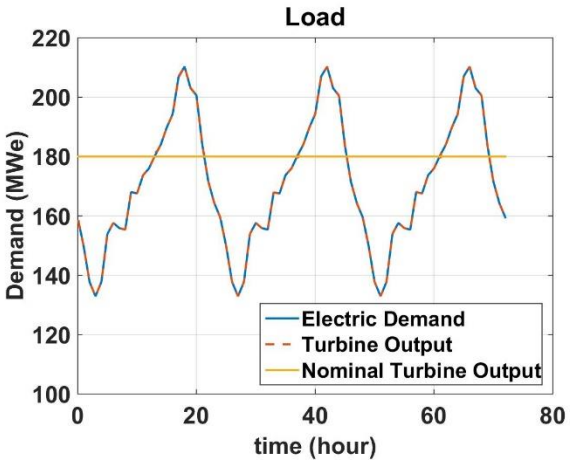

Figure 6.50: Turbine Output and Demand

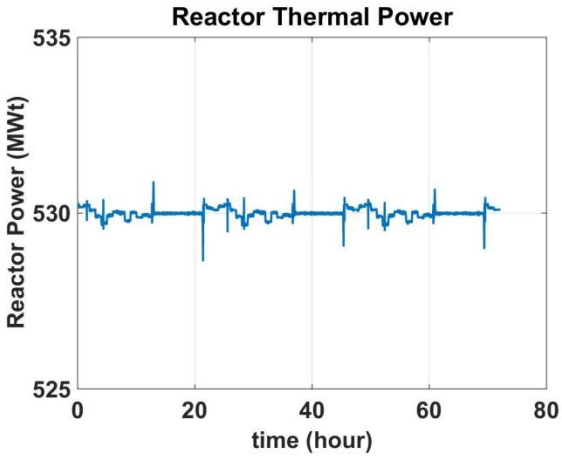

Figure 6.51: Reactor Power

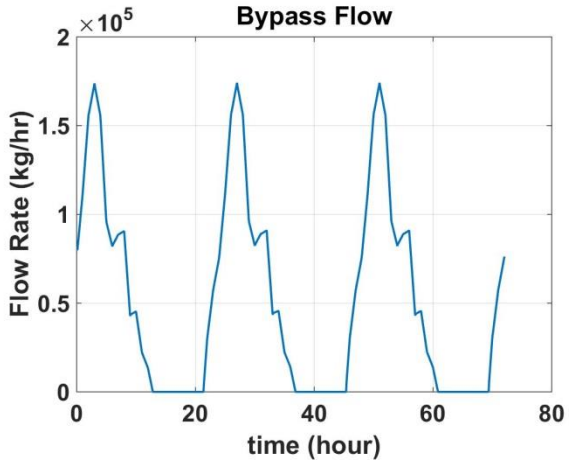

Figure 6.52: Auxiliary Bypass Flow

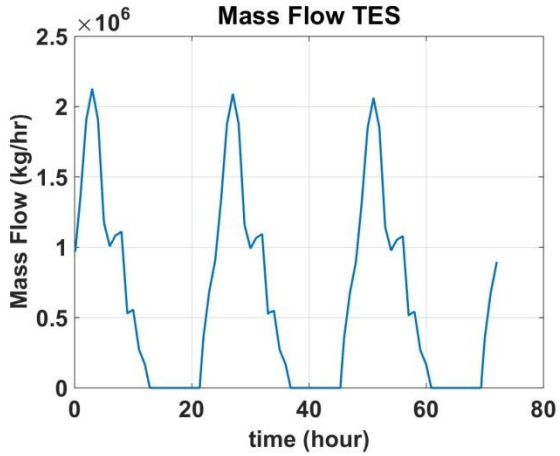

Figure 6.53: Flow of TES Fluid from Cold Tank to Hot Tank

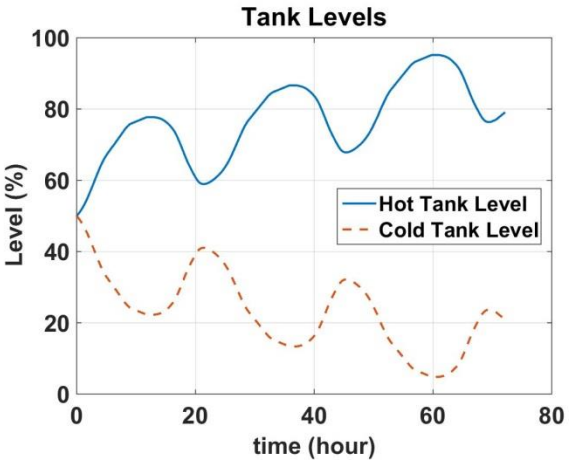

Figure 6.54: Hot and Cold Tank Level

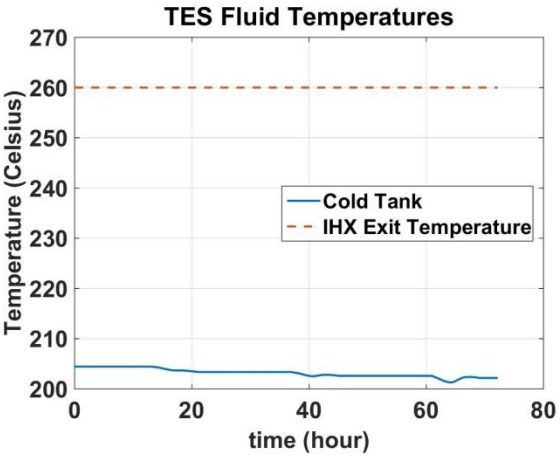

Figure 6.55: TES Fluid Temperature

6.3.2. Three Summer Days with 15% Solar Penetration (Third Day Cloudy)

The second of the simulations is three summer days with 15% solar penetration where the third day is cloudy, thus limiting the solar output. Figure 6.56 and Figure 6.57 demonstrate that load is met throughout the entire 72 hour run while maintaining nominal reactor thermal output. Bypass into the TES system and TES fluid flow from the cold tank to the hot tank is roughly the inverse of the load as shown in Figure 6.58 and Figure 6.59. Figure 6.60 demonstrates the effect of a cloudy day on realigning tank levels. During the first two sunny days, when nominal solar output is present, the hot tank goes from 50% full to about 70% full. However, the following 24 hours when only 10% nominal solar output

is available the additional peaking requirements causes the hot tank to drop to ~40% full. This weather variability necessitates the need for additional charging on days when nominal renewable output is available. The TES fluid temperature entering the hot tank is again maintained at the reference set point as seen in Figure 6.61.

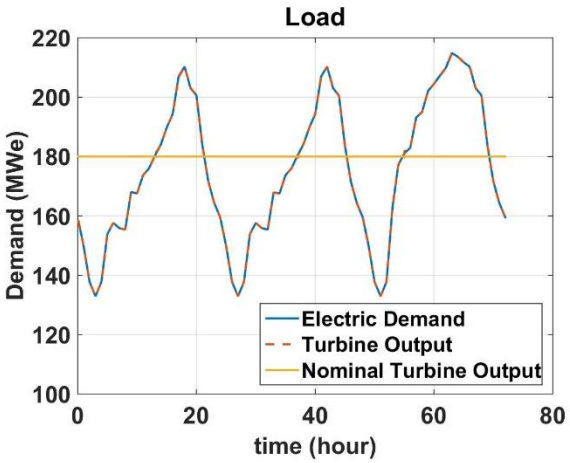

Figure 6.56: Turbine Output and Demand

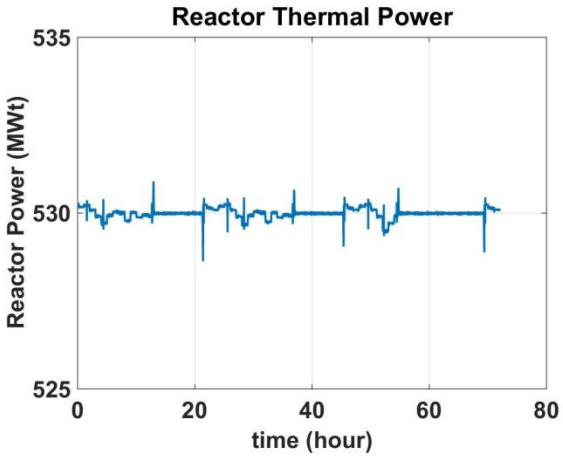

Figure 6.57: Reactor Power

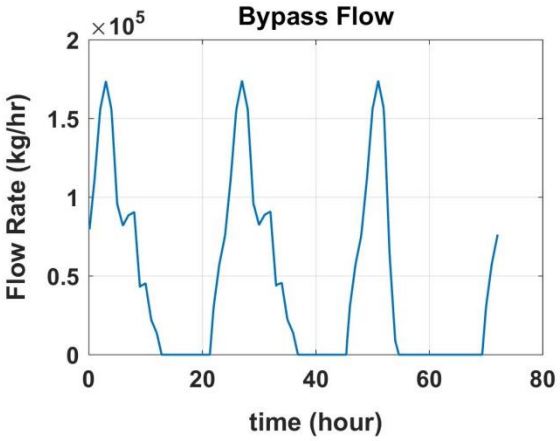

Figure 6.58: Auxiliary Bypass Flow

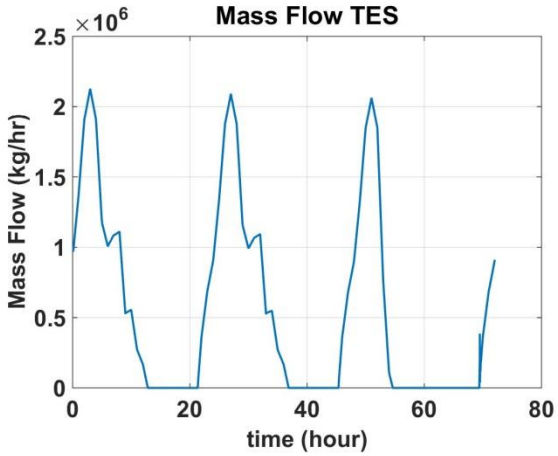

Figure 6.59: Flow of TES Fluid from Cold Tank to Hot Tank

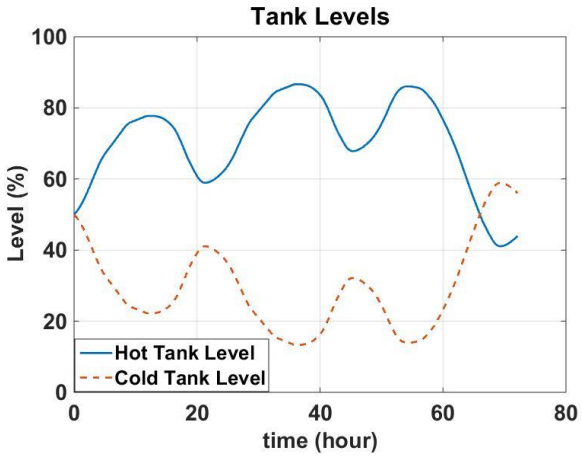

Figure 6.60: Hot Tank and Cold Tank Level

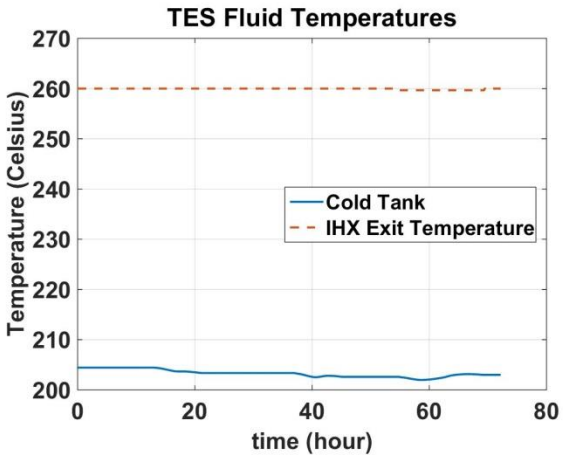

Figure 6.61: TES Fluid Temperature

6.3.3. Three Winter Days with 15% solar penetration

In addition to typical diurnal electric demand there is also seasonal demand. To further test system versatility, a three day winter run was completed with 15% solar penetration. The first and third days are sunny days with nominal solar output while the second day is rainy and overcast. It can be seen in Figure 6.62 and Figure 6.63 that the load is met while reactor power is maintained at approximately 100%. Mass flows through the TES system and tank levels are shown in Figure 6.64 through Figure 6.66. TES exit fluid temperature is maintained at the reference 260C throughout.

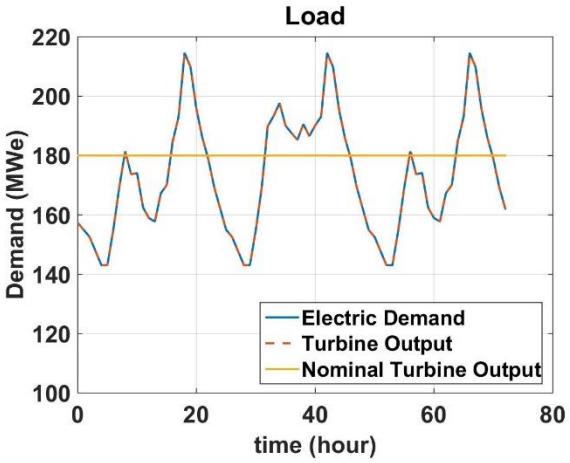

Figure 6.62: Turbine Output and Demand

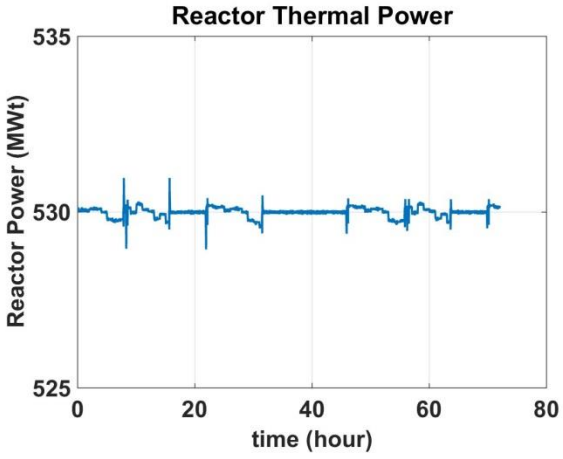

Figure 6.63: Reactor Power

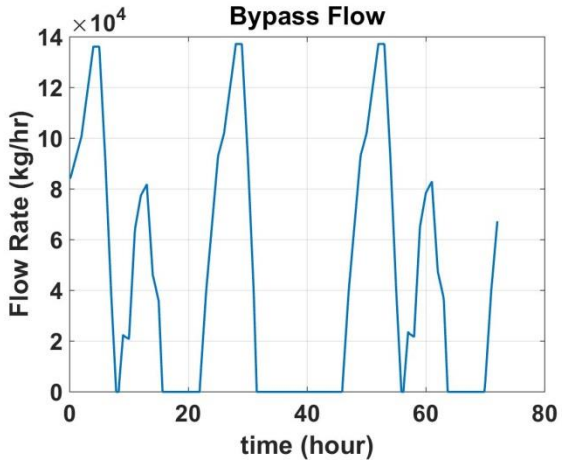

Figure 6.64: Auxiliary Bypass Flow

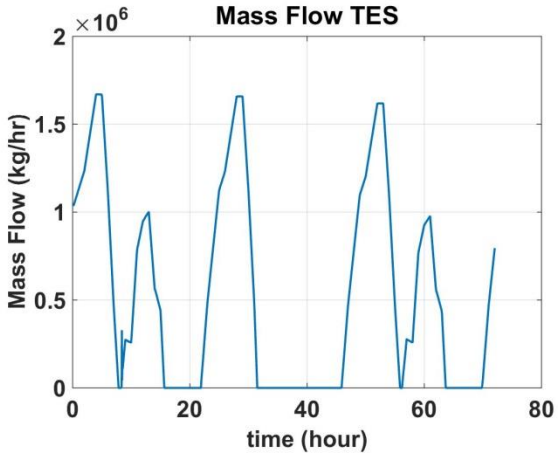

Figure 6.65: Flow of TES Fluid from Cold Tank to Hot Tank

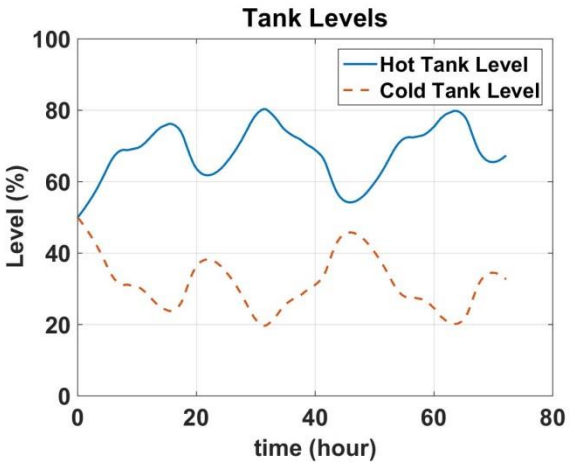

Figure 6.66: Hot Tank and Cold Tank Level

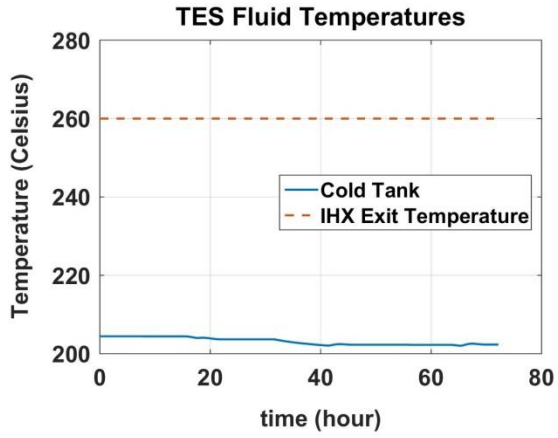

Figure 6.67: TES Fluid Temperature

6.4 Steam Applications

As opposed to using the TES system to supplement electric demand the system can alternatively be used for process steam applications. These applications include chilled water production and water desalination. Desalination can be accomplished through two main methods. One is Reverse Osmosis which just requires electrical input. Multi-stage flash desalination on the other hand requires a constant steam supply [12]. Another process considered is chilled water production using absorption chillers; this process requires low temperature, low pressure steam.

6.4.1. Multi-Stage Flash Desalination

Multi-stage flash desalination is a process that requires constant steam supply. The desalination process simulated is a 24 stage MSF system used to produce 7.2 MGD of product water requiring 189,100 kg/hr of steam at approximately 25 psia [52]. To show the capabilities of the TES system when configured to produce process steam, a 24 hour desalination run was simulated starting at midnight of a typical summer day with 226,500 m^3 tanks. While operating under these conditions, the TES system is both charging and discharging simultaneously. Over the 24 hour simulation period, turbine load and reactor power were kept at approximately 100% as shown in Figure 6.68 and Figure 6.69. Illustrated in Figure 6.70 bypass flow into the IHX is an x-axis reflection of the load as expected. TES fluid temperature entering the hot tank is maintained at the reference temperature and the target steam flow is met throughout the run. For this 24 hour simulation a 226,500m^3 tank size is sufficient for a single day. However, to support this level of continuous desalination in the long term would require the tanks to be sized consistent with expected daily demands. However, these results show that a TES system operating in conjunction with MSF desalination while simultaneously charging and discharging is feasible and capable of maintaining reactor power at 100%.

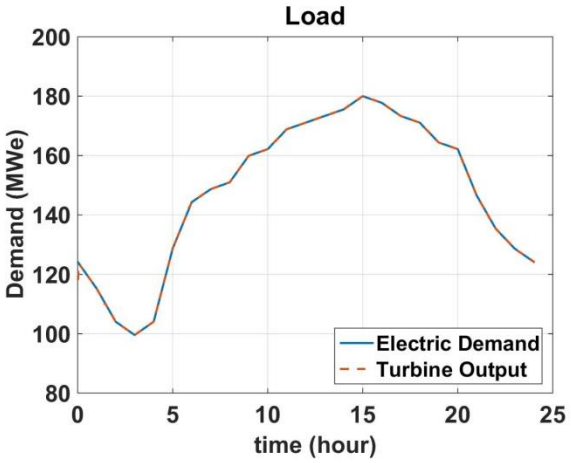

Figure 6.68: Turbine Output and Demand

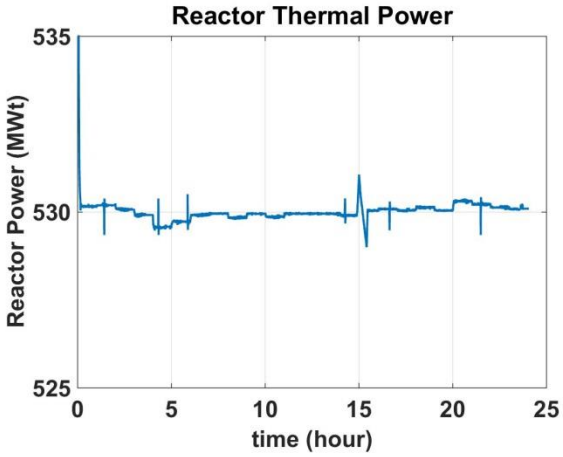

Figure 6.69: Reactor Power

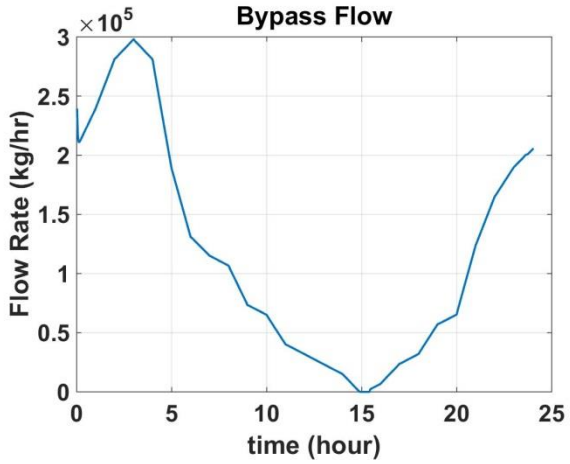

Figure 6.70: Auxiliary Bypass Flow

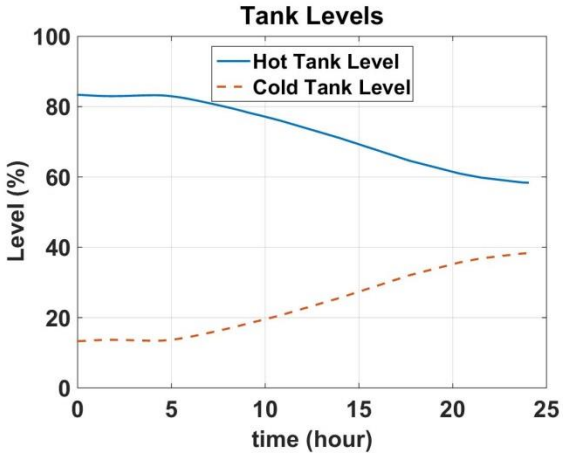

Figure 6.71: Hot Tank and Cold Tank Level

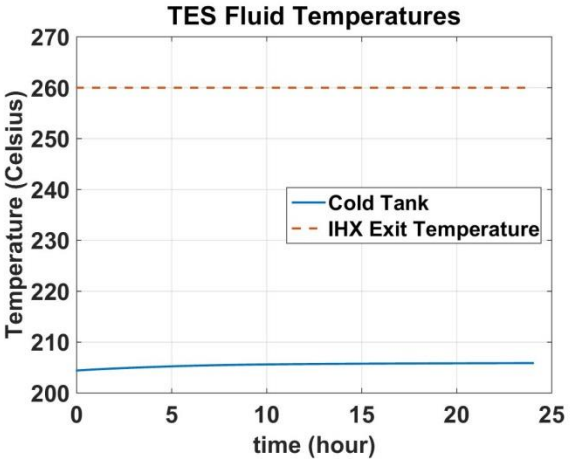

Figure 6.72: TES Fluid Temperature

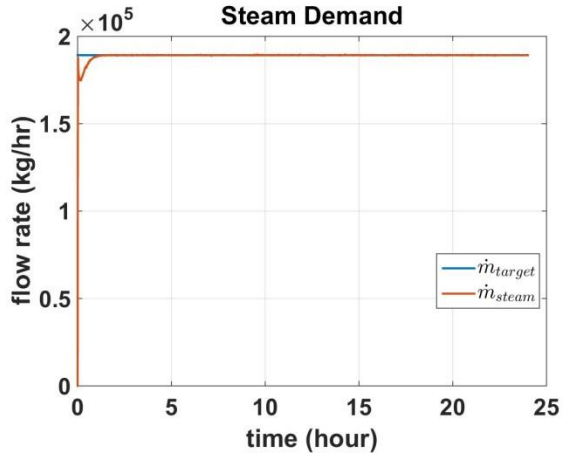

Figure 6.73: Ancillary Steam Demand and Flow

6.4.2. Chilled Water Production coupled to Flash Vessel Model

The large amount of condensate collected in the IHX hot well, provides additional opportunities for applications that can utilize low grade heat. This low grade heat is perfect for absorption chillers. This section explores coupling a chilled-water storage system to the flash vessel model. Previous studies completed by Misenheimer [53] have shown that using steam from a low-pressure turbine tap to supply absorption chillers is unable to significantly offset load variations and due to variations in steam conditions down stream of the turbine control valves is limited to narrow bands of operation. The flash vessel configuration has several benefits over the low-pressure turbine tap configuration. Specifically,

the flash vessel system enables use of condensate that would normally be dumped to the condenser. In addition, the various pressure control valves in Figure 5.1 modulate to maintain steam pressure sent to the chillers roughly constant, thereby ensuring more ideal absorption chiller operation. As mentioned in Chapter 1 absorption chillers are used in conjunction with a stratified chilled-water storage tank to offset cooling loads synonymous with an office space. Misenheimer [47] ran simulations showing absorption chiller performance when connected to the flash vessel model developed here. Runs were completed with electric demand identical to the load profile depicted in Figure 6.1 for a typical summer day. Further simulation details are available in Table 6.2.

Table 6.2: Absorption Chiller and Flash Vessel Parameters.

Parameter	Value
Number of 4,843 kW absorption chillers	4
Stratified chilled-water storage tank capacity	18,827 m^3 (5,000,000 gallons)
Size of conditioned office space	92,903 m^2 (1,000,000 ft^2)
Evaporator flow rate	0.208 m^3/s (3,305 gpm)
Condenser flow rate	0.31248 m^3/s (4,960 gpm)
Number of 3,407 kW cooling towers	13
Chiller valve open setpoint	Tank below 25%
Chiller valve close setpoint	Tank above 98%
Flash vessel volume	3,398 m^3 (120,000 ft^3)
Flash vessel condensate level setpoint	3.353 m (11 ft)
PCV_1; PCV_2; PCV_3; PCV_4 setpoint	241; 241; 248; 255 kPa (35; 36; 36; 37 psia)
$P_{impulse2}$ setpoint	212 kPa (30.7 psia)
$P_{chiller}$ setpoint	193 kPa (28 psia)

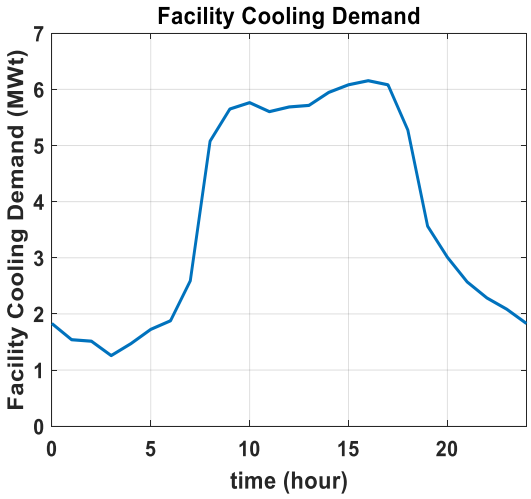

Figure 6.74: Facility cooling demand

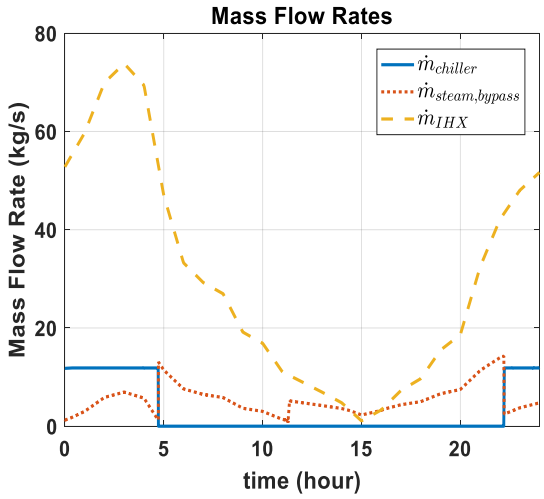

Figure 6.75: Mass flow rates

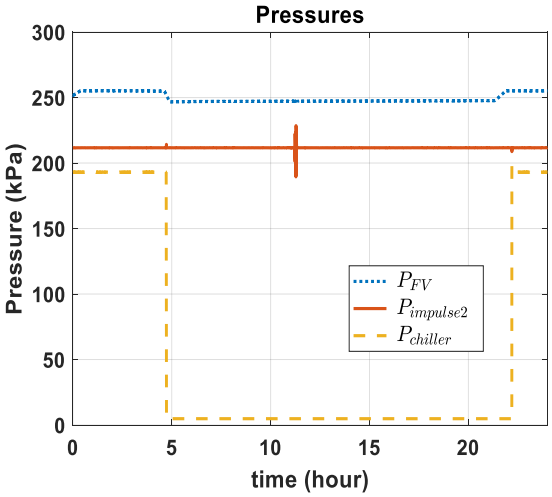

Figure 6.76: Flash vessel system pressures

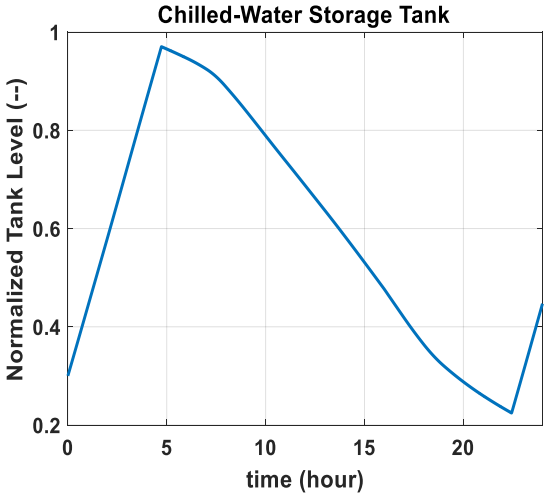

Figure 6.77: Stratified chilled-water storage tank level

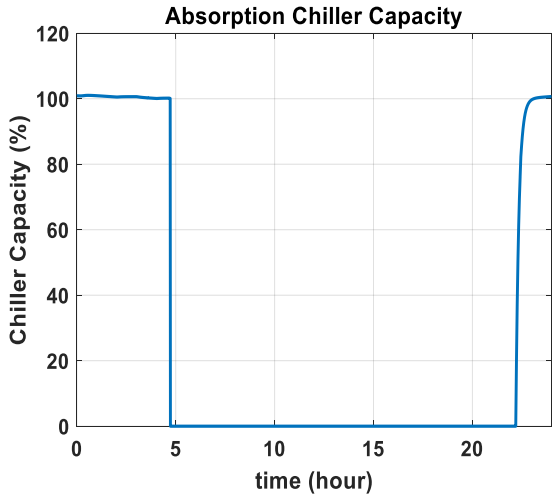

Figure 6.78: Absorption chiller capacity

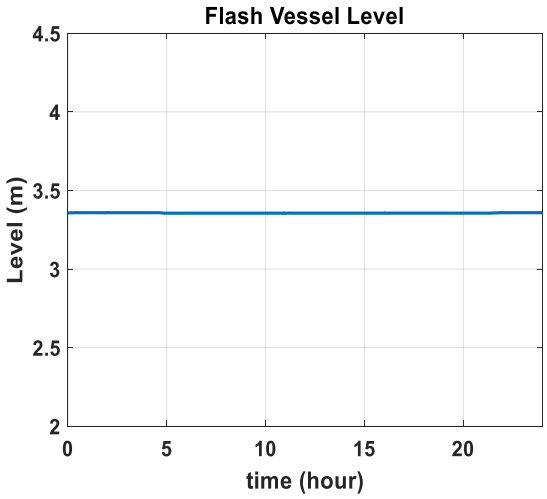

Figure 6.79: Condensate level in flash vessel

Simulation results run by Misenheimer [47] are depicted in Figure 6.75 through Figure 6.79. The simulations begin at midnight. The amount of mass flow into the flash vessel is governed by the operation of the ACV in the condensate line between the IHX of the TES system and the flash vessel. The ACV modulates to maintain condensate level in the IHX hotwell constant. Therefore, the condensate mass flow rate to the flash vessel, shown in Figure 6.75, is roughly the x-axis inverse of the electric demand curve illustrated in Figure 6.1, and a maximum during periods of low electric demand. The bank of four pressure control valves move based on their specific pressure setpoints in order to keep pressure in the flash vessel approximately constant. Each pressure control valve in the bank of four leaving the flash vessel is equipped with a unique setpoint, provided in Table 6.2. This control strategy enables the pressure in the flash vessel to stay roughly constant over the course of the simulation, as depicted in Figure 6.76. Meanwhile, Figure 6.79 shows that the LCV successfully modulates to maintain a fixed level of condensate in the flash vessel.

The success of the control strategies surrounding the flash vessel model enables near constant pressure steam to be delivered to the absorption chillers. As a result, the absorption chillers are able to achieve capacities in excess of 100%, as shown in Figure 6.78. High absorption chiller capacities mean that reduced chilled-water flow rates are not necessary in order to chill the water below the 7.2°C temperature threshold for storage and satisfying local facility cooling loads. The use of nominal chilled-water flow rates is twofold: the stratified chilled-water storage tank can be charged faster, and tank losses from mass and temperature diffusion across the thermocline are reduced at higher inlet and outlet storage tank flow rates. Lastly, four absorption chillers can consume a significant portion of the steam produced from flashing the high-pressure condensate in the flash vessel. Once the chilled water storage

tank becomes full, the absorption chillers are ramped down, and chilled-water in the tank is sent to the facility to satisfy HVAC loads. When the level in the tank falls below its lower setpoint, the chiller valve opens, the absorption chillers warmup, and chilled water is sent to the tank for storage. Unlike the low-pressure turbine tap configuration, the absorption chillers achieve nominal capacities during times of excess reactor capacity. Results demonstrate the ability to maintain the reactor thermal output at 100% and match turbine output with an electric demand profile characteristic of a typical summer day down to 60% load, while simultaneously using four large absorption chillers to charge a 18,927 m^3 stratified chilled-water storage tank to offset HVAC loads of an adjacent office space. Further studies completed by Misenheimer [47] on the functionality of this configuration have shown that using this configuration allows the absorption chiller system to piggyback on the existing TES reactor configuration throughout all foreseeable load profiles [47].

Chapter 7 Accident Scenarios

The addition of the TES System inherently increases the potential number of accident scenarios. A reactor trip results in lost hours of operation and profits and subjects the reactor to significant thermal and mechanical stresses. Thus, a TES caused trip would essentially eliminate the benefits of its addition. This section focuses on potential TES system accident scenarios and how different accident scenarios affect the reactor system. Accident scenarios considered are: auxiliary bypass valve tripped open, flow control valve tripped open, and hot tank full. Since the purpose of these simulations is to examine system behavior in the presence of TES component failures, rather than perform a Chapter 15 type safety analysis, normal control functions not associated with the failure were assumed to be active. While not exhaustive, these upsets provide some insight into potential threats to reactor safety due to the addition of the TES system. Reactor system trip set points outlined in Table 7.1 are consistent with the IRIS reactor [54], modified to reflect the different operating conditions of the mPower system. The system is configured as an electrical peaking unit consistent with simulations from Chapter 6.

Table 7.1: Reactor System Trip Setpoints [54].

Trip	Value
High Neutron Flux (% Nominal)	118
Low Reactor Coolant Flow (% Nominal)	87
Hogh Pressurizer Pressure (MPa)	16.64 (2414psia)
High Feedwater Flow (% Nominal)	108
Low Feedwater Flow (% Nominal)	75
Low Pressurizer Pressure (MPa)	13.79 (2000psia)
High Pressurizer Level (%)	95
Low Steam Generator Exit Temp (°C)	276.6 (530°F)

7.1 Auxiliary Bypass Valve Trips Open

The first accident scenario considered is one of the auxiliary bypass valves that connects the pressure equalization header with the TES charging system failing open. The bank of auxiliary bypass valves is a direct connection between the TES system and the reactor BOP. The most limiting case would occur with the valve going from full closed to full open. Since the bypass valves are normally open during times of low load it is more limiting to assume the valve fails open with the turbine at 100% load. This accident can be broken up into three distinct phases: Immediate effects [0 seconds, ~3 seconds], Intermediate effects [3 seconds, 18 seconds], and long-term effects [18 seconds, 58 seconds].

Immediate Effects [0 seconds, ~3 seconds]

At time zero one of the four banked auxiliary bypass valves fails open (Figure 7.1). As illustrated in Figure 7.2 the mass flow rate from the steam generator to the IHX increases causing the pressure in the steam generator to decrease (Figure 7.3). Even though steam flow exceeds feed flow (Figure 7.4), increased vapor generation due to depressurization causes a short term increase in the steam generator dryout location (Figure 7.5) and corresponding reduction in the steam generator exit temperature (Figure 7.6).

This initial increase in dryout position and reduction in secondary side pressure causes the primary coolant temperature to drop as the heat transferred to the secondary side increases (Figure 7.7). This drop in coolant temperature coupled with a large negative moderator temperature coefficient causes reactor power (Figure 7.8) to increase. The slight delay in this power increase is associated with the thermal time constant of both the fuel and primary coolant system.

Intermediate Effects [3 seconds, 18 seconds]

As steam generator pressure drops, the TCV's close to reestablish pressure control in the steam generator (Figure 7.9). Closing the TCVs reduces steam flow, turbine impulse pressure and turbine output as seen in Figure 7.3, Figure 7.4,and Figure 7.10. Following the short term increase in boiling length, steam flow in excess of feed flow results in a reduction in the boiling length and corresponding increase in the steam generator exit temperature.

Longterm Effects [18 seconds, 58 seconds]

Diversion of steam through the TBV results in turbine output not meeting demand (Figure 7.10). This causes the FCV to open to let more feed flow into the steam generator (Figure 7.14). Feed flow exceeds steam flow (Figure 7.4) increasing the dryout location (Figure 7.5). As the dryout location increases this leads to more surface area for effective heat transfer between the primary and secondary sides and ultimately leads to lower moderator temperatures and a higher average reactor power as reactor power tries to match the increased steam demand. Control rod motion is governed by two error signals, the first being the difference between average moderator temperature (T_{ave}) and reference T_{ave} (-) and the second being the difference between relative reactor power and relative turbine output (+). Control rod motion is limited due to the compensating effects of these two error signals (Figure 7.11). As the dryout location increases, this ultimately leads to the steam generator exit temperature decreasing to the point that the reactor is tripped at 58 seconds to ensure the steam generator does not overfill (Figure 7.6).

Increases in reactor power result in a decrease in Minimum DNB Ratio (Figure 7.12) and in increase in maximum fuel centerline temperature (Figure 7.13), though neither approach typical thermal limits.

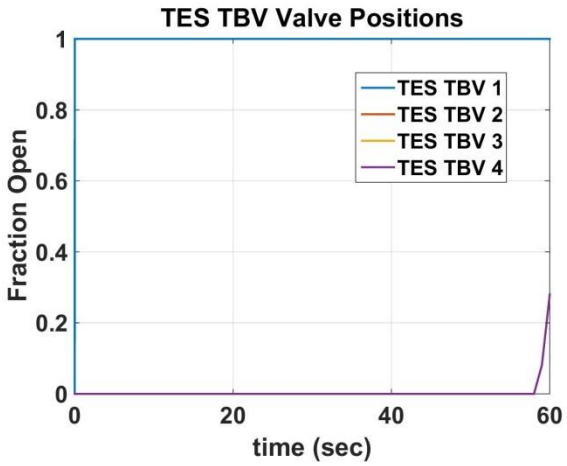

Figure 7.1: Auxiliary Bypass Valve Position

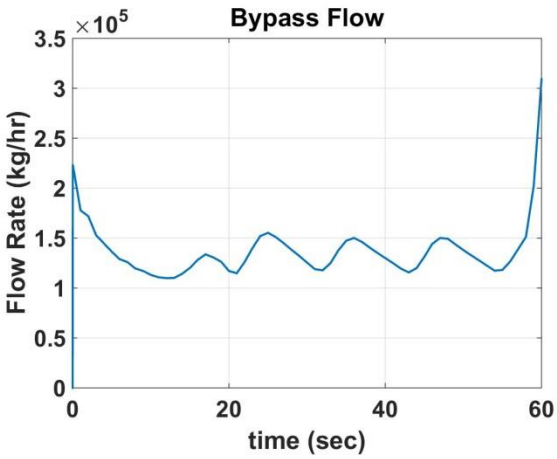

Figure 7.2: Auxiliary Bypass flow into IHX

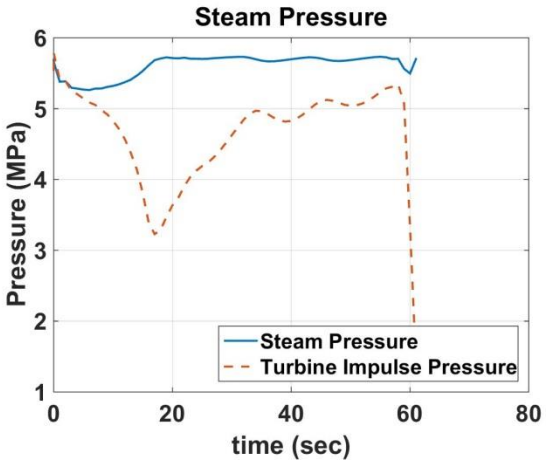

Figure 7.3: Steam Generator Pressure

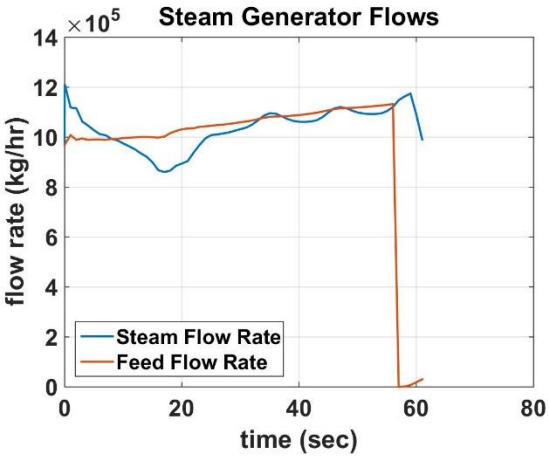

Figure 7.4: Steam Generator Flow Rates

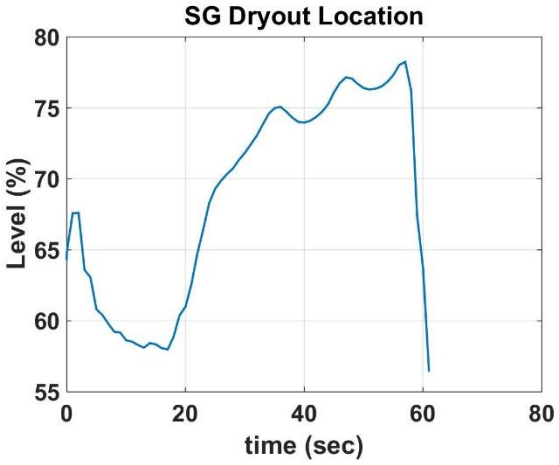

Figure 7.5: Steam Generator Dryout Location

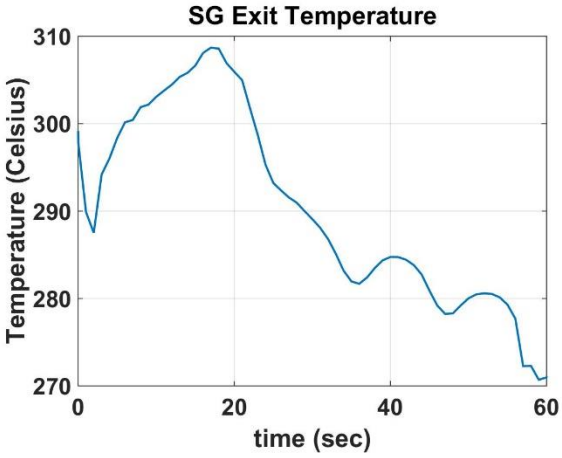

Figure 7.6: Steam Generator Exit Temperature

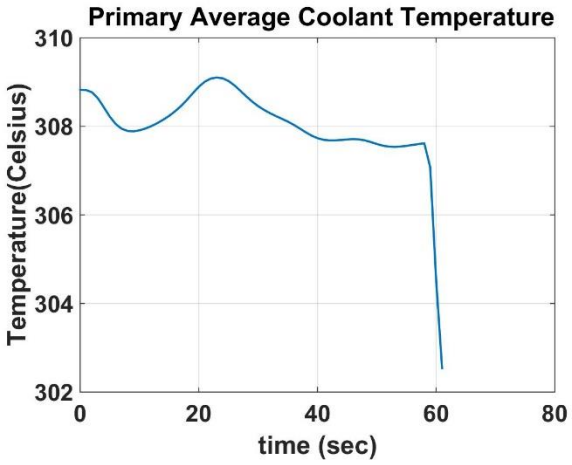

Figure 7.7: Primary Temperatures

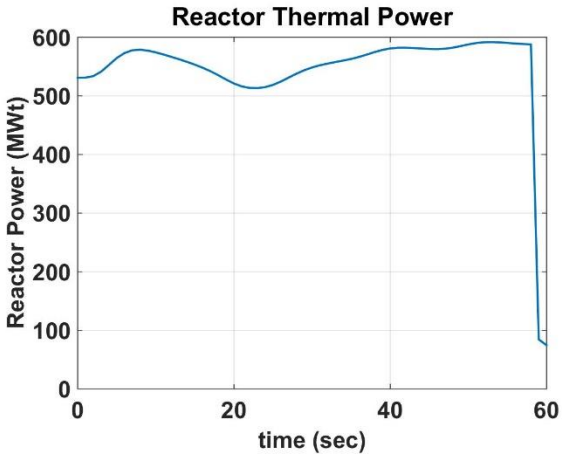

Figure 7.8: Reactor Power

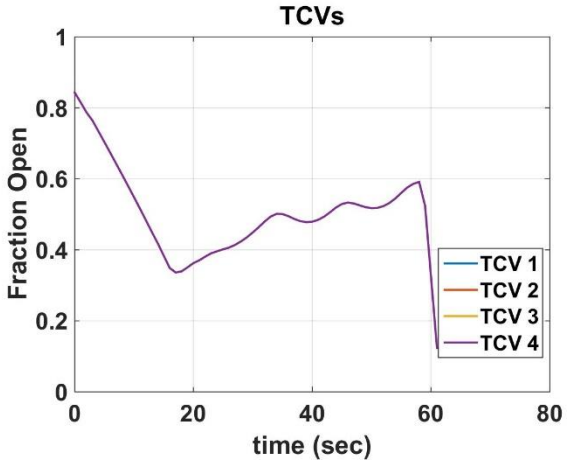

Figure 7.9: Turbine Control Valve Positions

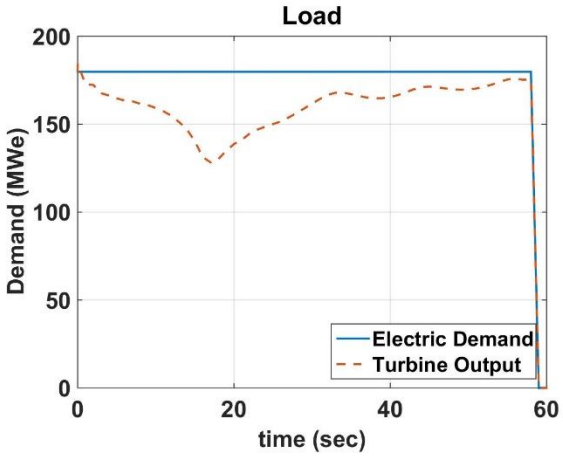

Figure 7.10: Turbine Output and Demand

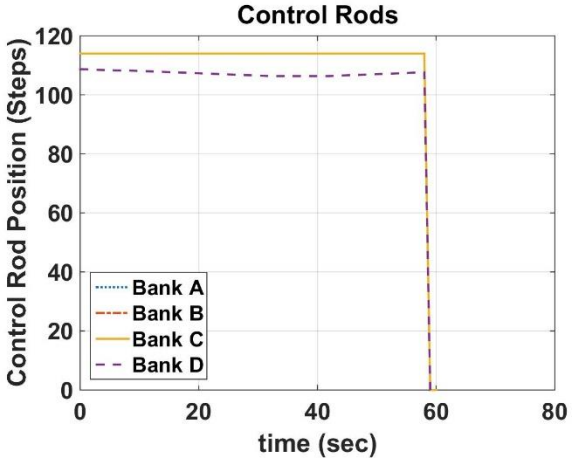

Figure 7.11: Control Rod Position

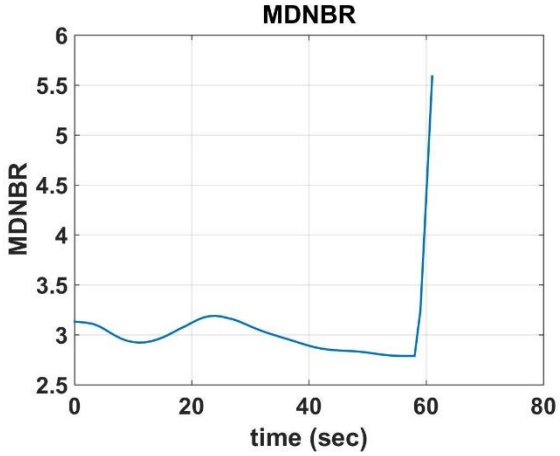

Figure 7.12: Minimum DNB Ratio

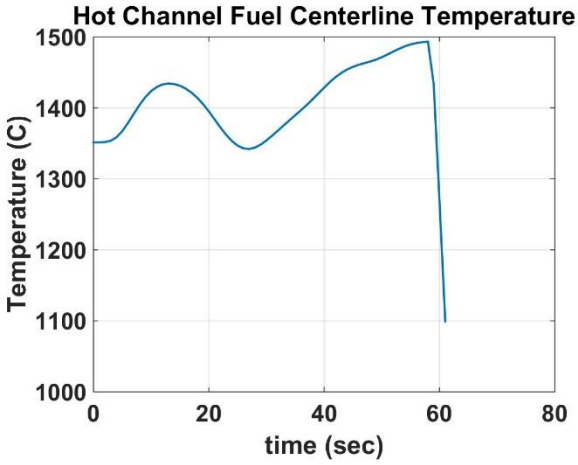

Figure 7.13: Fuel Centerline Temperature

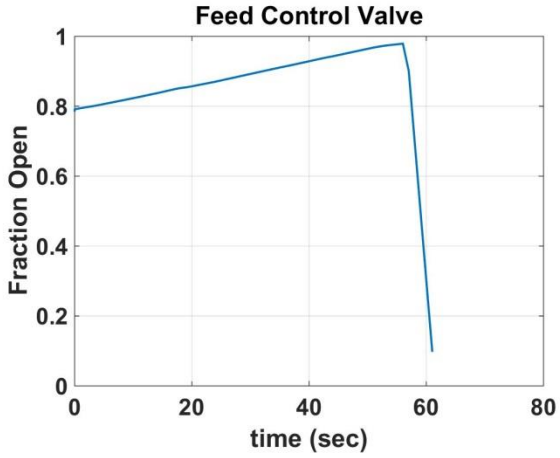

Figure 7.14: Feed Control Valve Position

7.2 TES Flow Control Valve Trips Open

An accident scenario unique to the addition of a Thermal Energy Storage System is if the flow control valve between the cold tank and the hot tank were to fail open. This scenario is most limiting at low power levels when the TES TBVs are open.

For this case the system is initially running at 88% capacity. This corresponds to a turbine output of 158.4 MWe. At time zero the FCV is instantly forced to full open as illustrated in Figure 7.16. Instantly, the mass flow between the cold tank and hot tank increases drastically thus increasing the heat transfer between the tube and shell sides. This increase in heat transfer leads to depressurization in the intermediate heat exchanger as shown in Figure 7.17. This depressurization allows for more bypass flow into the IHX ultimately leading to a slight decrease in steam generator pressure seen in Figure 7.20. This decrease in pressure causes an increase in heat transfer between the primary and secondary sides and a slight decrease in primary temperature. This leads to the minor increase in reactor power seen in Figure 7.15. However, this increase is less than a megawatt and insignificant. The slight increase in reactor power leads to a slight increase in steam generator pressure (Figure 7.20) causing the TCVs to open (Figure 7.22) therefore causing an increase in the steam flow rate (Figure 7.21) and turbine output over the initial 200 seconds of the simulation (Figure 7.19).

Ultimately, the TES FCV being full open continues to depressurize the TES system until it reaches equilibrium at 220°C. Bypass is still being sent to the TES system, however because the TES FCV is full open there is no temperature control on the hot tank (Figure 7.18). In addition, as the TES TBV

controller is active, the reactor is maintained at 100% power and the load is being met. The end result is that the hot tank fills to capacity. Until this occurs this upset has little effect on the reactor.

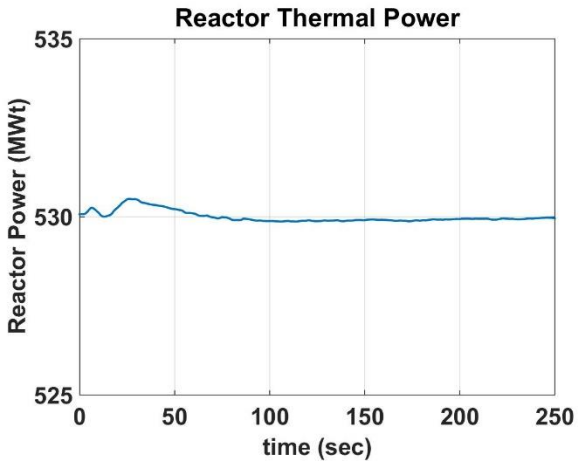

Figure 7.15: Reactor Thermal Output

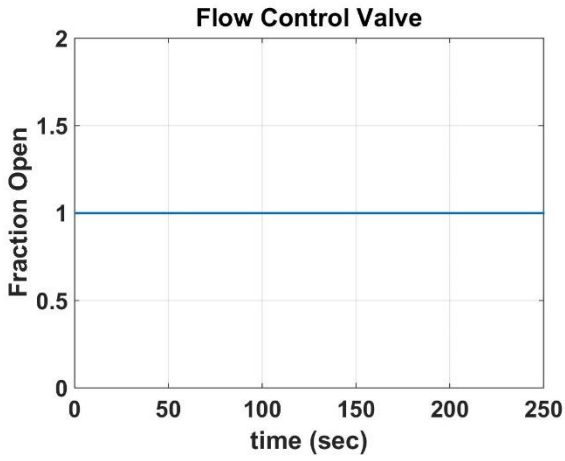

Figure 7.16: Flow Control Valve Position

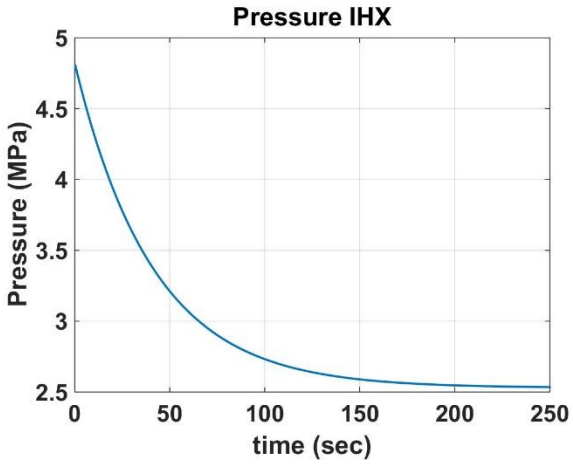

Figure 7.17: Pressure of the Intermediate Heat Exchanger

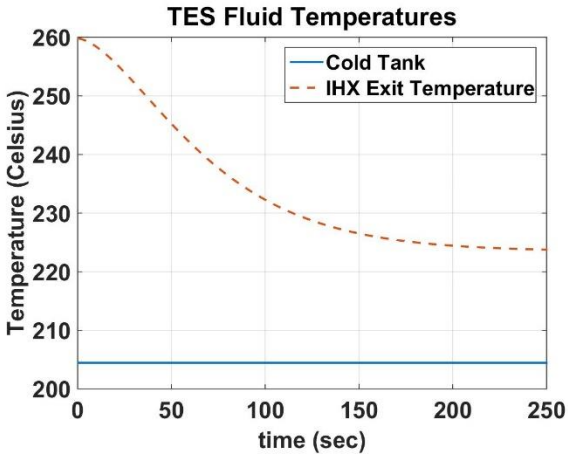

Figure 7.18: TES fluid temperature

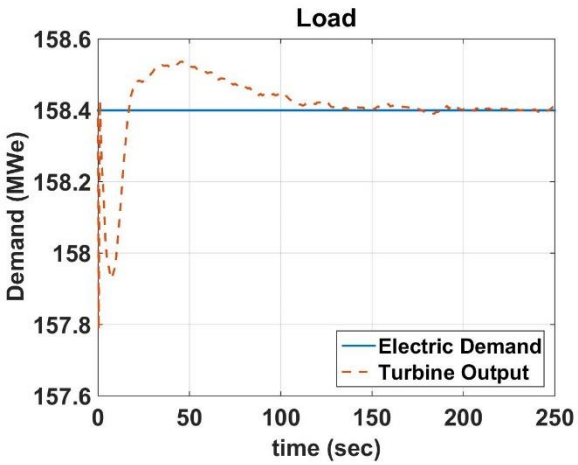

Figure 7.19: Turbine Output and Demand

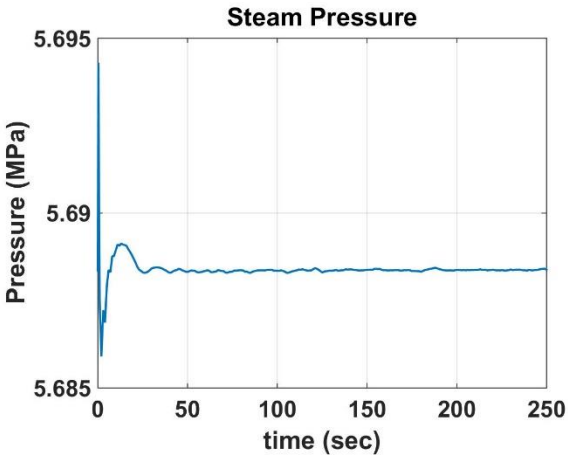

Figure 7.20: Steam Generator Pressure

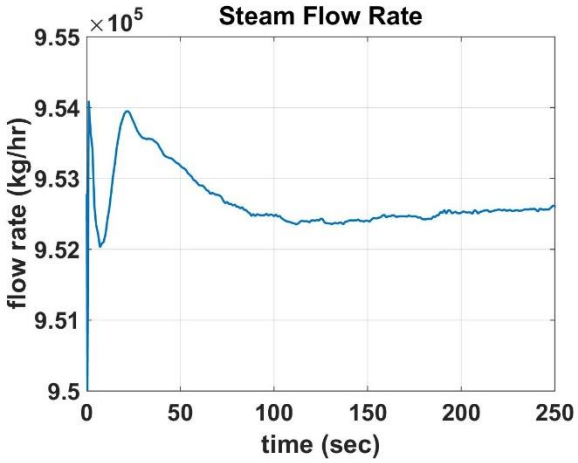

Figure 7.21: Steam Generator Steam Flow Rate

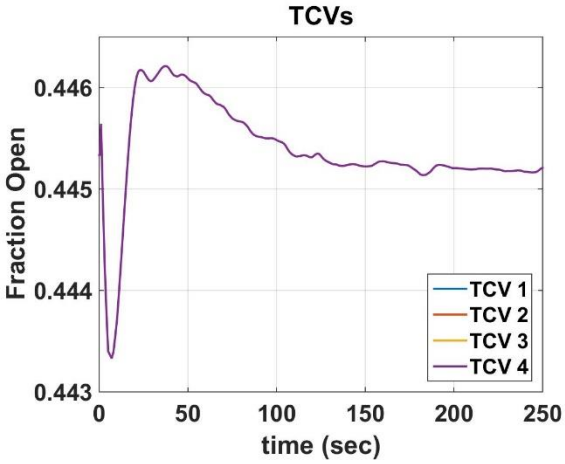

Figure 7.22: Turbine Control Valve Positions

7.3 Hot Tank Fills Up

The last scenario to be considered is when the hot tank fills to capacity and bypass flow is still being sent to the Intermediate Heat Exchanger. This condition will be most limiting at low power levels when the bypass demand is at its greatest. Simulation parameters for this run are as follows: Turbine Demand stable at 88% nominal load, hot tank 94% full with a stop valve set point of 95% full. For the first 700 seconds of the simulation everything runs normally. At 700 seconds the stop valve between the cold tank and hot tank closes as shown in Figure 7.24, stopping all flow in the line to ensure the hot tank does not overfill (Figure 7.28). At this point the heat transfer between the tube side and shell side of the

IHX is insufficient to condense the steam being sent into the intermediate heat exchanger. The pressure in the IHX rises rapidly until the pressure relief valve setpoint is hit as illustrated in Figure 7.25. At this point the PRV opens until the lower pressure setpoint is reached and the PRV closes. This oscillatory behavior continues indefinitely and ultimately causes the reactor power and load to oscillate in the same manner. However, the oscillations are not severe enough to trip the reactor. These oscillations will cause thermal and mechanical stress on the reactor but once these oscillations are recognized the TES system could be forced offline by an operator manually forcing the TES TBVs closed. One could also introduce an interlock system into the TES TBVs whereby if the stop valve closes the TES TBVs close. This would effectively put the reactor back in load follow mode. Finally, as opposed to the simple open/closed logic assumed here, the IHX PRV's could be programmed to modulate as conventional pressure control valves eliminating the oscillatory behavior.

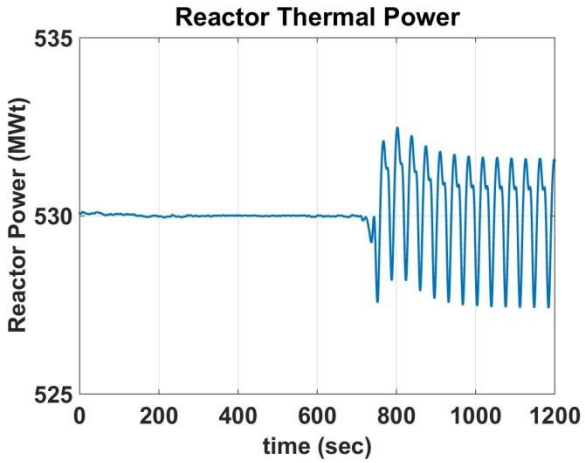

Figure 7.23: Reactor Thermal Power

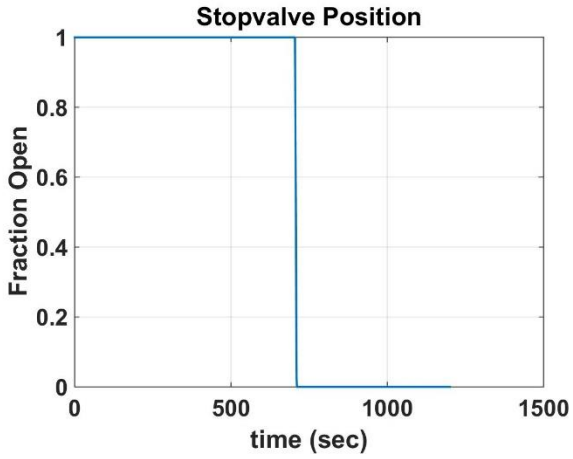

Figure 7.24: Stop Valve Position

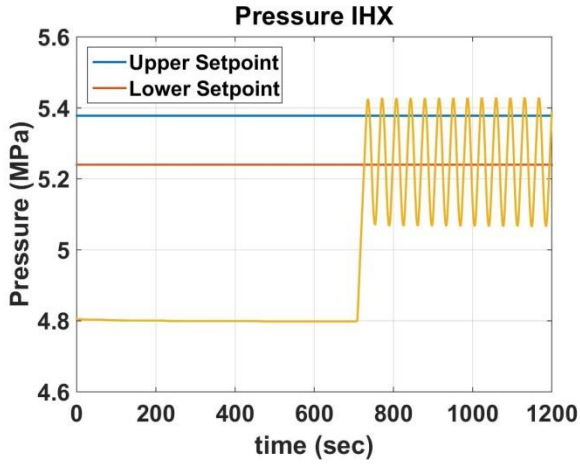

Figure 7.25: Pressure in the Intermediate Heat Exchanger

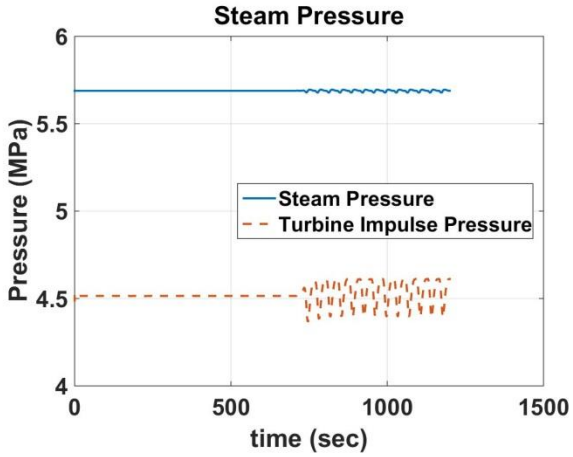

Figure 7.26: Steam Generator Pressure

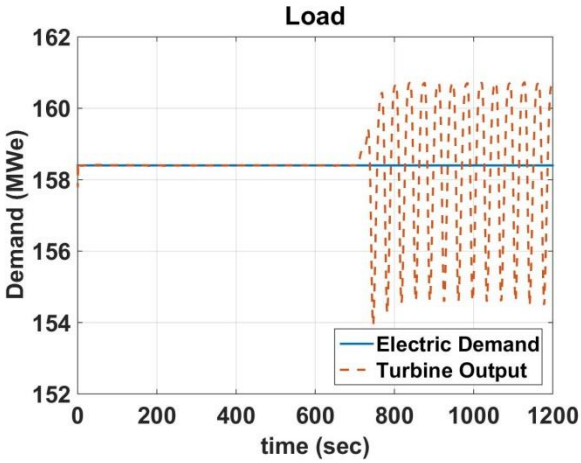

Figure 7.27: Turbine Output and Demand

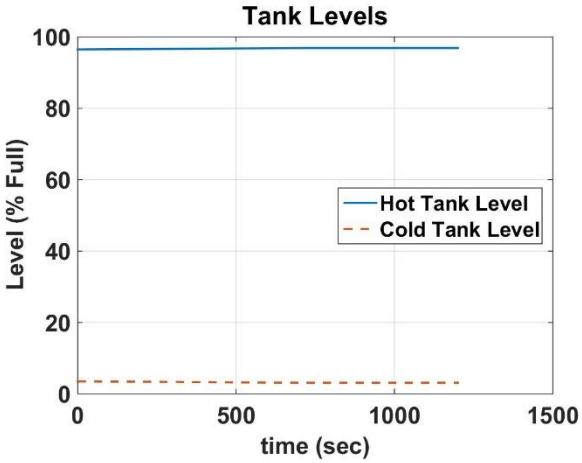

Figure 7.28: Tank Levels

Chapter 8 Conclusions

If SMRs are to be deployed in conjunction with intermittent power sources such as wind and solar, load variations can be significant. Current SMR designs allow for bypass off the pressure equalization header prior to the turbine control valves thus providing approximately constant steam conditions perfect for sensible heating thermal energy storage systems. This study investigates the prospect of coupling existing small modular reactor designs with a two-tank sensible heat thermal energy storage system to minimize power swings during periods of variable electric load.

The results presented demonstrate the feasibility of using TES systems coupled to Small Modular Reactors to minimize power swings during periods of variable electric load. During times of low electric demand, excess steam is bypassed into the TES system at a rate sufficient to maintain full reactor power. The thermal energy can be recovered later for either electric peaking or ancillary applications requiring steam such as multistage flash desalination.

Furthermore, it has been shown that the addition of the sensible heat storage system provides a source of high pressure, low grade heat that can be utilized for other process steam applications such as chilled-water production. The additional ancillary applications increase the overall efficiency of the system increasing its economic benefit.

Coupling the TES system to the reactor inherently introduces potential accident scenarios. Of the limited accident scenarios considered only TES TBV valve failure caused any significant concern. However, existing reactor trip set points caught the failure and tripped the reactor on low steam generator exit temperature. The other two accidents: hot tank fill up and TES FCV failure produced only minor perturbations in nominal system parameters.

With the implementation of these TES systems, decreases in capacity factor and increased stresses on plant components associated with load follow operation can be minimized, improving economic return over the lifespan of the reactor.

.

REFERENCES

[1] Appunn, K (2017, January 02). Why power prices turn negative. Retrieved December 4, 2017, from https://www.cleanenergywire.org/factsheets/why-power-prices-turn-negative.

[2] P. Denholm, M. O'Connel, G. Brinkman and J. Jorgenson, "Overgeneration from solar energy in California: a field guide to the duck chart, National Renewable Energy Laboratory (NREL), Denver, CO, NREL/TP-6A20-65023," 2015.

[3] "Renewable Energy and Electricity," 20 June 2016. [Online]. Available: http://www.worldnuclear.org/information-library/energy-and-the-environment/renewable-energy-and-electricity.aspx. [Accessed 08 July 2016].

[4] "Western Wind and Solar Integration Study Dataset," [Online]. Available: http://www.nrel.gov/electricity/transmission/wind_integration_dataset.html. [Accessed 19 March 2015].

[5] D. INGERSOLL, C. COLBERT, Z. HOUGHTON, R. SNUGGERUD, J. GASTON, and M. EMPEY. "Can Nuclear Power and Renewables Be Friends?" *Proceedings of ICAPP* (2015): 3129-3137. Print.

[6] S. M. Bragg-Sitton, R. Boardman, C. Rabiti, J. S. Kim, M. McKellar, P. Sabharwall, J. Chen, M. S. Cetiner, T. J. Harrison and L. A. Qualls, "Nuclear-Renewable Hybrid Energy Systems: 2016 Technology development program plan, Idaho National Laboratory (INL), Idaho Falls, ID, INL/EXT-16-38165," 2016.

[7] J. Pollak, "California's New Desalination Plant Wins International Award," 24 April 2016. [Online]. Available: http://www.breitbart.com/california/2016/04/24/san-diego-desalination-plant-winsinternational-award/. [Accessed 25 June 2016].

[8] P. Rogers, "Nation's largest ocean desalination plant goes up near San Diego; Future of the California coast?," 29 May 2014. [Online]. Available: http://www.mercurynews.com/science/ci_25859513/nationslargest-ocean-desalination-plant-goes-up-near. [Accessed 25 June 2016].

[9] "How Desalination by Multi-stage Flash Distillation Works," brighthubengineering.com, 23 December 2009. [Online]. Available: http://www.brighthubengineering.com/power-plants/29623-how-desalinationby-multi-stage-flash-distillation-works/. [Accessed 25 June 2016].

[10] International Atomic Energy Agency, "Introduction of Nuclear Desalination : A Guidebook," Vienna, 2000.

[11] "How Does Reverse Osmosis Plant Work?," 23 December 2009. [Online]. Available: http://www.brighthubengineering.com/power-plants/29624-how-does-reverse-osmosis-plant-work/. [Accessed 25 June 2016].

[12] M. A. Darwish and N. M. Al-Najem, "Energy consumption by multi-stage flash and reverse osmosis desalters," Applied Thermal Engineering, pp. 399-416, 2000.

[13] "Hydrogen Production: Natural Gas Reforming," Office of Energy Efficiency and Renewable Energy, [Online]. Available: http://energy.gov/eere/fuelcells/hydrogen-production-natural-gas-reforming. [Accessed 27 June 2016].

[14] D. Ingersoll, Z. Houghton, R. Bromm, C. Desportes, M. McKellar and R. Boardman, "EXTENDING NUCLEAR ENERGY TO NON-ELECTRICAL APPLICATIONS," in The 19th Pacific Basin Nuclear Conference (PBNC 2014), Vancouver, 2014.

[15] Climate Action Tracker. (2017, November 6). Retrieved February 05, 2018, from http://climateactiontracker.org/countries/usa.html.

[16] United Nations (2016). *Paris Agreement*. Paris: United Nations.

[17] Office of Energy Efficiency & Renewable Technology, "Hydrogen Production: Electrolysis," [Online]. Available: http://energy.gov/eere/fuelcells/hydrogen-production-electrolysis. [Accessed 11 July 2016].

[18] J. Kim, S. Bragg-Sitton, and R. Boardman. “Status Report on the High-Temperature Steam Electrolysis Plant Model Developed in the Modelica Framework (FY17)”. United States. doi:10.2172/1408745. http://www.osti.gov/scitech/servlets/purl/140875.

[19] R. K. Suri, A. M. R. Al-Marafie, G. P. Maheshwari, F. Al-Juwayadal, S. Al-Jandal, K. Al-Madani, and H. Abushaid, “Experimental Investigation of Chilled-Water Storage Technique for Peak Power Shaving,” *Int. J. Refrig.*, **12**, pp.213-219.

[20] A. M. R. Al-Marafie, “Stratification Behaviour in a Chilled-Water Storage Tank,” *Int. J. Refrig.*, **10**, pp. 213-219 (1987).

[21] C. T. Misenheimer and S. D. Terry, “Modeling Hybrid Nuclear Systems with Chilled-Water Storage,” *ASME J. Energy Resourc. Technol.*, **100**, (2016).

[22] California Energy Commission, "Renewables Portfolio Standard (RPS)," 22 April 2016. [Online]. Available: http://www.energy.ca.gov/portfolio/. [Accessed 27 June 2016].

[23] National Renewable Energy Laboratory, "Ivanpah Solar Electric Generating System," 20 November 2014. [Online]. Available: http://www.nrel.gov/csp/solarpaces/project_detail.cfm/projectID=62. [Accessed 27 June 2016].

[24] K. Fagan, "Desalination plants a pricey option if drought persists," 15 February 2014. [Online]. Available: http://www.sfgate.com/news/article/Desalination-plants-a-pricey-option-if-drought-5239096.php. [Accessed 27 June 2016].

[25] H. Cooley and M. Heberger, "Key Issues for Seawater Desalination in California: Energy and Greenhouse Gas Emissions," Pacific Institute, 2013.

[26] DriveClean, "Hydrogen Fuel Cell," California Air Resources Board, [Online]. Available: http://www.driveclean.ca.gov/Search_and_Explore/Technologies_and_Fuel_Types/Hydrogen_Fuel_Cell. php. [Accessed 27 June 2016].

[27] Electric Light and Power, "SDG&E energizes 117 mile, 500,000 volt transmission line," 18 June 2012. [Online]. Available: http://www.elp.com/articles/2012/06/sdg-e-energizes-117-mile-500-000-volttransmission-line.html. [Accessed 27 June 2016].

[28] C. McDaniel, "Solar Energy in Yuma a boon for electric grid," 18 January 2015. [Online]. Available: http://www.yumasun.com/business/solar-energy-in-yuma-a-boon-for-electric-grid/article_46f6652c9d44-11e4-a3be-efafa287ff9e.html. [Accessed 18 July 2016].

[29] F. Weaver, "The unprecedented water crisis of the American Southwest," theweek.com, 01 February 2014. [Online]. Available: http://theweek.com/articles/451876/unprecedented-water-crisis-americansouthwest. [Accessed 25 June 2016].

[30] S. Bragg-Sitton, R. Boardman, J. Collins, M. Ruth, O. Zinaman and C. Forsberg, Integrated NuclearRenewable Energy Systems: Foundational Workshop Report, Idaho National Laboratory, 2014.

[31] "Iowa: State Profile and Energy Estimates," U.S. Energy Information Administration, 17 March 2016. [Online]. Available: http://www.eia.gov/state/analysis.cfm?sid=IA. [Accessed 25 June 2016].

[32] "Coal Plant Retirements," [Online]. Available: http://www.sourcewatch.org/index.php/Coal_plant_retirements. [Accessed 08 July 2016].

[33] K. Powell and T. Edgar, "Modeling and control of a solar thermal power plant with thermal energy storage”.," Chemical Engineering Science, vol. 71, pp. 138-145, 2012.

[34] S. Kuravi, J. Trahan, D. Y. Goswami, M. Rahman and E. Stefanakos, "Thermal energy storage technologies and systems for concentrating solar power," Progress in Energy and Combustion Science, vol. 39, pp. 285- 319, 2013.

[35] Advances in Small Modular Reactor Technology Developments; A supplement to IAEA Advanced Reactors Information System (ARIS), IAEA (2014)

[36] H. Shen, “Advanced Feedwater Control for Next Generation Nuclear Power Systems,” PhD Thesis, Nuclear Engineering Department, North Carolina State University, (2006).

[37] Alan S. Rominger and J. Michael Doster , “Fast Valving for Small and Medium Sized Reactors”, Proceedings of the 7th International Topical Meeting on Nuclear Plant Instrumentation, Control and Human Machine Interface Technologies (NPIC&HMIT 2010) Las Vegas, Nevada, November 2010

[38] Alan S. Rominger and J. Michael Doster , “Benefits of Small Modular Reactors for Challenging Electric Grid Operation”, Proceedings of the 8th International Topical Meeting on Nuclear Plant Instrumentation, Control and Human Machine Interface Technologies (NPIC&HMIT 2012) San Diego, CA, July, 2012

[39] Andrew J. Petrarca and J. Michael Doster, “Low Power Feedwater Control in Helical Steam Generators”, Proceedings of the 8th International Topical Meeting on Nuclear Plant Instrumentation, Control and Human Machine Interface Technologies (NPIC&HMIT 2012) San Diego, CA, July, 2012

[40] Sohal, M. S., Ebner, M. A., Sabharwall, P., & Sharpe, P. (March 2010). Engineering Database of Liquid Salt Thermophysical and Thermochemical Properties. Idaho National Laboratory. INL/Ext-10-18297

[41] *Therminol-66*; MSDS 150000093438 [Online]; Eastman Chemical Company: 200 South Wilcox Drive, Kingsport, TN 37660-5280, April 11,2017. http://ws.eastman.com/ProductCatalogApps/PageControllers/MSDS_PC.aspx?Product=71093438 (accessed Dec 04, 2017).

[42] OpenStax College, Chemistry OpenStax College. 11 March 2015. <http://cnx.org/content/col11760/latest/>.

[43] Solutia: Applied Chemistry, Creative Solutions*, Therminol 66: High Performance Highly Stable Heat Transfer Fluid.*

[44] Solutia: Applied Chemistry, Creative Solutions*, Therminol 68: Highly Stable Low Viscosity Heat Transfer Fluid.*

[45] Solutia*, Therminol 75: Synthetic, Aromatic, High-temperature Heat Transfer Fluid.*

[46] J. Doster, "Brent's Algorithm," [Online]. Available: http://www4.ncsu.edu/~doster/NE400/Computing/Brent.pdf. [Accessed 08 July 2016].

[47] C. Misenheimer, *Modeling Chilled-Water Storage System Components for Coupling to a Small Modular Reactor in a Nuclear Hybrid Energy System*, PhD Dissertation, Department of Mechanical and Aerospace Engineering, North Carolina State University, 2017.

[48] K. Frick*, Coupling and Design of a Thermal Energy Storage System for Small Modular Reactors,* Masters of Science Thesis, Department of Nuclear Engineering, North Carolina State University, 2016.

[49] Search Import Export Data of India. (n.d.). Retrieved December 04, 2017, from https://www.zauba.com/import-therminol 66-hs-code.html

[50] U.S. Energy Information Administration - EIA - Independent Statistics and Analysis. (n.d.). Retrieved December 04, 2017, from https://www.eia.gov/beta/realtime_grid/#/summary/demand?end=20160725 &start=20160625®ions=00g

[51] Richardson, L. (2017, May 09). Do Solar Panels Work at Night or On Cloudy Days? | EnergySage. Retrieved December 08, 2017, from https://news.energysage.com/solar-panels-work-night-cloudy-day/

[52] El-Dessouky, H. T., & Ettouney, H. M. (2002). *Fundamentals of Salt Water Desalination*. Amsterdam: Elsevier Science.

[53] C. Misenheimer, S. Terry, J.M. Doster, and S. Bragg-Sitton, "Analysis of a Nuclear Hybrid Energy System using Absorption Chillers and Stratified Chilled-Water Storage with an mPower Reactor," in *10th International Topical Meeting on Nuclear Plant Instrumentation, Control and Human Machine Interface Technologies*, San Francisco, CA, 2017.

[54] IRIS Preliminary Safety Assessment. WCAP-16082-NP. July 15,2003.

APPENDIX

TES Standalone System Response

9.1 NuScale Size System

The system was designed to accommodate 85% steam dump from a NuScale size system for 24 hours. To accommodate this demand, large storage tanks were installed. To ensure that neither tank over pressurizes the combined amount of TES fluid in both the hot and cold tanks is slightly less than what either one could hold on their own. System design parameters are given in Table 9.1.

Table 9.1: NuScale Size System Parameters

Parameter	Value
TES Fluid	Therminol®-66
Hot tank Volume	2,000,000 ft^3
Cold Tank Volume	2,000,000 ft^3
IHX reference Exit Temperature	500F
Number of TBV's	4
TES maximum steam accommodation	85% Nominal conditions of NuScale size reactor
Pressure Relief Valve Upper Setpoint	780 psi
Pressure Relief valve Lower Setpoint	735 psi
Turbine Header Pressure	825 psi
Shell Side (outer loop) IHX Volume	755.443 ft^3
Number of tubes	12190
Length of tubes	36 ft
Tube Inner Diameter	0.044 ft
Tube Outer Diameter	0.058 ft
Mass of Hot Tank Fill Gas	$1.122x10^5$ lbm
Mass of Cold Tank Fill Gas	$1.309x10^5$ lbm
Temperature of Cooling Water	50F
Volume of Condenser (Shell Side)	7607 ft^3
Number of tubes in Condenser	76824
Length of tubes in Condenser	24.1ft
Mass Flow of Cooling Water	$3.411x10^7$ lbm/hr
Condenser Tube Inner Diameter	0.044 ft
Condenser Tube Outer Diameter	0.058 ft

9.1.1 Aggressive Load Profile

To test the robustness of the TES system an aggressive load profile was made for the system ranging from 85% bypass all the way down to 30% bypass over a sixteen hour run. This load profile is not typical of standard electrical demand profiles and is only used to test the robustness of the TES system model. If this demand can be met then it stands to reason that other less aggressive profiles should be easily accommodated given proper sizing of the system.

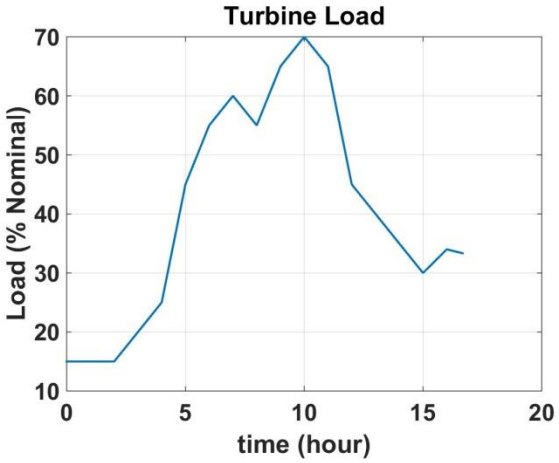

Figure 9.1: Aggressive Load Profile

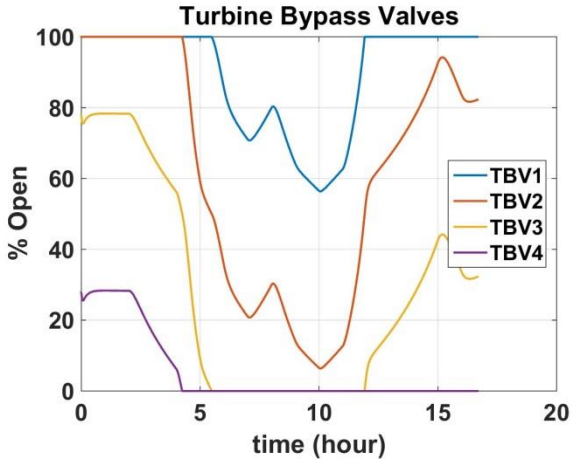

Figure 9.2: Auxiliary Bypass Valve Position

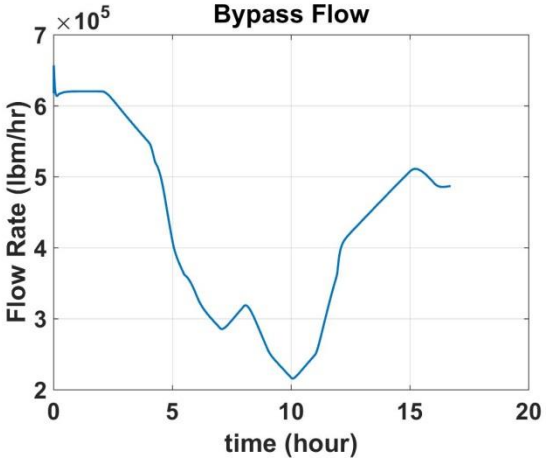

Figure 9.3: Bypass Flow

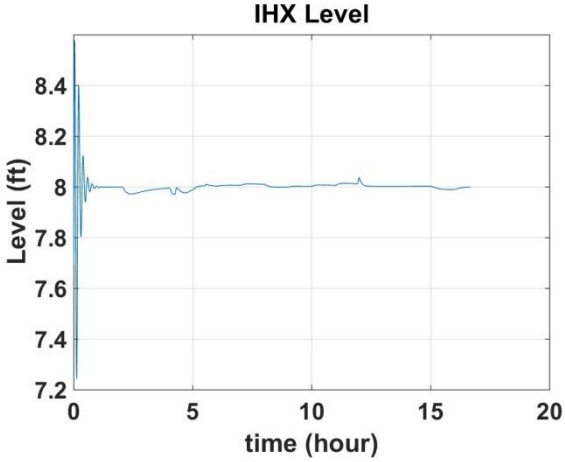

Figure 9.4: Level in the Intermediate Heat Exchanger

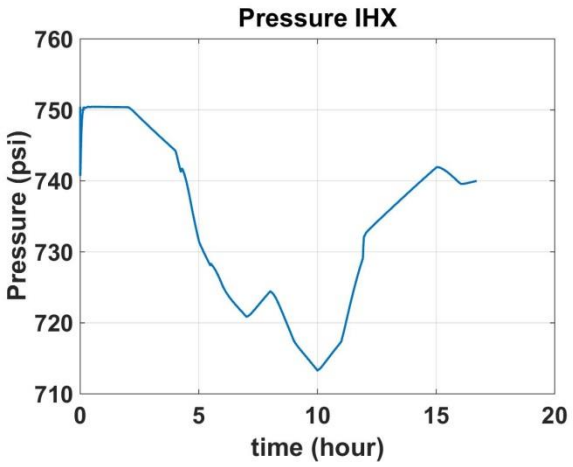

Figure 9.5: Pressure in the Intermediate Heat Exchanger

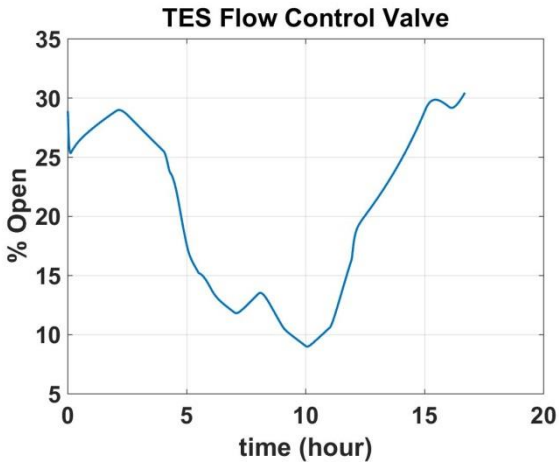

Figure 9.6: TES Flow Control Valve Position

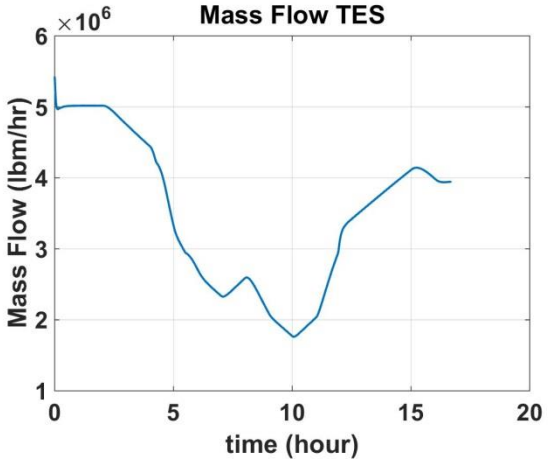

Figure 9.7: Mass Flow of the Therminol-66 from the cold tank to the hot tank

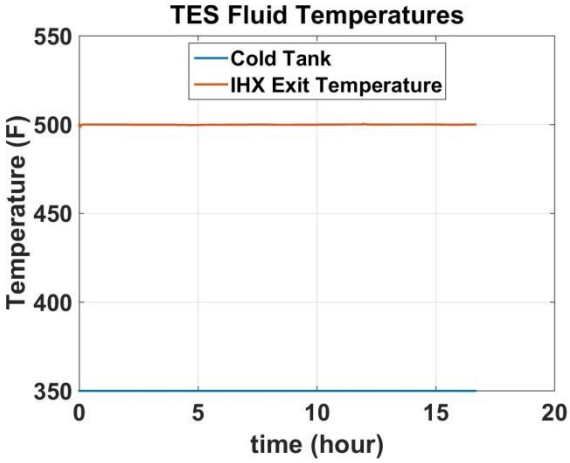

Figure 9.8 TES Fluid Temperature at exit of IHX

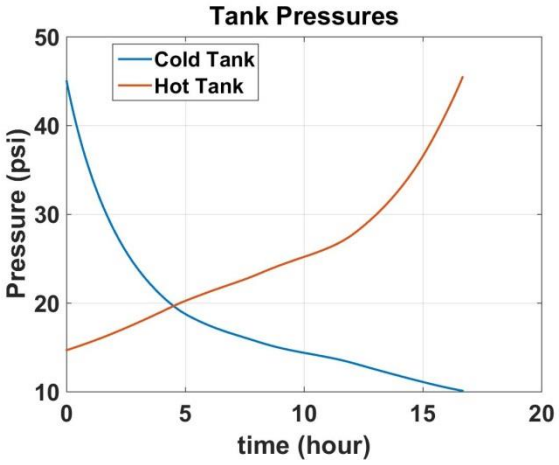

Figure 9.9 Hot and Cold Tank Pressures

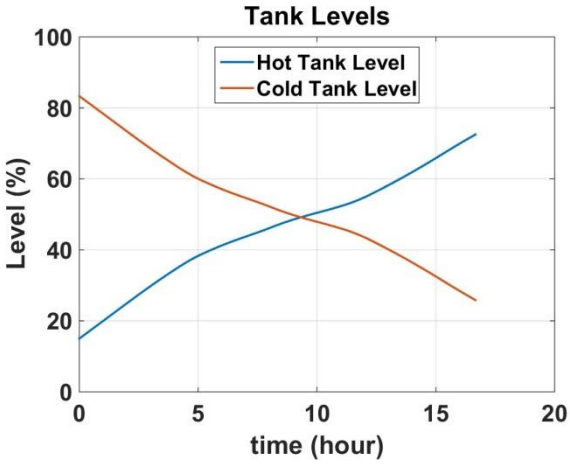

Figure 9.10: Hot and Cold Tank Levels

The system has a nominal output of ~160 MWth. As seen in Figure 9.1 the system initially starts with about 15% load on the turbine. This small turbine load means that the TES system is in full charging mode as 85% of the net reactor capacity is being pushed through the TES system. At this demand level all four of the auxiliary turbine bypass valves are open to allow steam into the IHX.

As the turbine load increases the bypass valves begin to close and subsequently the heat transfer rate to the inner loop decreases. When the heat transfer rate decreases so does the TES fluid exit temperature causing the FCV to close to keep the temperature at the set point value. The closing of the FCV reduces the charging rate between the hot and cold tanks as seen in Figure 9.7. At the end of the run the cold tank has gone from 82% full down to about 26% full while the hot tank has gone from 15% full up to about 72% full.

At the full design criteria of 85% steam dump with the cold tank relatively full, the FCV is ~25% open. This extra 75% capacity in the FCV is to accommodate full 85% steam dump when the hot tank approaches its design capacity.

9.2. mPower Size System

In the next scenario, a TES system designed to handle bypass from a mPower size reactor was simulated. mPower has an electric output of 180MWe with a 530MWth operating power. The TES system bypass lines have been designed to accommodate ~45%-50% bypass from the reactor at an IHX

shell side operating pressure of 750psi. The Condenser for this model has been designed to accommodate 530MW.

Table 9.2: Design Parameters for a mPower size TES system.

Parameter	Value
TES Fluid	Therminol®-66
Hot tank Volume	8,000,000 ft^3
Cold Tank Volume	8,000,000 ft^3
IHX reference Exit Temperature	500F
Number of TBV's	4
TES maximum steam accommodation	~45% Nominal
Pressure Relief Valve Upper Setpoint	780 psi
Pressure Relief valve Lower Setpoint	760 psi
Turbine Header Pressure	825 psi
Shell Side (outer loop) IHX Volume	1171 ft^3
Number of tubes	19140
Length of tubes	36.9 ft
Tube Inner Diameter	0.044 ft
Tube Outer Diameter	0.058 ft
Mass of Hot Tank Fill Gas	$5.235x10^5$ lbm
Mass of Cold Tank Fill Gas	$4.489x10^5$ lbm
Temperature of Cooling Water	50F
Volume of Condenser (Shell Side)	7607 ft^3
Number of tubes in Condenser	76824
Length of tubes in Condenser	24.1ft
Mass Flow of Cooling Water	$3.411x10^7$ lbm/hr
Condenser Tube Inner Diameter	0.044 ft
Condenser Tube Outer Diameter	0.058 ft

9.2.1. Typical Summer Day

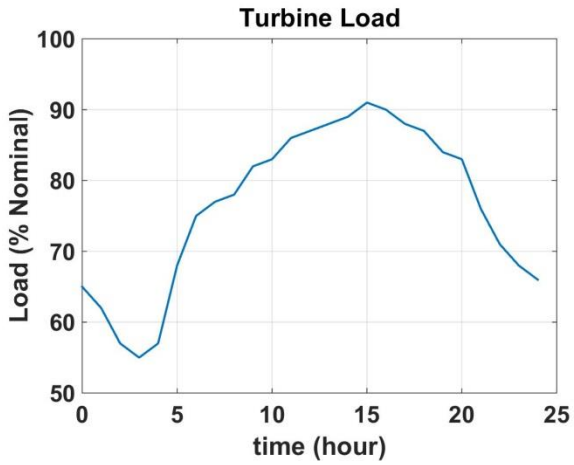

Figure 9.11: Summer Day Load Profile

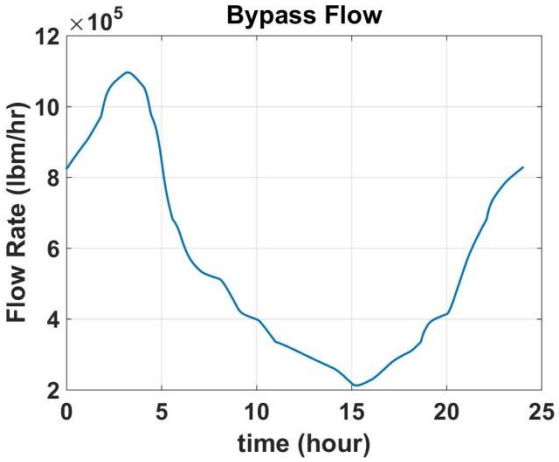

Figure 9.12: Bypass Flow

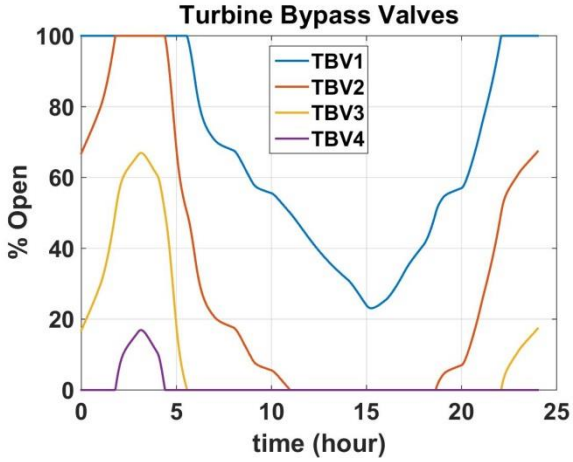

Figure 9.13: Position of TES Bypass Valves

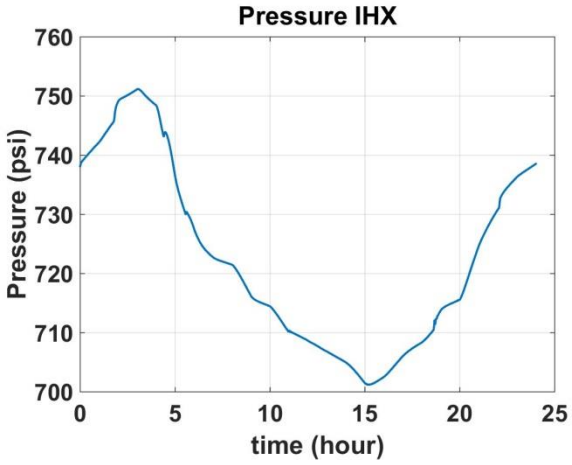

Figure 9.14: Intermediate Heat Exchanger Pressure

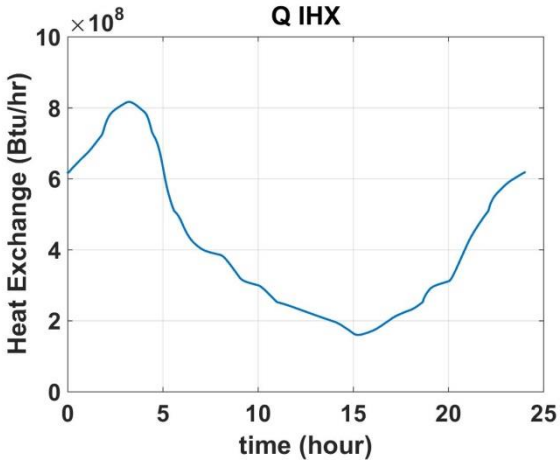

Figure 9.15: Heat Transfer Rate Across the Intermediate Heat Exchanger

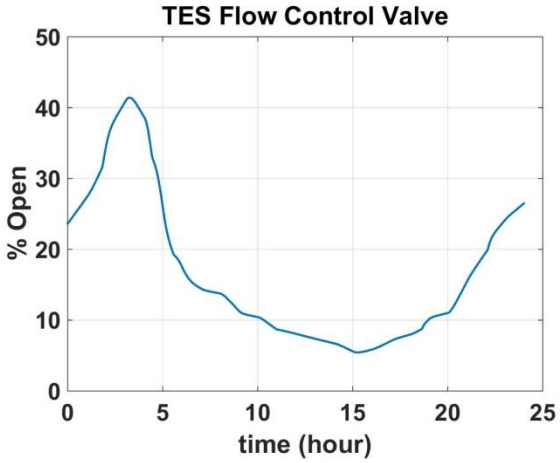

Figure 9.16: Position of TES Flow Control Valve

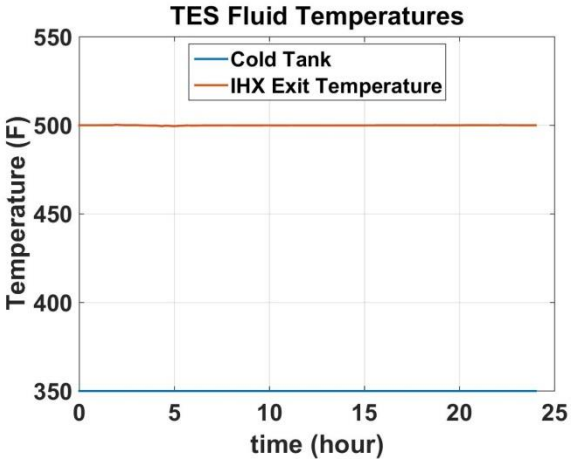

Figure 9.17: Temperature of the TES fluid leaving the IHX.

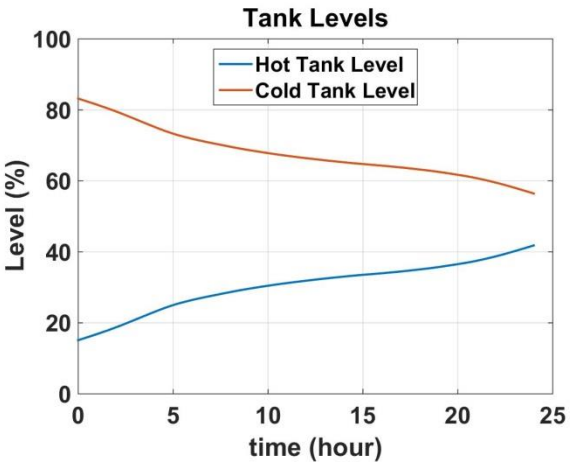

Figure 9.18: Hot and Cold Tank Levels

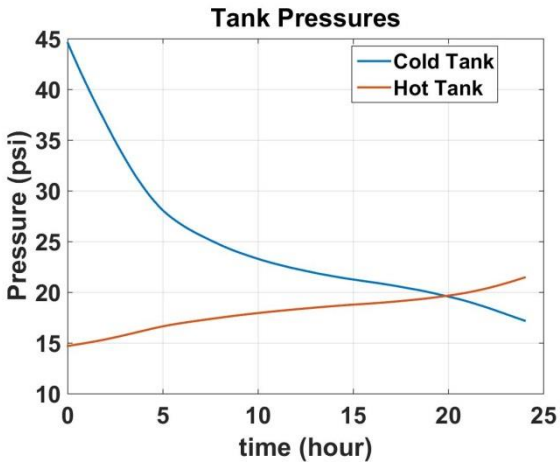

Figure 9.19: Hot and Cold Tank Pressures

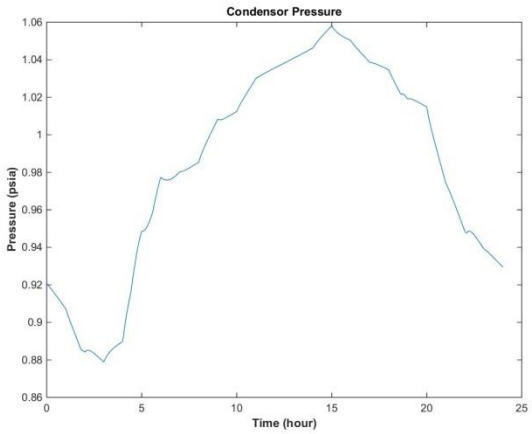

Figure 9.20: Condenser Pressure

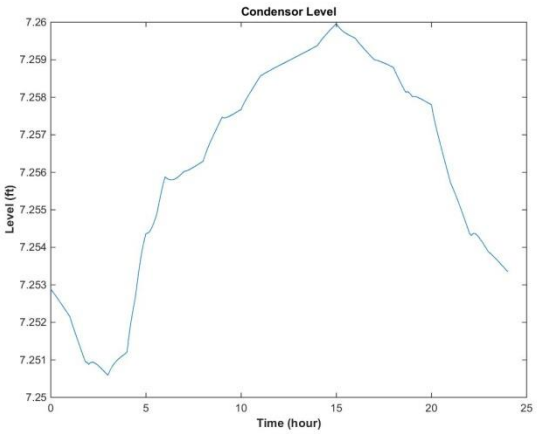

Figure 9.21: Condenser Level

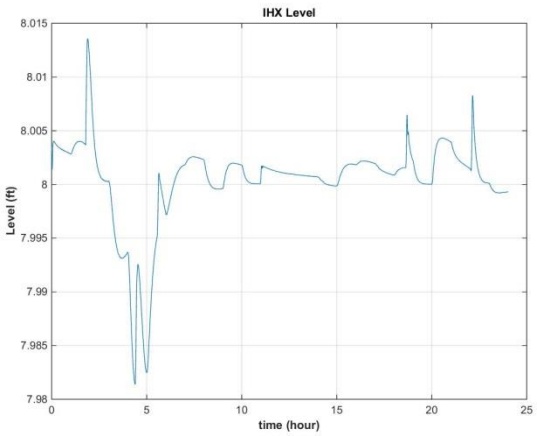

Figure 9.22: Level in the IHX.

The reactor system was assumed to have sufficient capacity to meet 100% load on the most extreme summer day. The run shown above is representative of a typical summer day. As a result, there will always be some bypass demand. Bypass demand goes as nominal reactor output-turbine demand. For the run shown we have bypass ranging from ~45% bypass down to ~7-8% bypass. Figure 9.13 shows that we are able to meet bypass demand as the valves never fully open or shut. Figure 9.14 shows the operating pressure at 45% bypass at the 750 psi design pressure, and over the course of the run reaches a minimum of ~700psi. As the pressure does not fall below 680psi, the shell side saturation temperature remains above the tube side set point temperature of 500F. Should the pressure in the IHX fall below this value the set point temperature on the tube side could not be reached. Further, the pressure in the IHX never reaches the setpoint of 780psi at which point the Pressure Relief Valves would open. Since the Pressure Relief Valves do not open this means zero energy is bypassing the TES system through the PRV's.

As shown in Figure 9.16 the flow control valve is ~24% open at the beginning of the simulation, it continues to move to ~42% open as bypass into the IHX increases. It then begins to close down to ~8% open as the amount of bypass flow into the IHX decreases later in the simulation. Figure 9.17 shows the flow control valve is able to maintain TES exit temperature at ~500F over the entire 24 hour simulation.

As the hot tank fills and the cold tank empties, the pressures in the tanks change due to compression and expansion of the cover gases. As the pressures change the relative position of the FCV required to achieve the same mass flow rate of TES fluid changes. As a result, the FCV is more open towards the end of the 24-hour run than the beginning despite the same demand levels.

Over the course of the day condenser pressures vary from 0.86psi to 1psi, despite the condenser cooling water temperatures and flows remaining constant. The level of the IHX remains steady about the reference value of 8 feet.

9.2.2. Typical Winter Day

During the winter months there tends to be two peaks in the load profile. One associated with morning activities around 8-10am and a second when people are returning home for the evening. Given that bypass flow goes as 1-relative demand, the overall bypass demand on the system is larger in the winter than in the summer months.

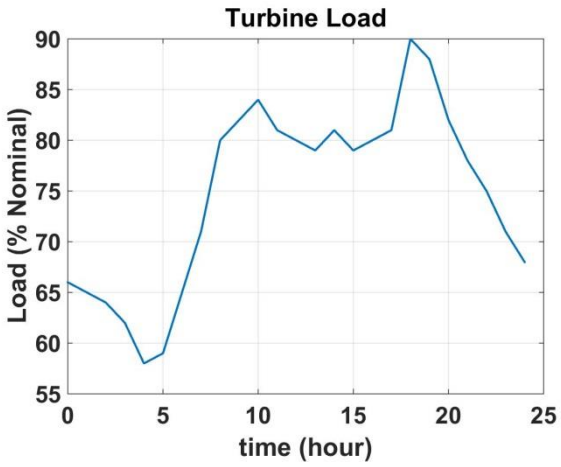

Figure 9.23: Winter Day Load Profile

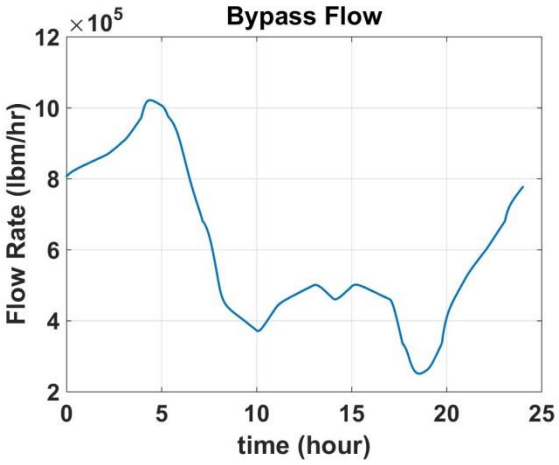

Figure 9.24: Bypass Flow

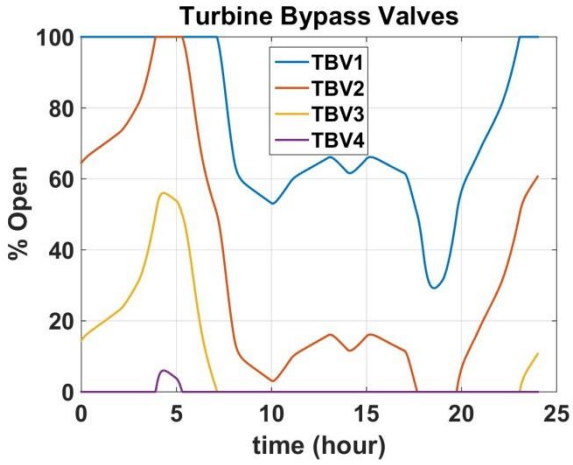

Figure 9.25: Position of TES Turbine Bypass Valves

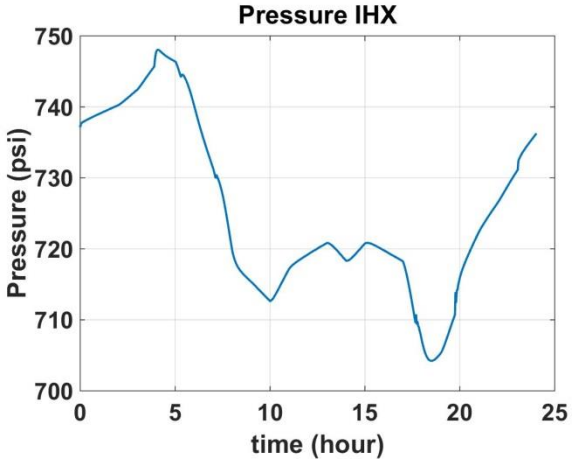

Figure 9.26: Pressure on the shell side of the IHX.

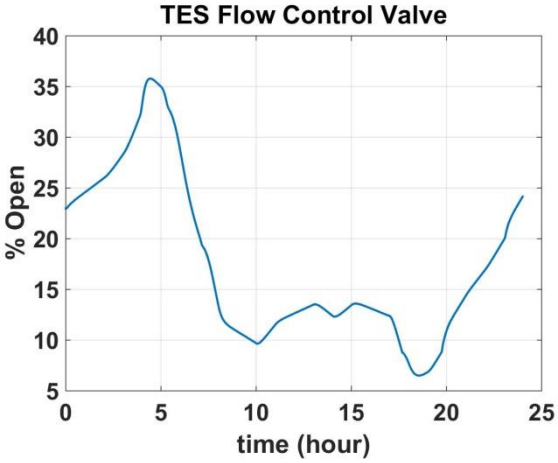

Figure 9.27: TES Flow Control Valve Position.

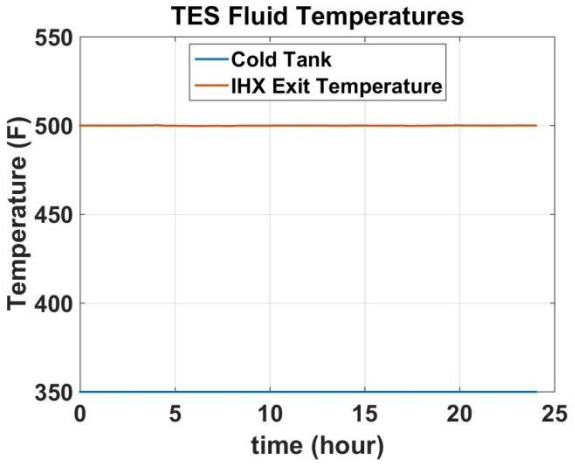

Figure 9.28: Temperature of TES fluid at exit of IHX.

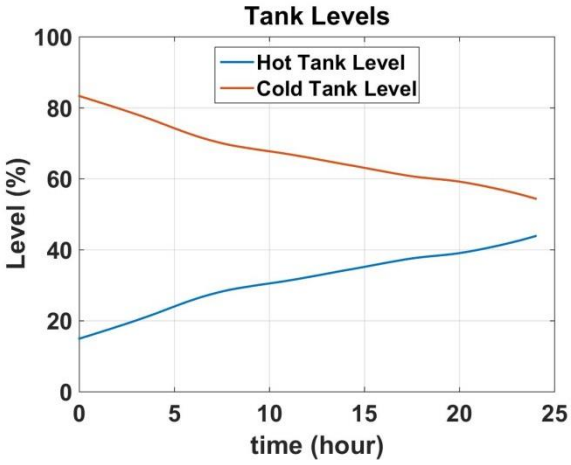

Figure 9.29: Hot and Cold Tank Levels.

As indicated in Figure 9.23 the turbine load goes from a minimum of ~57% up to 90% demand. This means the bypass demand is ranging from 43% nominal flow down to 10% nominal flow. In Figure 9.25 we see the turbine bypass valves never all go full open or full shut. This means we are never getting into a situation where the bypass demand is not met. Pressure in the IHX can be seen in Figure 9.26 and over the course of the run never falls below the target saturation pressure of 680psi or goes above the PRV set point of 780psi. With the pressure staying above 680psi the saturation temperature in the IHX stays above the reference temperature of 500F. Likewise, the pressure remaining below 780psi over the course of the entire 24-hour run ensures the PRV's remain closed. With the PRV's remaining closed all of the potential heat from the reactor is transferred into the TES fluid rather than bypassing straight to the condenser. From Figure 9.27 the flow control valve can be seen to never fully open or fully close. This means the system is never at the limits of its capacity and should be able to maintain the temperature at the top of the IHX over the course of the entire 24-hour run. This can be seen in Figure 9.28. As the flow control valve modulates flow to maintain the TES fluid temperature, the hot tank begins to fill as seen in Figure 9.29.

9.2.3. Summer Day –Including Solar

The summer day load profile was modified to reflect upwards of 40MWe installed solar capacity. The reactor system was again assumed to have sufficient capacity to meet 100% load on the most extreme summer day. When applied to a standard summer day as in the previous example the output from solar influences the load drastically. Figure 9.30 shows the solar output over a 24-hour period. Solar output increases from zero power from midnight to 4am to near full power from 8am to 3pm. Since solar

generation tends to have grid priority in most areas this directly affects the demand profile seen by the nuclear plant. This difference in load can be seen in Figure 9.31 when comparing the overall demand with the demand on the reactor. The reactor demand curve is the result of taking the overall demand and subtracting the solar output from Figure 9.30.

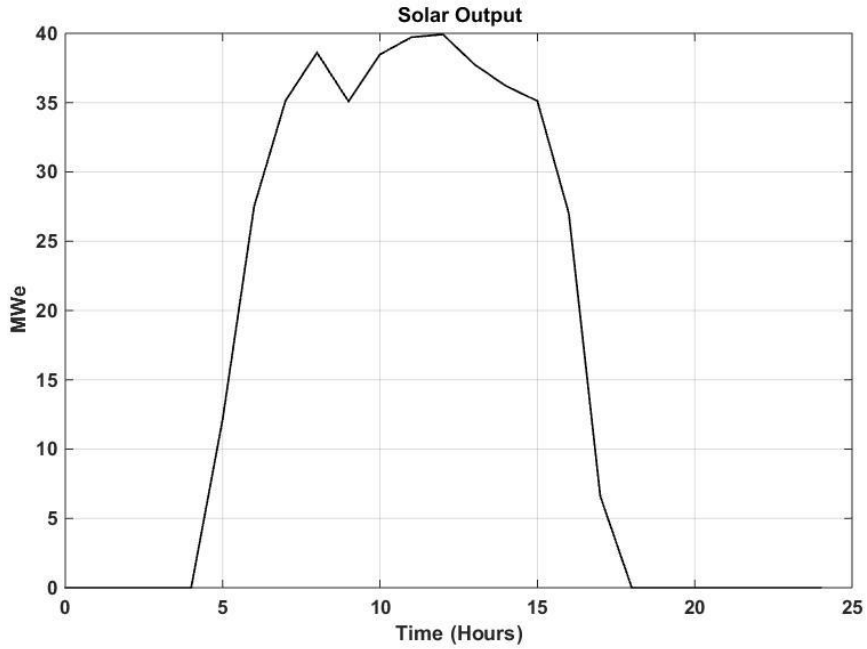

Figure 9.30: Typical Solar Output for a Summer Day

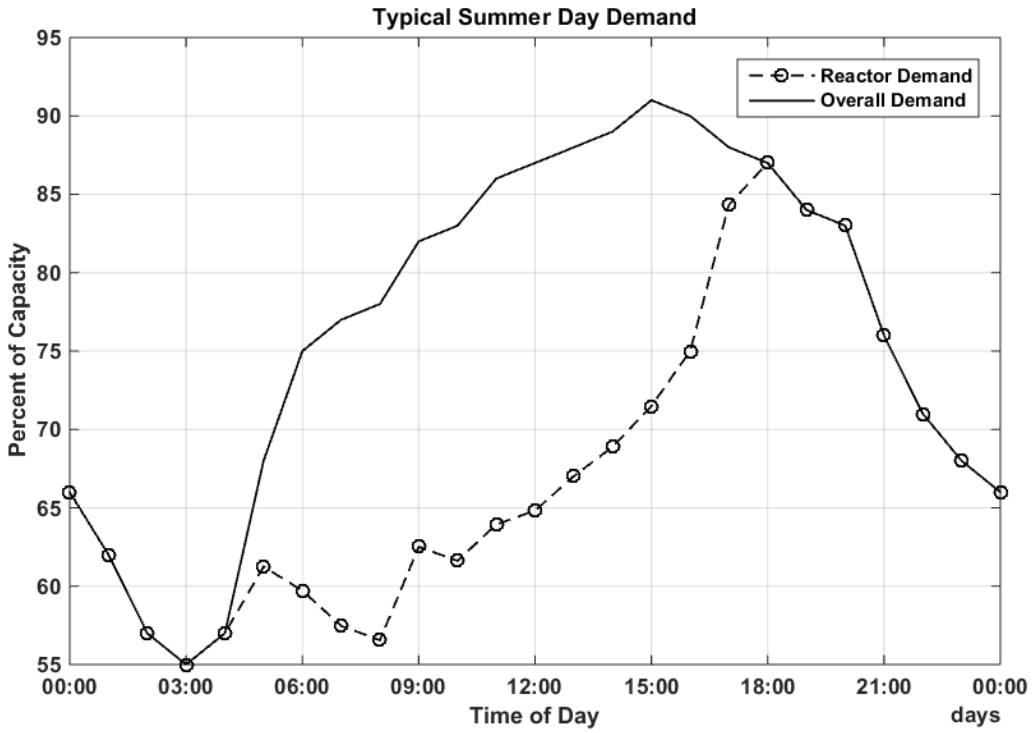

Figure 9.31: Demand profiles of a typical summer day with and without solar

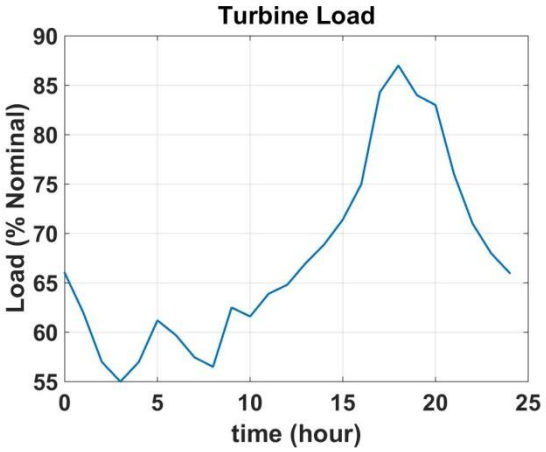

Figure 9.32: Summer Load Profile With Solar Generation

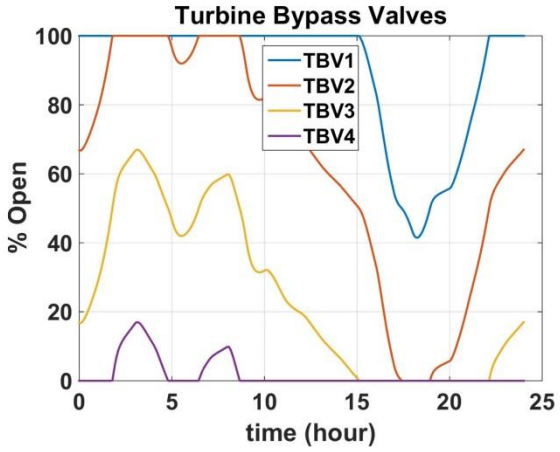

Figure 9.33: TES Bypass Valve Position

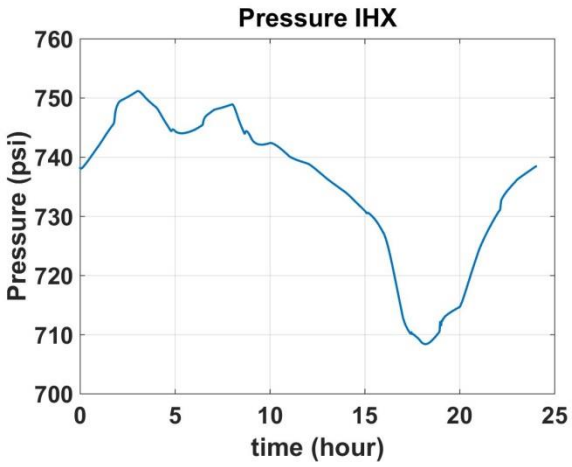

Figure 9.34: Pressure in the IHX.

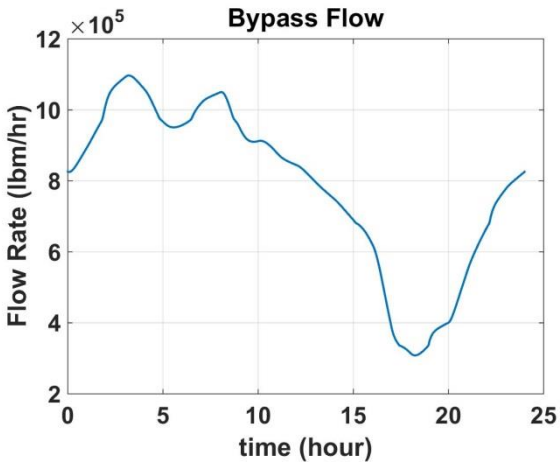

Figure 9.35: Bypass Flow

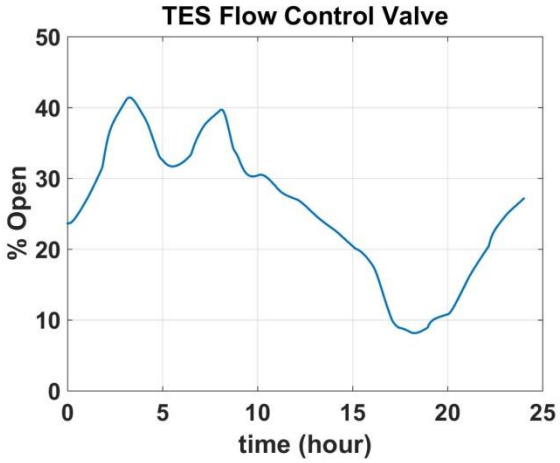

Figure 9.36: Flow Control Valve Position

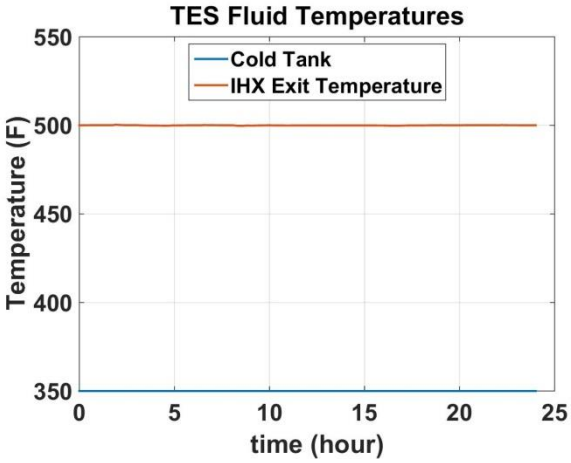

Figure 9.37: Temperature of TES fluid exiting the IHX.

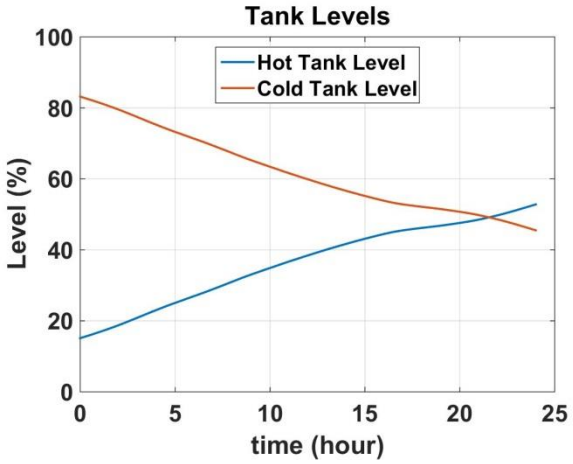

Figure 9.38: Hot and Cold Tank Levels.

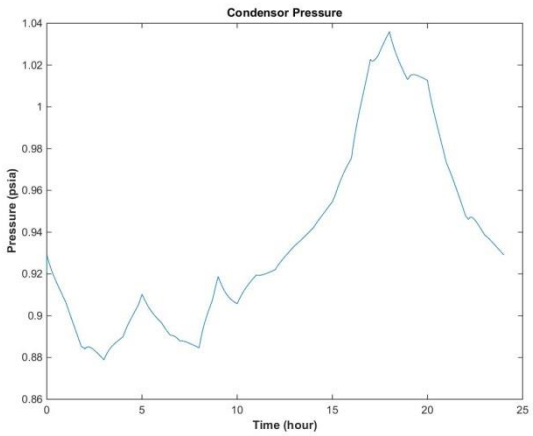

Figure 9.39: Condenser Pressure

Over the course of the simulation bypass flow ranges from 45% down to a bypass flow rate of ~13%. During this time Figure 9.33 shows the bypass valves initially start with one full open, two partially open, and one closed. The two partially open valves are at positions of ~17% and 67%. This 50% difference is due to a 50% overlap in the opening and closing set points for the valves. As the run progresses and the bypass demand is reduced, the valves close such that at 18 hours into the simulation all but one of the valves are completely closed. As the valves close and heat continues to be transferred from the shell side of the IHX to the tube side, shell side pressure decreases. Pressure ranges from 750psi to ~707psi, but remains above 680psi corresponding to the reference temperature of the IHX. Further, the pressure never reached the set point of 780psi that would open the PRV's.

As seen in Figure 9.36 and Figure 9.37 the flow control valve is moving to insure the temperature at the exit of the IHX is maintained at 500F. Figure 9.38 shows the tanks are able to accommodate the full 24 hour cycle.

9.2.4. Summer Day –Including Wind

Solar generation is only available when the sun is shining. Wind power on the other hand is variable throughout the day. This inability to predict wind availability necessitates the need to lower the penetration level of wind power compared to solar power. While solar generation tends to coincide with the highest power demand parts of the day, wind can be producing power at full capacity during times that demand is already low. If the wind penetration is sufficiently large this could create a situation where the bypass valves are full open and the bypass demand cannot be met. In this situation, the reactor would likely be required to reduce power.

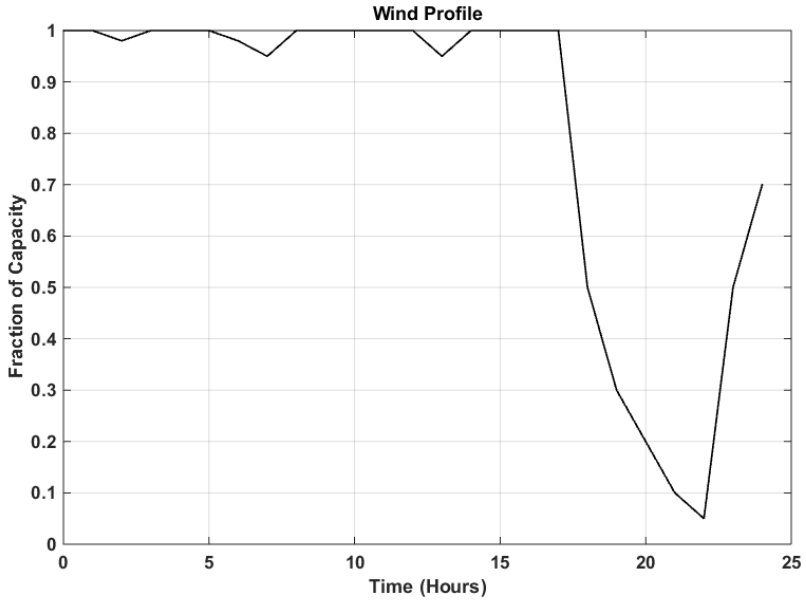

Figure 9.40: Wind availability profile.

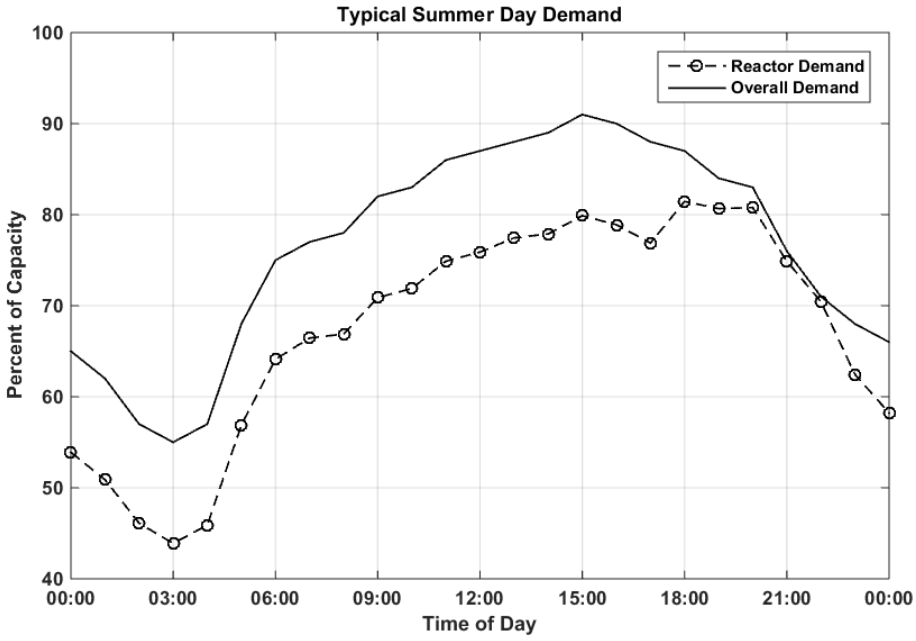

Figure 9.41: Typical summer day profile with 20MW wind capacity installed.

The demand on the reactor is the overall demand minus power provided by the wind plant. This decrease in turbine demand, seen in Figure 9.41 increases the amount of bypass flow allowed into the system. The bypass demand is upwards of 55% around 3am. This large amount of bypass is slightly more than the TES capacity, as seen in Figure 9.43.

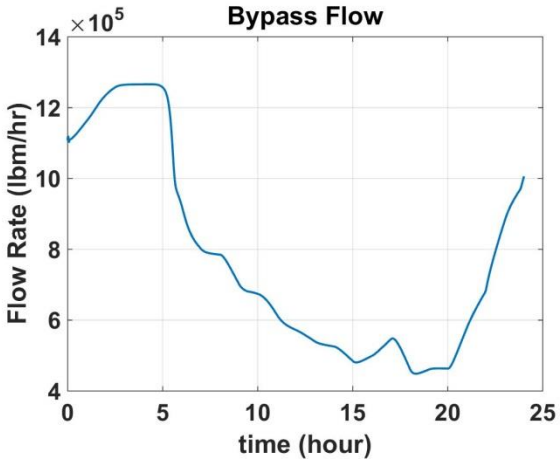

Figure 9.42: Bypass Flow

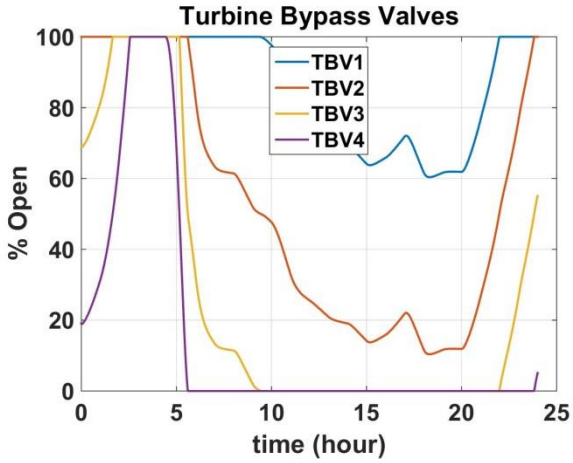

Figure 9.43: TES Turbine Bypass Valve Positions

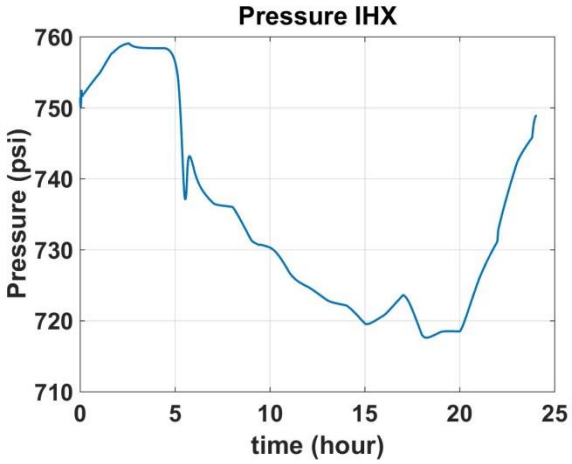

Figure 9.44: Pressure in the IHX.

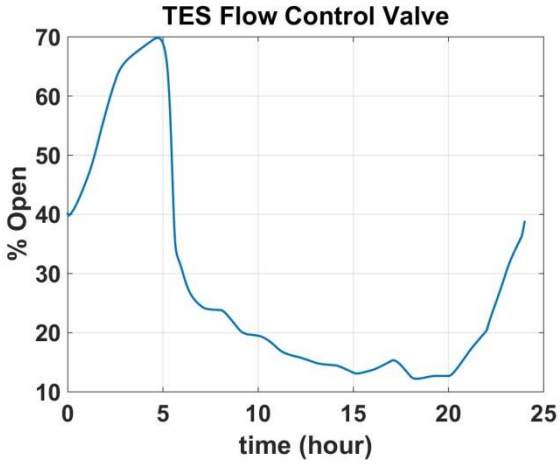

Figure 9.45: TES Flow Control Valve Position

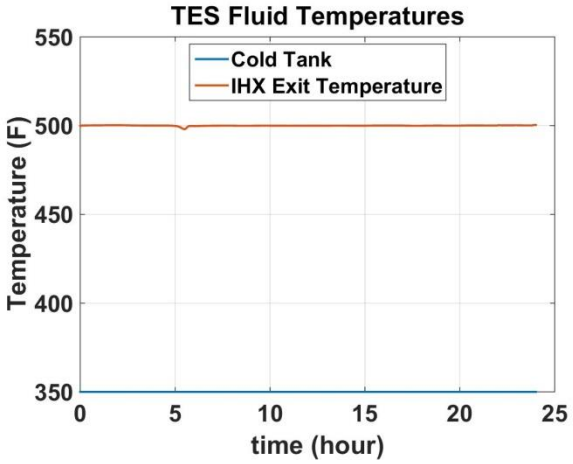

Figure 9.46: Temperature at the exit of the IHX.

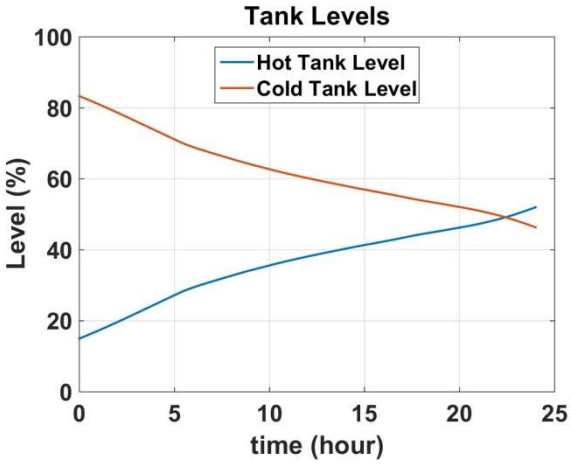

Figure 9.47: Hot and Cold Tank Levels

For the load profile considered above the bypass demand reaches around 55%. When attempting to accommodate this large bypass demand the bypass valves go full open. At their full open position, the valves are unable to provide the bypass flow necessary to keep the reactor at 100% power. In this situation the reactor would have to decrease power. While the bypass valves are full open the pressure in the IHX increases. Fortunately, over the course of the run the pressure stays below the PRV set point of 780psi meaning the PRV's are never forced to open. As bypass demand decreases later in the day, the bypass valves close and pressure in the IHX decreases. Figure 9.45 and Figure 9.46 show that over the course of the run the FCV went from 38% to 68% open as the FCV is modulating to maintain the reference temperature at the top of the IHX. For a brief period when the pressure in the IHX was dropping quickly the heat transfer rate across the IHX also drops. As the heat transfer rate across the IHX decreased rapidly the temperature at the exit of the IHX dropped significantly and it took the FCV a while to ultimately catch up. Therefore there is a small period of time (~5-10 minutes) where the TES fluid temperature leaving the IHX is slightly less than the reference temperature.